LIÈGE université
Gembloux
Agro-Bio Tech

Mechanisms underlying cyclic lipopeptide-induced resistance in plants

Jelena Pršić

COMMUNAUTÉ FRANÇAISE DE BELGIQUE
UNIVERSITÉ DE LIÈGE – GEMBLOUX AGRO-BIO TECH

Mechanisms underlying cyclic lipopeptide-induced resistance in plants

Jelena PRŠIĆ

Dissertation originale présentée (ou essai présenté) en vue de l'obtention du grade de doctorat en sciences agronomiques et ingénierie biologique

Promoteur(s) : Marc ONGENA
Année civile : 2024

Abstract

In recent years, the induced systemic resistance (ISR), triggered by elicitors produced by plant beneficial bacteria, emerged as a promising strategy for implementation in sustainable agriculture. Compared to chemical pesticides, ISR has certain advantages, such as provision of long-lasting and broad-spectrum protection and a low risk of development of resistant pathogens. Among ISR elicitors, cyclic lipopeptides (CLPs) are particularly important. Being reported in high diversity of phytopathosystems, the most studied CLP as an ISR elicitor is surfactin (Srf) produced by beneficial bacilli. However, the success of plant beneficial bacteria as stimulators of ISR has been rather limited due to a number of factors, including our global lack of knowledge about the mode of action of their elicitors. The aim of this work was therefore to investigate the elusive phenomena of ISR induced by these beneficials, using Srf as a model elicitor.

To tackle this complex question, this work integrated biophysical, *in silico*, and *in planta* approaches. The first method was to compare immune responses triggered by Srf and a well-known pattern triggered immunity (PTI) elicitor flagellin 22. Being the first steps in immunity elicitation, perception by the plant cells and mechanisms for early immune events elicitation were firstly investigated. Furthermore, a genome-wide transcriptome analysis was performed to compare these two types of responses at the transcriptional level. The data indicated that Srf does not rely on previously described elicitors sensing receptors, but rather interacts with the lipid phase of plant plasma membrane (PPM). More specifically, Srf interacts with a specific class of lipids, causing changes in PPM lipid organization, structural and rheological properties. Such membrane changes have been described in the literature to be perceived via mechanosensitive ion channels, and this work shows that representatives of these channels are required for early immune responses activation and induction of ISR by Srf. In addition, genome-wide transcriptome analysis revealed that plant responses to Srf and during the onset of PTI significantly differ. Considering that the bioactivity of Srf is influenced by the presence of particular PPM lipids, other structurally different CLPs were tested, and it was observed that the affinity for lipids differs among them. This indicates that in different species, CLPs/PPM lipids interaction will result in different immune responses depending on plant's plasma membrane lipid profile. Further structure activity studies revealed that CLP activity is a finely tuned process where structural changes in both the peptide and the acyl chain can cause loss of activity.

Through in-depth data mining of results of the RNAseq analysis conducted on *Arabidopsis thaliana* roots, this work also provided data that could be used to decipher signaling during the onset of Srf-triggered ISR, as well as the mechanism for enhancing plant defense responses.

To our best knowledge, this is not only the first time that a perception of an ISR elicitor has been described, but also the first time that this peculiar way of perception of an immunity elicitor was described. Moreover, by revealing the perception pathway and the transcriptional changes induced upon Srf treatment, this work provides clues for further elucidation of Srf triggered ISR.

Résumé

Ces dernières années, la résistance systémique induite (induced systemic resistance ISR), déclenchée par des éliciteurs produits par des bactéries bénéfiques pour les plantes, est apparue comme une stratégie prometteuse à mettre en œuvre dans l'agriculture durable. Par rapport aux pesticides chimiques, la résistance systémique induite présente certains avantages, tels qu'une protection durable et à large spectre et un faible risque de développement de pathogènes résistants. Parmi les éliciteurs RSI, les lipopeptides cycliques (LPC) sont particulièrement importants. La surfactine (Srf), produite par des bacilles bénéfiques, est le LPC le plus étudié en tant qu'éliciteur de l'ISR, car il est présent dans une grande diversité de systèmes phytopathologiques. Cependant, le succès des bactéries bénéfiques pour les plantes en tant que stimulateurs de l'ISR a été plutôt limité en raison d'un certain nombre de facteurs, y compris notre manque global de connaissances sur le mode d'action de leurs éliciteurs. L'objectif de ce travail était donc d'étudier le phénomène insaisissable de l'ISR induit par ces auxiliaires, en utilisant le Srf comme éliciteur modèle.

Pour aborder cette question complexe, ce travail a intégré des approches biophysiques, in silico et in planta. La première méthode a consisté à comparer les réponses immunitaires déclenchées par le Srf et un éliciteur bien connu de l'immunité déclenchée par les motifs (pattern triggered immunity - PTI), la flagelline 22. Etant les premières étapes de l'élicitation de l'immunité, la perception par les cellules végétales et les mécanismes d'élicitation des événements immunitaires précoces ont d'abord été étudiés. En outre, une analyse du transcriptome à l'échelle du génome a été réalisée pour comparer ces deux types de réponses au niveau transcriptionnel. Les données indiquent que Srf ne dépend pas des récepteurs de détection des éliciteurs précédemment décrits, mais interagit plutôt avec la phase lipidique de la membrane plasmique de la plante (PPM). Plus précisément, Srf interagit avec une classe spécifique de lipides, provoquant des changements dans l'organisation des lipides de la PPM, ainsi que dans ses propriétés structurelles et rhéologiques. De tels changements membranaires ont été décrits dans la littérature comme étant perçus via des canaux ioniques mécanosensibles, et ce travail montre que des représentants de ces canaux sont requis pour l'activation des réponses immunitaires précoces et l'induction de l'ISR par le Srf. En outre, l'analyse du transcriptome à l'échelle du génome a révélé que les réponses des plantes au Srf et pendant le début de le PTI diffèrent de manière significative.

Étant donné que la bioactivité du Srf est influencée par la présence de lipides PPM particuliers, d'autres CLP structurellement différents ont été testés et il a été observé que l'affinité pour les lipides diffère entre eux. Cela indique que chez différentes espèces, les CLP ont une affinité différente pour les lipides.

Cela indique que chez différentes espèces, l'interaction CLP/lipides PPM entraînera des réponses immunitaires différentes en fonction du profil lipidique de la membrane plasmique de la plante. D'autres études sur la structure et l'activité ont révélé que l'activité des CLP est un processus finement réglé dans lequel des changements structurels dans le peptide et la chaîne acyle peuvent entraîner une perte d'activité.

Grâce à l'exploration approfondie des résultats de l'analyse RNAseq menée sur les racines d'Arabidopsis thaliana, ce travail a également fourni des données qui pourraient être utilisées pour déchiffrer la signalisation pendant le début de l'ISR déclenché par le Srf, ainsi que le mécanisme d'amélioration des réponses de défense de la plante.

A notre connaissance, c'est non seulement la première fois qu'une perception d'un éliciteur ISR a été décrite, mais aussi la première fois que ce mode particulier de perception d'un éliciteur d'immunité a été décrit. De plus, en révélant la voie de perception et les changements transcriptionnels induits par le traitement au Srf, ce travail fournit des indices pour une élucidation plus poussée de l'ISR déclenché par le Srf.

Acknowledgements

This thesis is not a product made in isolation, but rather in synergy with people that supported this work, but also with ones supporting me and thus this thesis as well.

Everyone who spoke to me at least once in the last two years about my thesis know that it was not all butterflies and flowers, especially at the end. In reality the finalization of this thesis didn't happen thanks to the strength I had in me, but to the strength I gathered from the support I had from the people surrounding me. Expressing my gratitude to these people would make this manuscript 100 pages longer and anyways the words won't do. So, I will keep it short.

In the front line of this battlefield there was always one more person standing by and supporting - my supervisor Marc Ongena. His supervisorship helped me to improve not only research but also life skills both of which will surely contribute to my future professional development. Thus, thank you Dr Ongena.

Besides Dr Ongena, it is really important for me to express my sincere gratitude to the members of the thesis committee, professors: Monica Höfte, Barbara De Coninck, Magali Deleu, and Philippe Jacques who directed this thesis and improved its quality with their highly valuable advices.

Furthermore, I would like to thank the whole MiPI and LBMI labs. Thank you, my dear teammates Sofija, Anthony, Grég, Thibault, Nell, Guillaume B., Farah, Adrien, Augustin, Francois and Virginie. Also, thank you Cathy, Séb, Aurélien, Romain, Katrien, Olivia, Marguerite, and Marina for all the help and support you provided. Considering her knowledge of biophysics at the beginning of this thesis, this author owes a great gratitude for achieved improvement to the team of the LBMI, Estelle, Catherine, Guillaume G., Aurélien, Willy, and Magali. Last but not least, special thanks to you Valeria as well, you were also one of these people that put love for biophysics in my heart.

In addition, I am immensely grateful to my climbing girls that were there through my best rises and worst falls, literally and metaphorically :D The end of this thesis was possible also thanks to you, dhanyavaad Arpita, mulțumesc Andreea, thank you Hillary, and merci Sigrid! My dear Flemish and BioBest friends, you came at the very end but actually just on time! An, Luisa, Felipe, Eva, Lara, Sanne, Cindy, Soraya thank you for your support and understanding, it came when it was most needed.

For all the hours listening to all the versions of the presentation, me whining about the thesis, for never complaining about it, for literally correcting with me this manuscript when I could not anymore, for keeping an eye on the prize when I could not anymore... Special thanks to you Jan, I will be grateful forever.

It is not possible to finish these acknowledgements without mentioning people that were not only there for me last 6 years, but for a long period of my life, in happy, sad, crazy, in all we shared. Vesna, Violeta, Vale, Katka, Anna, love you guys!

Na kraju, veliko hvala mojoj porodici bez koje ovo, ni početak, ni kraj, ni ono između ova dva, ni ono pre, ne bi bilo moguće. Volim vas najviše <3

Table of contents

List of figures

List of tables

List supplementary figures

List supplementary tables

List of acronyms

AHL	Acyl-homoserine lactone
Aza	Azelaic acid
BAK1	BRI1-associated receptor kinase
BIK1	BOTRYTIS-INDUCED KINASE 1
CaM	Calmodulin
CBL	Calcineurin B-like proteins
CDPK	Ca2+- dependent protein kinases
CLP	Cyclic lipopeptide
CMLs	CaM-like proteins
CNGC	Cyclic nucleotide-gated channels
Col-0	Columbia-0
Cyt	Cytosolic
DAMP	Damage-associated molecular patterns
DEG	Differentially expressed genes
DLS	Dynamic light scattering
EFR	ELONGATION FACTOR-TU RECEPTOR
ERF	Ethylene response factor
ET	Ethylene
ETI	Effector-triggered immunity
fah1fah2	FATTY ACID HYDROXYLASE 1 and 2
FC	Fold change
flg22	Flagellin 22
FLS2	FLAGELLIN-SENSING 2

GIPC	Glycosyl inositol phosphorylceramides
GLR	Ionotropic glutamate receptors
GluCer	Glucosylceramides
GP	Generalized polarization
IG	Indolic glucosinolates
ISR	Induced systemic resistance
ITC	Isothermal titration calorimetry
JA	Jasmonic acid
loh1	LONGEVITY ASSURANCE GENE ONE HOMOLOG 1
LORE	LIPOOLIGOSACCHARIDE-SPECIFIC REDUCED ELICITATION
LOX	Lipoxygenase
LUV	Large unilamellar vesicles
MAMP	Microbe-associated molecular patterns
MAPK	Mitogen-activated protein kinase
MCA	Mid1-complementing activity channels
MD	Molecular dynamics
MSC	Mechanosensitive ion channel
MSL	Mechano-sensitive channels of small conductance-like
NIA	Nitrate reductase
NOS	Nitric oxide synthase
NPR1	Nonexpressor of pathogenesis-related genes 1
NR	Neutron reflectivity
NRPS	Non-ribosomal peptide synthetases

OPDA	Oxo-phytodienoic acid
OSCA	Reduced hyperosmolarity-induced [Ca2+]cyt increase channels
PAD3	PHYTOALEXIN DEFICIENT 3
PAL	Phenylalanine ammonia-lyase
PAMP	Pathogen-associated molecular patterns
PBB	Plant beneficial bacteria
PBL	PBS1-like
PLPC	1-palmitoyl-2-linoleoyl-sn-glycero-3-phosphocholine
PPM	Plant plasma membrane
PR	Pathogenesis-related (proteins)
PRR	Pattern-recognition receptors
PTI	Pattern-triggered immunity
RNAseq	RNA sequencing
RNS	Reactive nitrogen species
ROS	Reactive oxygen species
SA	Salicylic acid
SAR	Systemic acquired resistance
SD	Standard deviation
Sito	ß-sitosterol
SLD	Scattering length density
SOBIR	Suppressor of BIR
Srf	Surfactin
TPC1	Two-pore channel 1

Publications in scientific journals

Pršić J. and Ongena M. (2020) Elicitors of Plant Immunity Triggered by Beneficial Bacteria. Front. Plant Sci. 11:594530. doi:10.3389/fpls.2020.594530

Crouzet J., Arguelles-Arias A., Dhondt-Cordelier S., Cordelier S., Pršić J., Hoff G., Mazeyrat-Gourbeyre F., Baillieul F., Clément C., Ongena M., and Dorey S. (2020) Biosurfactants in Plant Protection Against Diseases: Rhamnolipids and Lipopeptides Case Study. Front. Bioeng. Biotechnol. 8:1014. doi: 10.3389/fbioe.2020.01014

Hoff G, Arguelles Arias A, Boubsi F, Pršić J, Meyer T, Ibrahim HMM, Steels S, Luzuriaga P, Legras A, Franzil L, Lequart-Pillon M, Rayon C, Osorio V, de Pauw E, Lara Y, Deboever E, de Coninck B, Jacques P, Deleu M, Petit E, Van Wuytswinkel O, Ongena M. (2021). Surfactin stimulated by pectin molecular patterns and root exudates acts as a key driver of the Bacillus-plant mutualistic interaction. mBio 12:e01774-21. https://doi.org/10.1128/ mBio.01774-21

Rondelli, V., Koutsioubas, A., Pršić, J., Deboever E., Crowet J. M., Lins L., Deleu M. (2021). Sitosterol and glucosylceramide cooperative transversal and lateral uneven distribution in plant membranes. Sci Rep 11, 21618. https://doi.org/10.1038/s41598-021-00696-7

Bacha K., Chemotti C., Monboisse JC, Robert A., Furlan A., Smeralda W., Damblon C., Estager J., Brassart-Pasco S., Mbakidi JP., Pršić, J., Bouquillon S., Deleu M. Encapsulation of Vitamin C by Glycerol-Derived Dendrimers, Their Interaction with Biomimetic Models of Stratum corneum and Their Cytotoxicity. Molecules. 2022;27(22). doi:10.3390/molecules27228022

Gilliard G, Furlan AL, Smeralda W, Pršić J, Deleu M. Added Value of Biophysics to Study Lipid-Driven Biological Processes: The Case of Surfactins, a Class of Natural Amphiphile Molecules. Int J Mol Sci. 2022;23(22):13831. doi:10.3390/ijms232213831

Communications in scientific conferences

Plant immunization by the Bacillus lipopeptide surfactin: insights into the mechanistics of perception at the plasma membrane, (19.11.2020). Plant BioProTech symposium, Marrakech, Marocco (19-22.11.2019), oral presentation

Elicitation of induced systemic resistance in plants by cyclic lipopeptides (04.10.2021). UMRT BioEcoAgro (webinar), oral presentation

Structural features driving the plant immunity elicitor activity of bacterial lipopeptides (26.01.2022). 15èmes Rencontres Plantes Bactéries (VISIOCONFERENCE) (25 – 27.01.2022), oral presentation

Structural features driving the plant immunity elicitor activity of bacterial lipopeptides (11 – 14.07.2022). miCROPe Vienna, Austria, poster presentation

Mechanistics of surfactin perception for plant immunity stimulation (21.09.2022). EOS workshop – Bacterial lipopeptides: from (physico) chemistry to ecology, Liege, Belgium (21-23.09.2022), oral presentation

Chapter 1

General introduction

1. Potential of biological control agents in sustainable agriculture

1.1. *Crop protection - then and now*

The main challenge agriculture is facing nowadays is the global food security due to a world's fast-growing population with changing dietary habits (Avermaete *et al*., 2023). Besides abiotic factors (weather and soil conditions), pathogens and pests are the most important biotic factors that negatively impact crop yields and thus global food security. The yield reduction of the world's most important crops due to pathogens and pests was estimated by Savary *et al*., (2019) to be 21.5% for wheat, 30.0% for rice, 22.5% for maize, 17.2% for potato, and 21.4% for soybean, at the global level.

In modern farming practices, the management of agricultural yield reduction caused by living organisms is achieved through the application of pesticides. These products prevent, eradicate, or control harmful organisms (referred to as 'pests') and diseases, while also ensuring the protection of plants and their associated products throughout the stages of production, storage, and transportation. In the early days of pest management, people mainly relied on natural substances like sulfur, as well as extracts from plants, animals, or minerals. However, synthetic chemical pesticides have assumed a predominant role as the primary means of pest and disease management in agriculture over the last century. With their drastic improvement, they not only ensured maximum yields, but also provided food free of toxins harmful to humans, such as mycotoxins secreted by pathogens (Mahato *et al*., 2019; Umetsu and Shirai, 2020).

At the global level, in 2018, the use of these chemicals was the most prevalent in Asia (about 50% of the global consumption in two categories total weight to crop land, and average kg/ha applied), followed by Americas (30 %), and Europe in the third place (in both aforementioned categories) (FAOSTAT site). In Europe, the most commonly used pesticides are for the control of phytopathogens (fungicides and bactericides, acting against fungal and bacterial diseases respectively) and herbicides (acting against weeds), each

accounting for about 40-45% of total consumption (total weight to crop land) (FAO.Org).

However, years of application showed that extensive use of pesticides is harmful for the environment, poses a risk to human health and induces development of phenomena called “resistance” manifested through lower sensibility of pathogens, pests, and weeds towards pesticides (Kole *et al*., 2019). Consequently, nowadays there is an increased interest in sustainable, ensuring rational use of pesticides, and in organic agriculture characterized by a strong restriction in commercial pesticides used (FAO.Org). In Europe alone, between 2000 and 2021, the area of certified organic cropland increased from around 4 million ha to 16,5 million ha (FAOSTAT site). These new agricultural trends have opened the door for biological control agents and increased their share of total pesticides used in agriculture.

1.2. *Bacillus spp. and Pseudomonas spp. as biocontrol agents*

Biological control involves the use of non-living nature-based substances and/or living biocontrol agents among which plant beneficial bacteria (PBBs) are being extensively researched and exploited. Amongst many rhizobacterial genera (*Lysobacter* spp., *Streptomyces* spp., *Paenibacillus* spp., *Burkholderia* spp., *Serratia* spp., *Azospirilum* spp., *Pseudomonas* spp., *Bacillus* spp.) that demonstrates beneficial effects, *Pseudomonas* spp. and *Bacillus* spp. are the most studied (Baliah *et al*., 2018; Dame *et al*., 2021).

The immense potential of these genera for application as biocontrol agents mainly relies on the vast diversity of their genetical pool enabling production of numerous bioactive compounds (enzymes, antibiotics, immunity elicitors, growth-promoting substances) (Chen *et al*., 2020; Müller and Behrendt, 2021). Additionally, these species demonstrate strong competition with other microorganisms and fast adaptation to environmental stresses which together result in successful soil establishment often associated with naturally disease suppressive soils (Ganeshan and Kumar, 2005; Baliah *et al*., 2018).

However, in the downstream process towards registration, obstacles imposed on pseudomonads due to the risk of acting as opportunistic human pathogens and the short shelf-life period make this genus less suitable. Despite the difficulties, some *Pseudomonas* sp.-based products are registered in Belgium (**Table 1**).

On the other hand, *Bacillus* species, which currently account for half of the registered commercial bacterial biocontrol products in the world, show a higher potential (**Table 1**). This is mainly due to the fact that bacilli are considered to be generally safe and are successful in forming endospores that allow survival under unfavorable conditions, thus ensuring a longer shelf life (Dimopoulou *et al*., 2021).

Generally, biocontrol agents are affecting pathogens with direct and/or indirect inhibition. Directly, they are successful competitors for nutrients and environmental niches, secreting metabolites acting as antimicrobials, and inhibiting colonization of the host plant by pathogens. Indirectly, these microbes rely on plant growth- and health promotion, where health promoting effect is supported by the induction of systemic resistance (induced systemic resistance, ISR) (Dimopoulou *et al*., 2021). From an agronomic perspective, the importance of PBB-triggered ISR rests in the provision of long-lasting and broad-spectrum protection, with low fitness costs, and low risk of resistant pathogen development (Köhl *et al*., 2019).

Product name	Pesticide category	Active microorganism	Pathogens/pests affected
Amylo-X WG	Fungicide	*Bacillus amyloliquefaciens* subsp. *plantarum* D747	*Botrytis cinerea*, *Oidium* spp., *Sclerotinia* spp., *Trichoderma aggressivum*
Serenade ASO	Fungicide	*Bacillus velezensis* QST 713 (formerly *Bacillus subtilis* QST 713)	*Alternaria* spp., *Erwinia amylovora*, *Cercospora beticola*, pathogens causing seedlings damping off, *Fusarium* spp., *Oidium* spp., *Botrytis cinerea*, *Rhizoctonia solani*, *Sclerotinia* spp., *Pseudomonas syringae*
Taegro	Fungicide	*Bacillus amyloliquefaciens* FZB24	*Alternaria* spp., downy mildew, *Oidium* spp., *Botrytis cinerea*
Serifel	Fungicide	*Bacillus amyloliquefaciens* MBI 600	*Botrytis cinerea*, *Sclerotinia* spp., *Trichoderma aggressivum*
Turex WG	Insecticide	*Bacillus thuringiensis* ssp. *aizawai* GC-91	Caterpillars of butterflies and moths (Lepidoptera)
Dipel DF	Insecticide	*Bacillus thuringiensis* ssp. *kurstaki*	Caterpillars and borers
Delfin WG	Insecticide	*Bacillus thuringiensis* ssp. *kurstaki* SA-11	Caterpillars
Proradix WP	Fungicide	*Pseudomonas* sp. DSMZ 13134	*Helminthosporium solani*, *Rhizoctonia solani*
Cerall	Fungicide	*Pseudomonas chlororaphis* MA342	*Tilletia* spp., *Fusarium* spp., *Septoria* spp.

Table 1 - Examples of bacterial biocontrol products registered in Belgium (source PHYTOWEB).

1.2.1. *Plant immunity induction*

Due to the sessile lifestyle, plants developed various defense systems in order to survive. Constitutively, these are manifested as chemical and physical barriers present in plants, whether or not there is an invader's attack. On the other hand, plants also developed defense mechanisms that are induced upon the perception of various hostile biotic (pathogens, insects) and abiotic (unfavorable environmental conditions) cues (Wiesel *et al*., 2014).

The plant plasma membrane (PPM) is the critical cell site not only for the perception of these unfavorable cues, but also for their transduction into signals that specify to the plants what type of stressor is present. Once the stressor is perceived, as a part of transduction into signal, early immune events are activated and via fine-tuned hormonal signaling the information is transmitted to neighboring and distant organs and the appropriate responses are activated (Oelmüller 2021).

In order to improve their defensive capacity, plants also developed an adaptive strategy – the phenomenon of induced systemic resistance (ISR) (Conrath *et al*., 2006). This work refers to ISR as a phenomenon triggered by PBB and their elicitors (referred to as ISR elicitors).

2. Structural properties of the plant plasma membrane: the main site for perception of the stimuli and transduction into signals

PPM is the key site for signal perception and transduction, the two components necessary for cell survival and proper functioning. It is therefore essential that the PPM is stable, but also fluid and adaptable in order to address the challenges of a constantly fluctuating environment. This complex system is mainly composed of lipids and proteins, where a molar ratio of 50–100 molecules of lipid for 1 protein could be expected (Cassim *et al*., 2019).

The main role of the lipids constituting the two-leaflet PPM is maintaining the structural balance of cells. The three main classes of plant membrane lipids are sphingolipids, phospholipids, and sterols, where the distribution of these lipids within the layers is laterally and transversally uneven (**Figure 1**).

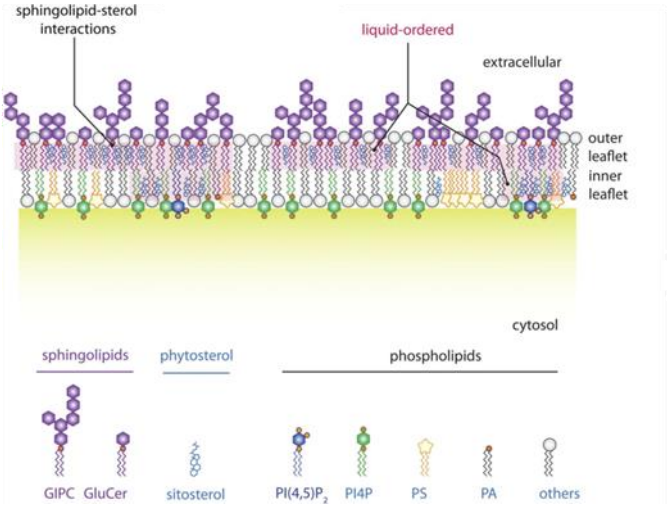

Figure 1 - Organization of the different classes of lipids in the PPM. Adapted from Jaillais and Ott, 2020.

Lipids dominating cytosolic, inner leaflet are phospholipids, whereas sphingolipids are mainly located on the outer leaflet, where they assemble with sterols thus forming microdomains (Cacas *et al*., 2016; Rondeli *et al*., 2021; Yu and Klaud, 2021). Complex sphingolipids glucosylceramides (GluCer) and glycosyl inositol phosphorylceramides (GIPC) constitute more than 40% of PPM lipids and are key components required for membrane integrity and functionality.

Being part of such a complex interface, proteins, like PPM lipids, also exemplify compartmentalization at the planar and transversal level where the lipid bilayer is used as a docking platform. At the planar level, protein clustering can occur with other proteins but also with the aforementioned lipid microdomains.

Besides being located, some proteins, such as protein receptors involved in the activation of plant immunity, are able to move laterally and colocalize in membrane domains in order to realize their activity or even be disactivated (Jarsch *et al*., 2014; Hao *et al*., 2014; Bücherl *et al*., 2017).

These microenvironments of specific proteins alone or segregated with lipids serve as functional hubs by playing the crucial role in cell surface signaling, modulating signal perception, and even activation of immune responses (Huby *et al*., 2020; Jaillais and Ott, 2020). As some of the latest research indicated, lipid/protein coalescences are not random but assumed by the specific interaction between the two (Legrand *et al*., 2019; Noack *et al*., 2021).

Transversally PPM located proteins can be transmembrane (integral proteins), such as ion channels, or membrane-associated (peripheral proteins), such as signal receptors. Most commonly, transmembrane proteins are static, whereas signal receptor proteins diffuse laterally allowing plants successful perception of extracellular signals (Jong and Munnnik, 2021).

3. Events underpinning immune responses to phytopathogens

The first step in eliciting immunity is always the recognition of elicitors via dedicated receptors which leads to the activation of early immune events, such as the production of reactive oxygen / nitrogen species, calcium influx, and ion fluxes resulting in medium alkalinization or change in media conductivity (**Figure 2**). Plant cells decipher this message by integrating the information from all the early immune events which results in activation of complex signaling and consequently plant defense responses (DeFalco and Zipfel, 2021).

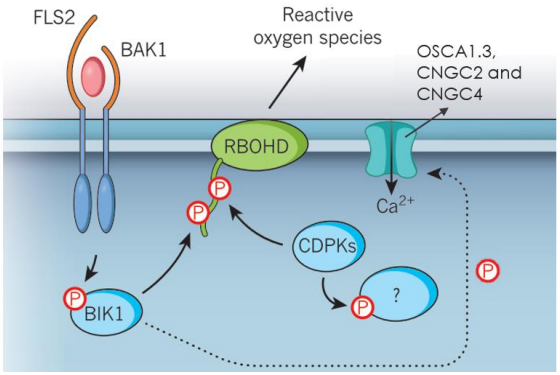

Figure 2 - Schematic representation of perception and induction of early immune events by flagellin 22 , a known elicitor described in plant pathogens interactions (Adapted from Zipfel and Oldroyd, 2017; Tian *et al*., 2019; Thor *et al*., 2020) FLS2 (FLAGELLIN-SENSING 2) a receptor recognizing bacterial flagellin protein flagellin 22; BAK1 (BRI1-Associated receptor Kinase) a FLS2 coreceptor; BIK1 (BOTRYTIS-INDUCED KINASE1) a receptor-like cytoplasmic kinase; RBOHD a NADPH oxidase; CDPK (Ca^{2+}-dependent protein kinases); OSCA1.3, CNGC2, CNGC4 Ca^{2+} channels, P phosphorylation.

3.1. *Perception of microbial immunity elicitors by the plant cells*

Plants are lacking specialized immune cells and the circulatory system like vertebrates, so they developed an extraordinary system in which each cell is

capable of perceiving immune elicitors and initiating the plant response (Spoel and Dong, 2012).

To successfully detect microbials, plants employ plethora of PPM embedded Pattern-Recognition Receptors (PRR). Being in a constant vicinity of potentially harmful microorganisms, plants rely on efficient PRRs and thus they are able to detect immune elicitors at nM concentrations and activate pattern-triggered immunity (PTI) (Han, 2019). Most commonly, PTI elicitors are classified as pathogen/microbe - associated molecular patterns (PAMPs/MAMPs, respectively), or as damage-associated molecular patterns (DAMPs) (Schellenberger *et al*., 2019). The best-known bacterial molecules, whose recognition by the immune system is mostly conserved in the plant kingdom, are flagellin, elongation factor Tu, lipopolysaccharides, and peptidoglycans (Zipfel and Oldroyd, 2017). In most instances, once the receptor/coreceptor complex recognizes an elicitor, it phosphorylates BIK1, or its homologue (PBS1-like) PBL1 (Wan *et al*., 2019), serving as a link between perception and early immune events activation (Oelmüller, 2021). To bypass the first line of PAMPs/MAMPs induced immune response, adapted pathogens use protein effectors injected into host cells to dampen PTI. In turn, plants have evolved intracellular nucleotide-binding leucine-rich repeat (NLR) receptors, that interfere with these effectors leading to the effector-triggered type of immunity (ETI) (Kanyuka and Rudd, 2019; Schellenberger *et al*., 2019). In both cases, when the elicitor is bound by the receptor, local early immune events are initiated as a first step following perception (Han, 2019).

3.2. *Early immune events triggered by elicitors*

Being involved in both abiotic and biotic stress signaling, plants use early immune events in a particularly balanced manner in order to activate specific, trigger-dependent immune responses. The most important events occurring during this phase are activation of secondary messengers, *i.e.*, production of reactive oxygen and nitrogen species, elevation of cytosolic Ca^{2+}, and medium alkalinization (Marcec *et al*., 2019).

3.2.1. *Reactive oxygen species*

Production of reactive oxygen species (ROS) is one of the earliest measurable plant defense responses, also playing an important role in the plant metabolism, growth, development, and autophagy (Turkan 2018; Li *et al*., 2020).

ROS is a collective term used for a group of high chemical reactivity molecules, such as OH^{-}, O_2, O^{2-}, and H_2O_2 (Janků *et al*., 2019). According to their synthesis site, ROS can be characterized as apoplastic ($[ROS]_{apo}$) (produced by cell wall peroxisomes, amine oxidase, oxalate oxidase, plasma membrane associated NADPH oxidase (Rboh)) and intracellular ($[ROS]_{intra}$) (mitochondria, chloroplast, peroxisomes, plasma membrane associated quinone oxidase) (Farnese *et al*., 2016). Among these, MAMPs perception is often triggering ROS production through the RBOH family of NADPH oxidase, resulting in a PTI-specific strong and rapid burst of $[ROS]_{apo}$ (Kadota *et al*., 2014; Lee *et al*., 2020).

Changed redox state caused by "signaling active" levels of ROS, is brought back to normal by antioxidants, thus creating a specific ROS signature (Noctor *et al*., 2018). Antioxidants can be categorized as enzymes and non-enzymatic low mass molecules (Kapoor, *et al*., 2019; Soares, *et al*., 2019). The apoplast is characterized by a low content of non-enzymatic antioxidants, which allows enhanced apoplastic oxidation state, implying a possible difference in signal translation of apoplastic and intracellular ROS (Janků *et al*., 2019). Besides antioxidants, additional factors shaping ROS signature are PPM aquaporins conducting ROS across the membrane. During activation of PTI, lack of ROS transfer from apoplast to cytosol restricts activation of defense responses, therefore demonstrating the important role it plays in plant immunity (Marcec *et al*., 2019).

All considered, plant immune responses induced by ROS are strongly influenced by species synthesized, the site of production, rapidity of synthesis and antioxidation, and transport across the membrane (Møller and Sweetlove, 2010; Noctor *et al*., 2018; Janků *et al*., 2019).

3.2.2. *Reactive nitrogen species*

Besides ROS, the production of reactive nitrogen species (RNS) is considered as an early immune response, without which resistance to pathogens is significantly reduced (Xu *et al*., 2013). Their actions influence immunity through MAPK activation, cell wall lignification, and immune stomatal closure (Kapoor *et al*., 2019; Lawrence *et al*., 2020).

RNS is as well a collective term under which nitric oxide (NO^-), peroxynitrite ($ONOO^-$), the NO_x compounds (NO_2, N_2O_3, and N_2O_4), and nitrous acid (HNO_2) are considered. The rest of the section focuses on NO^-, being the most studied one (Romero-Puertas and Sandalio, 2016; Tomar *et al*., 2021).

Possible routes for NO^- generation in plants are oxidative and reductive. Even though oxidative mechanism utilizing NO synthase (NOS) characteristic for animal cells, was demonstrated to be active in plants, the genes encoding related enzymes have not been identified thus far. The reductive route is also very active in plants, generating NO^- intracellularly and extracellularly. Intracellularly, NO^- can be synthesized in the cytosol by nitrate reductase [NADH] 1 (NIA1) and NIA2, and, though rarely, in the mitochondrial inner membrane probably via cytochrome c oxidase and/or reductase. On the other hand, extracellular NO^- is produced by membrane bound NiNOR which activity is suspected to be limited to the roots, and by the cell wall peroxisomal enzyme xanthine oxidoreductase, activated only in anaerobic conditions (Yu *et al*., 2014). Activation of the production site depends on the type of the elicitor. For instance, NO^- production triggered by pathogen *Pseudomonas syringae* pv. *maculicola* occurs via NIA1 NIA2 involved in the reduction pathway, whereas lipopolysaccharides trigger NOS-dependent synthesis (Zeidler *et al*., 2004; Mur *et al*., 2006).

The main way for NO^- to act is by post-translationally modifying proteins, thus changing their functionality and activity (Romero-Puertas and Sandalio, 2016). In this manner, target proteins are most commonly reversibly changed through S-nitrosylation, which impacts their conformation, activity, and/or localization, a process highly ubiquitous in the different kingdoms of life (Astier *et al*., 2018; Pande *et al*., 2021). S-nitrosylation is considered as an important event in plant immunity since it regulates cell death during the

hypersensitive response, facilitates NPR1 oligomerization thus its activation, and regulates ROS production. It is also suspected that S-nitrosothiols (S-nitrosylated proteins) have signaling role in systemic immune responses (Tada *et al*., 2008; Yun *et al*., 2011; Jedelská *et al*., 2021). Additionally, it has been shown that NO^- can interfere with hormonal signaling by influencing plant hormone levels (e.g., biosynthetic, degradation, and conjugation enzymes), their distribution (e.g., transport proteins) or signaling (e.g., receptors and signal transduction proteins), which emphasizes its role in plant immunity (Freschi, 2013).

Although the specificity of protein/NO^- interaction is not completely understood, it is postulated that the structure of the target and the local NO^- concentration are the main factors influencing this process (Feng *et al*., 2019; Cui *et al*., 2021).

3.2.3. *Cytosolic calcium increase*

Alongside ROS, increase in cytosolic Ca^{2+} ($[Ca^{2+}]_{cyt}$) is considered as the most important ubiquitous early immune event. Most of the plant Ca^{2+} channels are non-selective since they can conduct other cations, both mono- and divalent ones. Signaling $[Ca^{2+}]_{cyt}$ influx is most commonly activated by glutamate, glycine, ROS, ATP, and ADP (Demidchik *et al*., 2018).

Best described ion channel families for Ca^{2+} transport in cytosol are cyclic nucleotide-gated channels (CNGCs), ionotropic glutamate receptors (GLRs), two-pore channel 1 (TPC1), annexins, mechano-sensitive channels of small conductance-like (MSLs), Mid1-complementing activity channels (MCA), Piezo, and reduced hyperosmolarity-induced $[Ca^{2+}]_{cyt}$ increase channels (OSCAs) (Demidchik *et al*., 2018; Kong *et al*., 2020). Which of these channels will conduct the Ca^{2+} signaling influx depends on the origin of the trigger, however the data clearly showing the links elicitor/channel is scarce. For instance, when stimulated by well-known PAMP flg22, the Ca^{2+} influx is conducted through CNGCs and OSCA1.3 phosphorylated by BOTRYTIS-INDUCED KINASE1 (BIK1) which is activated by receptor/coreceptor complex (Tian *et al*., 2019; Thor *et al*., 2020). On the other hand, abiotic stresses, such as mechanical and osmotic, induce calcium influx through

families of channels MCAs and MSLs, collectively known as mechanosensitive ion channels (MSCs) (Basu and Haswell, 2017).

In order to restore normal Ca^{2+} levels and avoid Ca^{2+} toxicity upon calcium influx, efflux mechanisms are activated operating mainly through Ca^{2+}-ATPases and Ca^{2+} exchangers (Bose *et al*., 2011). The combination of magnitude, frequency, and shape of the stress signaling induced $[Ca^{2+}]_{cyt}$ elevations is creating a specific Ca^{2+} "signature" which depends on the nature, strength, and duration of the stimulus (Bose *et al*., 2011; Aldon *et al*., 2018). Specific calcium "signature" is deciphered by sensor binding proteins.

Plants are equipped with three primary families of calcium sensors, namely CaM (calmodulin), CBL (calcineurin B-like), and CDPKs (calcium-dependent protein kinases). While CaM and CBLs lack intrinsic enzymatic functions and rely on conveying calcium-induced structural alterations to target proteins, CDPKs, which are unique to plants and certain protists, exhibit both calcium-sensing and protein-kinase activities within a single polypeptide. Consequently, CDPKs are hypothesized to undergo direct activation through calcium binding, modulating target proteins via phosphorylation, albeit with varying affinities. Namely, calcium binding proteins exhibit diverse affinities for calcium ions, levels of expression, subcellular localization, and assembly in microdomains (Bose *et al*., 2011; Boudsocq *et al*., 2012; Demidchik and Shabala, 2018).

3.2.4. *Mitogen-activated protein kinase*

Mitogen-activated protein kinase (MAPK) cascades serve as highly conserved signaling pathways converting external stimuli into intracellular responses across various eukaryotic organisms. In the context of plants, these MAPK cascades play a significant role in orchestrating defense responses against pathogen attacks. Numerous PRRs have been demonstrated to initiate MAPK signaling upon detection of PAMPs (Meng and Zhang, 2013). A prototypical MAPK cascade typically comprises a minimum of three sequentially acting kinases: a MAP kinase kinase kinase (MAPKKK), a MAP kinase kinase (MAPKK), and ultimately, the MAP kinase (MAPK) itself (**Figure 3**). Phosphorylation plays a pivotal role in advancing the signal through the MAP kinase cascade, where, upon activation, MAPKs proceed to

phosphorylate various protein targets. These targets encompass a broad range of proteins, including other kinases, enzymes, cytoskeletal proteins, and transcription factors, within all eukaryotic cells (Jagodzik *et al*., 2018; Krysan and Colcombet, 2018; Zhang and Zhang, 2022).

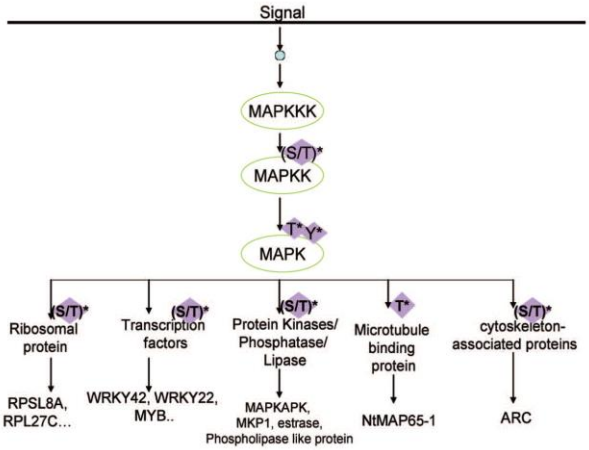

Figure 3 – Schematic representation of mitogen-activated protein kinase phosphorylation cascade (Taj *et al*., 2010).

3.2.5. *Medium alkalinization*

Even though not so commonly mentioned as $[Ca^{2+}]_{cyt}$ and ROS, medium alkalinization does play an important role in plant defense-associated early responses to various PAMPs (Boller, 1995, Falhof *et al*., 2016). It develops due to the activation of H^+-ATPases located on the plasma membrane, which at the expense of ATP transports H^+ from outside inside the cell. When H^+ influx occurs, newly established electrochemical gradient across the membrane triggers activation of numerous secondary transporters and channels, thus enabling normal cell functioning (Wang *et al*., 2014). Coordination between H^+-ATPase and transporters/channels can be established by ionic conditions in the cytosol (calcium ions and nitrate), cytosolic pH, nucleotides, malate, kinases and phosphatases, redox conditions, and membrane potential (Cosse and Seidel, 2021).

3.2.6. *Achieving signal specificity: secondary messengers' interplay*

Since using the same secondary messengers for underpinning a myriad of cellular processes, the manner in which plants are translating these signals into a final stressor-dependent specialized response is intriguing and still unknown. The current theory is that plant responses are determined by specific secondary messengers' signatures, which have been shown to be unique to particular environmental cues, and by a fine balance among these. This fine balance creates a "lock and key" mechanism, and it is often established by the mutual interplay amongst the early immune events (Marcec *et al*., 2019).

The best known example of interaction between early immune events is the Ca^{2+}/ROS hub. Namely, depending on the elicitor inducing the immune responses, Ca^{2+} and ROS appear to orchestrate the signature network, by activating, up- or down-regulating each other (Marcec *et al*., 2019). Additionally, in some cases such as flg22 triggered early immune responses, ROS production by RBOHD and $[Ca^{2+}]_{cyt}$ increase are two independent processes (Kadota *et al*., 2014). The participants in such an interplay may be different, thus NO^- and Ca^{2+} can also be involved in interaction. However, it has been shown that the influence of NO^- on $[Ca^{2+}]_{cyt}$ influx is restricted to specific cellular compartments, thus adding a layer of complexity on the interplay (Ali *et al*., 2007; Astier *et al*., 2011). Although not directly, RNS can also regulate ROS homeostasis in plants through S-nitrosylation (Wang and Chu, 2020).

Plants demonstrate deep complexity regarding secondary messengers' interplay, however its physiological function is yet to be deciphered. To reveal how a fine balance and interaction between messengers is influencing plant responses, a better comprehension of the production sites, specific signatures, and mechanisms for expressing activity of these cues is needed.

3.3. *Hormonal signaling in plant immunity*

Besides having a key role in growth, development, and reproduction, plant hormones also significantly participate in the onset of plant immunity. This complex signaling network influences immune responses by integrating information about the phytohormonal blend in the plant, relative concentration of each hormone, timing and sequence of initiation of each of these molecules, and their cross talk (Pieterse *et al*., 2012; Gimenez-Ibanez and Solano, 2013).

Molecules considered as immunity signaling hormones activated during pathogen attack are salicylic acid (SA), jasmonic acid (JA) with its derivatives (**Figure 4**), ethylene (ET), abscisic acid, gibberellins, auxins, cytokinins, and brassinosteroids. Among these, the role of phytohormones SA, JA, and ET has been most thoroughly described in pathogen triggered immunity. In *Arabidopsis*, even though there are exceptions, these signaling pathways are often correlated with the pathogen's lifestyle, biotrophs and hemi-biotrophs being fended off through SA signaling pathway, and necrotrophs by JA acting in alliance with ET. This is however an oversimplistic view since other hormones are also synergistically or antagonistically involved in signaling (Berens *et al*., 2017; Vlot *et al*., 2021).

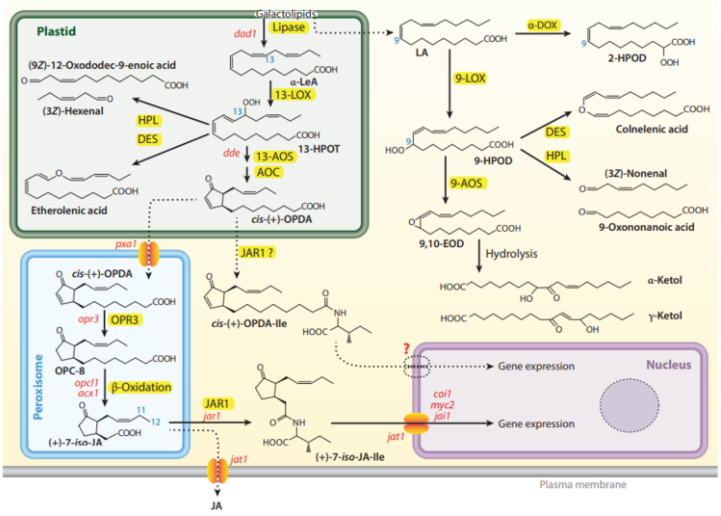

Figure 4 - Synthesis pathway of JA and oxylipins involved in plant defenses (Adapted from Wasternack and Feussner, 2018).

3.4. *Plant defense responses*

Upon recognition of immunity elicitors and following signaling, plants reallocate their resources from growth and reproduction to resistance achieved in three steps.

Firstly, plants activate production of cellulose, hemicellulose, pectin, and lignin to reinforce the cell wall. This physically restraints pathogens ingress and it is also considered as the most universal defense response (Wan *et al*., 2021). On the other hand, plants also activate synthesis of antimicrobial enzymes, proteins, or metabolites (also known as phytoalexins) involved in direct fight against attacker (Vos et al., 2013; Jeandet et al., 2014). Phytoalexins are compounds that can be categorized in two groups: nitrogen-containing molecules (alkaloids) and nitrogen-deficient molecules (terpenoids and phenolics) (Jeandet *et al*., 2014). Some of the commonly used markers of phytoalexins synthesis are lipoxygenase and phenylpropanoid pathway activation.

Lipoxygenase (LOX) pathway is involved in plant immunity in two ways, one being synthesis pathway of phytohormones jasmonates (Chapter 1 – section 3.3) and the second one being the pathway for production of oxylipins acting as antimicrobials (Thakur and Udayashankar, 2019; Deboever *et al*., 2020). Similarly, phenylpropanoid (PAL) pathway is involved in SA synthesis, but as well in the production of lignin and wide range of phenolic compounds directly acting against pathogens (Kim and Hwang, 2014).

Among the high diversity of so far identified phytoalexins, the crucial plant defense metabolite for *Arabidopsis*, the model plant used in this study, is an alkaloid phytoalexin called camalexin (Frerigmann *et al*., 2015). The first step in the biosynthesis of this molecule is the production of indole-3-acetaldoxime from tryptophan, which is further followed by several steps catalyzed by a set of enzymes finally resulting in the production of camalexin (**Figure 5**). Biosynthesis of this compound is also linked to tryptophan derived indolic glucosinolates production contributing to plant immunity by improving callose deposition. Depending on the pathogen challenge, activation of camalexin production can be triggered by different phytohormones SA, JA, or ET (Nguyen *et al*., 2022a). So far, camalexin has been described as an important

player in *Arabidopsis* resistance against some of the most important pathogens such as *Botrytis cinerea* and *Pseudomonas syringae* (Nguyen *et al*., 2022b).

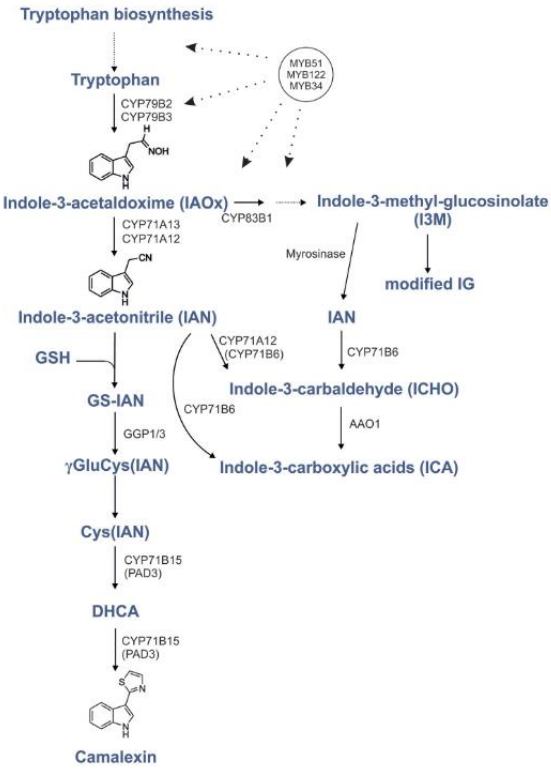

Figure 5 - Schematic representation of enzymes catalyzing reactions, intermediate products of camalexin biosynthesis pathway. Scheme also represents a possible link between camalexin synthesis and indolic glucosinolates (IG) production (Frerigmann *et al*., 2015).

Eventually, plants produce pathogenesis-related (PR) proteins that lower the pathogen occurrence or delay the disease spreading in plant organs that have not yet been infected. PR proteins achieve this through their dual function in cell wall lignification and synthesis of antimicrobial compounds and enzymes (such as chitinases and glucanases), thus playing a critical role in the plant immune response against a variety of pathogens (Ali *et al*., 2018).

4. *Plant immune responses triggered by beneficial bacteria*

One of the most commonly used tactics of PBB to protect plants from unfavorable cues is activation of ISR. Amongst vast number of beneficials reported to induce resistance in plants, elicitors have only been identified for a small fraction. Moreover, despite efforts, relatively little is known about the mechanisms underpinning ISR from elicitor perception to the elevated resistance upon pathogen attack (Stringlis *et al*., 2018; Shrestha *et al*., 2022; Yang *et al*., 2023; Pierre *et al*., 2023). In the subsequent sections, the chemical diversity and activity of ISR elicitors produced by PBB are highlighted, with their activity being influenced by both their structure and dosage. The emphasis is placed on compounds that have been rigorously tested in their pure form, at biologically relevant concentrations, and/or via specifically suppressed bacterial mutants. The studies cited are those in which the ability to induce systemic resistance was clearly shown to be independent from any direct antimicrobial effects of elicitors. Another factor considered was that the application of these elicitors was to a plant organ other than the one of pathogen infection.

4.1. *Elicitors of ISR produced by PBB*

Even though some proteins produced by *Brevibacillus laterosporus*, *B. amyloliquefaciens*, and *Saccharothrix yanglingensis* have also been proposed as PBB determinants responsible for ISR elicitation, in majority of cases these compounds have been reported to be small-size molecules (Wang *et al*., 2015, 2016; Zhang *et al*., 2018). Generally, PBB secondary metabolites identified as ISR elicitors can be divided in following groups: volatile organic compounds, Acyl-Homoserine Lactones, rhamnolipids, N-Alkylated Benzylamine Derivative, siderophores, compounds with antibiotic function, and the CLPs - the most studied ones (Pršić and Ongena, 2020).

4.1.1. *Volatile organic compounds*

Most of the well-characterized PGPR elicitors are soluble compounds, but some volatile organic compounds (VOCs) were as well-reported to induce systemic resistance in the host plant, showing that these metabolites can also act as infochemicals involved in inter-kingdom communication (Kai *et al*., 2016). The most studied VOC immunity elicitor is 2,3-butanediol (2,3-BD; **Figure 6-1**) produced from glucose in the central metabolism (Yang *et al*., 2013). Its bioactivity was first assessed on *Arabidopsis* by application on roots, where *B. subtilis* GB03 induced resistance against *Erwinia carotovora* subsp. *carotovora*, while mutants deprived in 2,3-BD or its precursor acetoin production were inactive (Ryu *et al*., 2004). Bioactivity, when treated on roots in relatively high mM concentrations, was demonstrated as well in the pathosystems maize/*Setosphaeria turcica*, tobacco/*Erwinia carotovora*, and in pepper against multiple viruses, where the immunity eliciting ability was structure dependent. Namely, among the three forms, 2R,3R-BD (R), 2S,3S-BD (S) and 2R,3S-BD (meso), the S form is the least active (Han *et al*., 2006; D'Alessandro *et al*., 2014; Kong *et al*., 2018). However, on pepper against *Xanthomonas axonopodis* pv. *vesicatoria*, another VOC 3- pentanol (10 µM, 1 mM; **Figure 6-2**) showed higher activity than 2,3-BD (Choi *et al*., 2014). Beside 3-pentanol, long-chain VOCs tridecane and hexadecane (**Figures 6-3,4**, respectively) showed bioactivity as well at µM (100) concentration (Lee *et al*., 2012; Park *et al*., 2013).

4.1.2. *Acyl-homoserine lactones*

Many gram-negative bacteria produce N-acyl-homoserine lactones (AHLs) as quorum-sensing molecules involved in cell-to-cell communication in order to monitor their behavior according to population density. Some AHLs are not only the mean of communication between bacterial cells, but also may be used as signal in inter-kingdom interaction and act as plant growth promoting compounds and/or as immunity elicitors (reviewed in Schikora *et al*., 2016). Firstly, it was showed by using an AHL-suppressed mutant of *Serratia liquefaciens* MG1, that induced resistance in tomato toward *Alternaria alternata* by this strain is AHL-dependent (Schuhegger *et al*., 2006). Several works performed with purified molecules further revealed that AHL

bioactivity is structure dependent. AHLs with short length acyl chains (C4, C6, C8) have been mostly demonstrated to promote plant growth, whereas AHLs with longer fatty acid (C12, C14) are better described as elicitors of resistance (Schenk *et al*., 2012; Zarkani *et al*., 2013; Schikora *et al*., 2016). The long-chain N-3-oxo-tetradecanoyl-L-homoserine lactone (oxo-C14-HSL; **Figure 6-5**) has been amply demonstrated for immunity elicitation in many pathosystems. Upon treatment at 6 µM, oxo-C14-HSL successfully induced systemic resistance against biotrophs (*Blumeria graminis* f. sp. *hordei*, *Puccinia hordei*, *Golovinomyces orontii*) and hemibiotroph (*P. syringae* DC3000) in barley and Arabidopsis, but not against the necrotrophs *Botrytis cinerea* and *Plectosphaerella cucumerina* BMM (Schikora *et al*., 2011; Schenk *et al*., 2012; Wehner *et al*., 2019). ISR-eliciting activity of oxo-C14-HSL was also observed in wheat and tomato against *Puccinia graminis* f. sp. *tritici* and *Phytophthora infestans*, respectively (Hernández-Reyes *et al*., 2014). Collectively, these data indicate that the plant defensive response triggered by the same oxo-C14-HSL molecule may not be efficient in enhancing resistance against phytopathogens with necrotrophic lifestyle.

4.1.3. *Rhamnolipids*

Rhamnolipids (RLs) are amphiphilic glycolipids produced by various species including pathogenic isolates, but also some plant beneficial *Pseudomonas* and *Burkholderia* species (Perneel *et al*., 2008; Abdel-Mawgoud *et al*., 2010). They are essential for bacterial surface motility and biofilm development (Vatsa *et al*., 2010; Chrzanowski *et al*., 2012). Mono- and di-RLs (**Figure 6-6**) tested as pure compounds have been shown to elicit plant defense responses and to induce resistance against various pathogens in grapevine, *Arabidopsis*, and *Brassica napus* using a wide range of concentrations from approximately 10 up to 300 µM (Varnier *et al*., 2009; Sanchez *et al*., 2012; Monnier *et al*., 2019, 2020). When tested for activation of plant immunity markers, RLs also show a structure dependent activity, with C12 being the most active variant in the C4-C18 range (Platel *et al*., 2018).

4.1.4. *N-Alkylated benzylamine derivative*

Although its function for bacterial life is not clear, an N-alkylated benzylamine derivative (NABD; **Figure 6-7**) produced by *P. putida* BTP1, was identified as immunity elicitor (Ongena *et al*., 2005). Treatment of bean and cucumber roots with pure NABD at low micromolar concentration elicited similar protective effect compared to living cells. On the other hand, in tomato, the pure elicitor induced a lower protective effect than observed with the producing strain, suggesting the synthesis of an additional ISR determinant in that case (Ongena *et al*., 2008).

4.1.5. *Siderophores*

To ensure their growth in iron-limited environments, microorganisms have evolved powerful Fe^{3+}-acquisition systems based on the secretion of high-affinity iron-chelating molecules termed siderophores. PGPR siderophores are also known to antagonize pathogen populations by decreasing iron amounts in soil, resulting in competition for this essential element (Kramer *et al*., 2020). However, some siderophores also act as plant immunity elicitors and pyoverdines (also referred to as pseudobactines; **Figure 6-8**) produced by various fluorescent pseudomonads were, in the 90's, among the first PBB metabolites proposed as ISR elicitors. Their key role in systemic resistance induction was notably shown for *P. fluorescens* CHA0 on tobacco infected by Tobacco necrosis virus, and in the protection provided by *P. fluorescens* WCS374 to radish against *Fusarium wilt* (Maurhofer *et al*., 1994; Leeman *et al*., 1996). These chromopeptides were further described as inducers of resistance in various plant species such as bean, tomato, Arabidopsis, tobacco, eucalyptus, and rice against a range of microbial pathogens (Meziane *et al*., 2005; Ran *et al*., 2005; De Vleesschauwer *et al*., 2008). In addition to pyoverdine, *P. aeruginosa* 7NSK2 also forms the chelating agent pyochelin (**Figure 6-9**) and its precursor salicylic acid (SA). When tested on pathosystem grapevine/*B. cinerea*, SA produced by *P. aeruginosa* 7NSK2 was crucial for mounting the plant immunity (De Meyer *et al*., 1999; Verhagen *et al*., 2010). However, for ISR stimulated in tomato by the same strain, an important role for SA could not be excluded, but probably combined with the action of other

metabolites including pyochelin which may somehow also retain some eliciting activity (Audenaert *et al*., 2002).

4.1.6. *Elicitors with antibiotic function*

To ensure fitness in the competitive rhizosphere niche, PBB produce a wide range of secondary metabolites best identified for their antimicrobial function such as non-ribosomal peptides, polyketides, bacteriocins, terpenes, phenazines, quinolones, or rhamnolipids (Raaijmakers and Mazzola, 2012; Zhao and Kuipers, 2016; Tracanna *et al*., 2017). Interestingly, some of these antibiotics were also shown to act as signal for ISR stimulation at similar concentrations, making them promising tools for biocontrol with dual action on pathogen populations (Sayyed 2019). One such antibiotic 2,4-diacetyl phloroglucinol (**Figure 6-10**), formed by *P. fluorescens*, is triggering resistance in *Arabidopsis* against various pathogens, such as *Peronospora parasitica*, *P. syringae* pv. *tomato*, and *B. cinerea*, upon application at relatively high 10–100 µM concentrations (Iavicoli *et al*., 2003; Weller *et al*., 2012; Chae *et al*., 2020). Besides other *Pseudomonas* antibiotics, phenazine type molecules were also reported to induce resistance. Notably phenazine- 1-carboxamide (**Figure 6-11**) in rice toward *M. oryzae* at 0.1–1 µM, in bean toward *R. solani*, and pyocyanin produced by *P. aeruginosa* 7NSK2 in the pathosystem tomato/*B. cinerea* (Audenaert *et al*., 2002; D'aes *et al*., 2011; Ma *et al*., 2016).

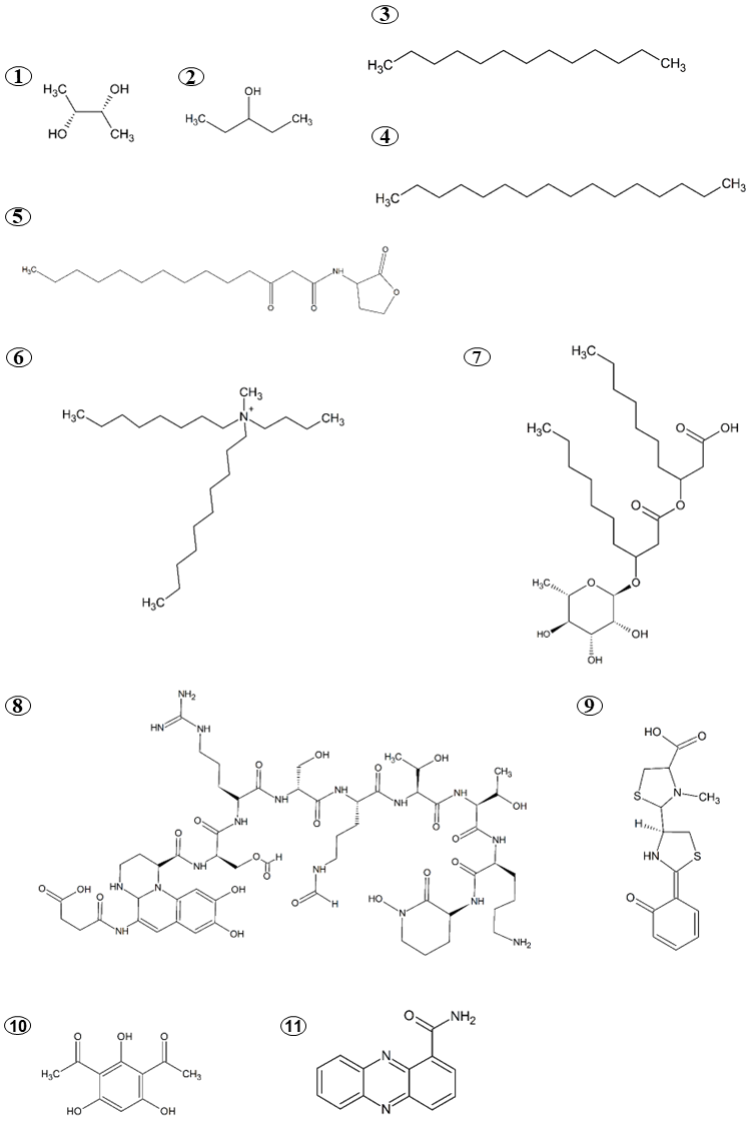

Figure 6 - Chemical structures of PBB produced ISR elicitors. (1) 2,3-butanediol; (2) 3-pentanol; (3) Tridecane; (4) Hexadecane (5) N-3-oxo-tetradecanoyl-L-homoserine lactone; (6) N,N-dimethyl-N- tetradecyl-N-benzylammonium; (7) Rhamnolipid, L-rhamnosyl-3-hydroxydecanoyl-3-hydroxydecanoic acid; (8) Pyoverdine; (9) Pyochelin; (10) 2,4-diacetyl phloroglucinol; (11) phenazine-1-carboxamide.

4.1.7. *Cyclic lipopeptides*

CLPs are multifunctional molecules produced by fungi *Aspergillus*, and various bacterial genera such as *Streptomyces, Pseudomonas* and *Bacillus*. These amphiphilic molecules are consisted of an oligopeptide lactone ring linked to a fatty acid tail (Raaijmakers *et al*., 2010). Due to production of a wide spectra of bioactive CLPs, potentially used in agricultural, chemical, food, and pharmaceutical industries, special interest is invested in studying CLPs produced by pseudomonads and bacilli (Roongsawang *et al*., 2011). CLPs have high structural diversity, thus they are categorized in families. CLPs produced by bacilli are divided in three families: surfactin, fengycin, and iturin. Compared to bacilli, beneficial pseudomonad species produce CLPs of much higher diversity, with so far 100 described structures divided in 14 families (viscosin, orfamide, amphisin, syringomycin, syringopeptin, tolaasin, bananamides, xantholysins, putisolvins, pseudofactins, syringopeptins, corpeptin, fuscopeptins) (Geudens and Martins, 2018). Variations in type and number of amino acids, their configuration in the peptide moiety, and in the length of the fatty acid tail consequently affect their biological activity (Raaijmakers *et al*., 2006). Thus, they can be possibly involved in biofilm formation, motility, colonisation, antimicrobial activity, and plant immunity elicitation (Ongena and Jacques, 2008).

In most instances CLPs shown to trigger ISR are produced by two bacterial genera *Pseudomonas* spp. and *Bacillus* spp. Being reported in high diversity of phytopathosystems, the most studied CLP as an ISR elicitor is surfactin (Srf; **Figure 7**) produced by bacilli. When applied on roots, this CLP demonstrates bioactivity in phytopathosystems, such as bean, tomato, tobacco/*B. cinerea*, melon/*Podosphaera fusca*, peanut/*Sclerotium rolfsii*, and *Arabidopsis*/*Pseudomonas syringae pv. maculicola* (Ongena *et al*., 2007; García- Gutiérrez *et al*., 2013; Cawoy *et al*., 2014; Rodríguez *et al*., 2018; Hoff *et al*., 2021; Altrão *et al*., 2022). However, on dicot leaves or monocot roots concentrations of Srf needed to mount the defense responses are much higher, indicating that there are certain limitations regarding the systems where it performs efficiently (Rahman *et al*., 2015; Yamamoto *et al*., 2015; Mejri *et al*., 2018). Besides Srf, bacilli also produce iturin and fengycin (**Figure 7)** which have also been reported to induce ISR. Via this mechanism, when applied together on rice roots these two CLPs cause *P. oryzae* disease reduction, which

can be further enhanced by their direct antimicrobial effect when applied at the site of pathogen infection (Lam *et al*., 2021). In addition, fengycin primes tomato plants against *B. cinerea* and grapevine against *Plasmopara viticola* (Farzand *et al*., 2019; Li *et al*., 2019), whereas iturin has same effect on strawberry, cotton, grapevine, and *Arabidopsis* (Yamamoto *et al*., 2015; Farace *et al*., 2015; Han *et al*., 2015; Wu *et al*., 2018; Altrão *et al*., 2022). Mycosubtilin, part of iturin family, showed efficacy as priming agent and direct antimicrobial against *Zymoseptoria tritici* in wheat (Platel *et al*., 2023). Besides Srf, iturin also shows certain specificity regarding the plant species. Namely, on cotton roots its bioactivity has effect at 50 µM concentration, while on strawberry and chili pepper leaves, and *Arabidopsis* roots 1–10 µM suffice for a protective effect by triggered ISR (Han *et al*., 2015; Kawagoe *et al*., 2015; Park *et al*., 2016; Altrão *et al*., 2022).

On the pseudomonad CLPs side, bioactivity in both monocots and dicots was reported. Research on pseudomonads CLPs triggering ISR showed that the ISR is specific regarding the pathogen. More specifically, in rice/*M. oryzae* phytopathosystem CLPs such as WLIP (**Figure 7)**, lokisin, and entolysin, induce resistance and significantly reduce disease symptoms. Nevertheless, orfamide, an ISR elicitor in rice against *Cochliobolus miyabeanus*, loses the eliciting effect in the aforementioned plant pathosystem, highlighting the CLP/pathosystem specificity (Ma *et al*., 2017; Omoboye *et al*., 2019).

On dicot plants, massetolide A, orfamide (**Figure 7)**, and sessilin were reported as ISR elicitors (Tran *et al*., 2007; Olorunleke *et al*., 2015; Ma *et al*., 2016). Interestingly, elicitation of ISR by orfamide and sessilin is exhibited only in the precise concentration range, 0.001-0.1 µM and 0.001-0.01 mg/L, respectively (Olorunleke *et al*., 2015; Ma *et al*., 2016).

Besides influencing the ecological role, the structure of CLPs also greatly influences their efficacy in triggering systemic resistance. For instance, on tobacco cells, linear and methylated derivatives of Srf are much less efficient in triggering early immune events indicating that the charge and cyclisation of the peptide moiety play an important role in the plant/Srf interaction. Moreover, activity is also assumed by the chain length since only homologs with long C14 and C15 acyl chains are active at inducing not only early immune-related events, but also ISR itself (Jourdan *et al*., 2009; Henry *et al*., 2011; Hoff *et al*., 2021). Additionally, cyclization and length of the b-hydroxy

fatty acid chain of CLPs can also influence the activation of defense genes (Kawagoe *et al*., 2015).

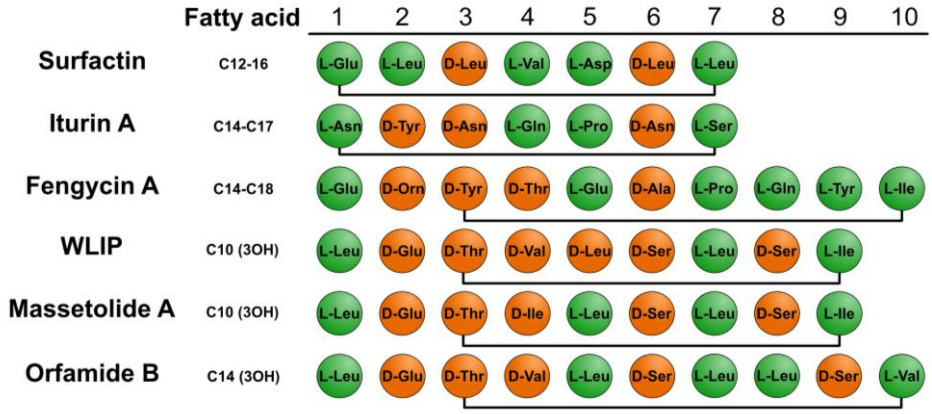

Figure 7 - Schematic representation of the structures of the CLPs described for ISR induction. Orange circles represent D-amino acids, green L-amino acids. The bar below the amino acids indicates amino acids included in the peptide cycle.

4.2. *Surfactin: an ISR elicitor showing a great potential*

Besides being plant immunity elicitors, the most active biosurfactant known today - Srf plays the main role in biofilm formation and motility improvement and acts as a shield of the bacteria synthetizing it (Götze and Stallforth, 2020; Andric *et al*., 2021). Among the three CLP families produced by plant associated beneficial bacilli, only Srf's synthesis gene is preserved in most of the species (Harwood *et al*., 2018; Théatre *et al*., 2021). In nature, it is produced as a mix of homologues with a fatty acid (FA) chain variating from 12 to 16 carbons and peptide moiety consisting of L-Glu1-L-Leu2-D-Leu3-L-Val4-L-Asp5-D-Leu6-L-Leu7 (Théatre *et al*., 2021b).

In general, bacilli and pseudomonads synthesize CLPs via non-ribosomal peptide synthetases (NRPSs), with one NRPS cluster can often produce various CLP variants. The structure of the peptide ring does not only depend on the genome of the species synthesizing it, but also on availability of amino acids being starting building material (Süssmuth and Mainz, 2017; Geudens and Martins, 2018). Among the surfactin family of cyclic lipopeptides (CLPs), Srf

is often referred to as the "canonical surfactin" and was the first CLP of the surfactin family to be described in the literature. In addition to Srf, *Bacillus* species produce Srf-like CLPs, with only two such CLPs commonly encountered in nature - lichenysin and pumilacidin (**Figure 8**). They are as well produced as a mix of homologues, where lichenysin has quite similar distribution of different length FA variants as Srf (12-16), while pumilacidin's range slightly differ (14-17). Additionally, the peptide moiety of both CLPs differs from Srf at two points, one being common for both, where in the position 7 Ile is positioned instead of Leu, and the second one in lichenysin being Gln1 instead of Glu1 and in pumilacidin Val4 substituted with Leu4 (Théatre *et al*., 2021).

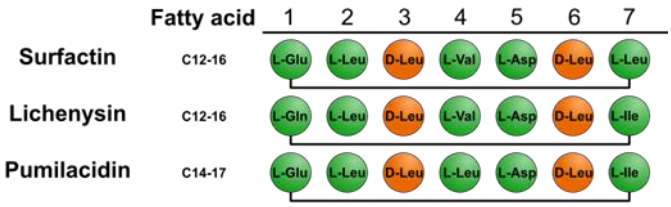

Figure 8 - Schematical representation of the structure of the CLPs belonging to Srf family. Orange circles represent D-amino acids, green L-amino acids. The bar below the amino acids indicates amino acids included in the peptide cycle.

With the positions 3, 5 and 6 being the same in all variants, further natural biodiversity can be increased in the positions 2, 4, and 7. As aforementioned, amino acids sequence of the peptide also depends on availability of amino acids, thus positions 2, 4, and 7 can possibly contain L-Leu, L-Val or L-Ile therefore creating new variants. In this manner, most commonly, together with Srf, bacilli are producing in very low amounts Srf with Val in position 7 (Théatre *et al*., 2021).

5. Points of convergence and distinctions between PTI and ISR

So far, ISR being not fully characterized, it is challenging to parallelly compare it with the PTI. However, even if limited, the data available for both of the phenomena already shows points of convergence and distinctions.

Namely, elicitors of immunity from both beneficials and pathogens share activation of ROS, RNS, Ca^{2+} influx, and alkalinization as early immune events, indicating that, as aforementioned, final immune responses highly depend on messengers' signatures and their interplay (Chapter 1 – section 3; De Vleesschauwer *et al*., 2006; Jourdan *et al*., 2009; Cawoy *et al*., 2014; Wang *et al*., 2014; Pande *et al*., 2021).

Moreover, once pathogen attacks, ISR does not induce ISR-specific plant defense mechanisms, but only reinforces plant immune responses triggered by pathogen infection, such as for example higher production of phytoalexin camalexin in primed plants. Thus, it remains unclear how plants selectively trigger phytoalexins production depending on the lifestyle of the colonizing microbe (beneficial or pathogenic) (Nguyen *et al*., 2022a,b).

On the other hand, more numerous points of contrasts between the two are exemplified through the amount and structure of elicitors triggering the response, hormonal signaling blend, promptness and robustness of the defense, and a consequent plant fitness cost.

Being in constant vicinity of potentially harmful microorganisms, plants depend on efficient recognition mechanisms and therefore pathogenic immunity elicitors are perceived by plant cells at nM concentrations. Intriguingly, plant's receptor equipment should enable detection of not only pathogenic, but MAMPs of rhizobial symbionts as well. Indeed, some findings show that MAMPs from PBB, such as flagellin and peptidoglycan, trigger ISR (Meziane *et al*., 2005; Ran *et al*., 2005; Liu *et al*., 2014; Rajamanickam and Nakkeeran, 2020). However new findings revealed that beneficial bacterial colonizers can silence immune responses induced by their MAMPs, thus

ensuring successful colonization (Boller and Felix, 2009; Stringlis *et al*., 2018).

On the other hand, PBB do produce specialized immunity elicitors though significantly different from PAMPs. Namely, even though receptors of PBB elicitors are not known, they mostly induce immune responses at µM, thus thousand times higher concentrations, when compared to PAMPs (Pršić and Ongena, 2020). Additionally, the size of the PBB ISR elicitors described in Chapter 1, significantly distinguishes them from PAMPs, since the majority is identified as small-size compounds and rarely proteins (Stringlis *et al*., 2018; Pršić and Ongena, 2020).

Although PTI and ISR show similarities in the phytohormones used, SAR and ISR additionally use for signaling azelaic acid (Aza). Aza is an oxylipin produced in plastid membranes by the hydrolysis of C18 fatty acids, such as oleic acid (18:1), linoleic acid (18:2), and linolenic acid (18:3) (Shine, *et al*., 2019). This hydrophobic oxylipin has been identified as a systemic signal that travels by vascular sap and enhances the systemicity of the immune responses, and thus it is required for SAR and ISR induction. Additionally, application of this molecule itself can induce SAR (Jung *et al*., 2009; Cecchini *et al*., 2015 Oelmüller, 2021).

In the last decade, production of coumarins, plant-derived secondary metabolites produced via the phenylpropanoid pathway, emerged as a specific pathway of PBB induced immunity (Stringlis *et al*., 2019). Namely, it was demonstrated that beneficial pseudomonads' volatiles trigger coumarin synthesis dependent ISR, whereas the two well-known PAMPs, flg22 and chitin, are not able to activate marker genes of this pathway *MYB72* and *BGLU42* (Zamioudis *et al*., 2015). Moreover, overexpression of the gene encoding the enzyme b-glucosidase BGLU42 involved in the production of coumarins, results in constitutive resistance against *Botrytis cinerea*, *Pseudomonas syringae* pv. *tomato* DC3000 and *Hyaloperonospora arabidopsidis* in *Arabidopsis* indicating that elicitors activating this pathway could possibly induce ISR against these pathogens (Zamioudis *et al*., 2014).

Finally, it is considered that in situations when they are attacked by pathogens due to the resource restrictions, plants are forced to prioritize growth or defense, which results in growth–defense trade-offs (Huot *et al*., 2014). On

the contrary, even though priming has a low fitness cost, once plants are in hostile conditions primed plants outperform unprimed plants, thus resulting in overall positive cost–benefit balance (Martinez-Medina *et al*., 2016).

6. Dissertation objectives and research approach

Thanks to the ISR effect, plant beneficials and their bioactive elicitors represent promising approaches for phytopathogen control in sustainable agriculture. However, the success of PBBs as stimulators of plant defenses is so far rather limited due to a number of factors, including our global lack of knowledge about the nature and mode of action of their elicitors. Namely, tremendous progress has been made in the last decades in understanding the MAMP perception during PTI, but the mechanistic of PBB elicitor recognition at the plant plasma membrane level and the molecular events underlying PBB - induced priming remain largely obscure. Answering this complex question would not only better implement ISR as an approach for phytopathogen control in sustainable agriculture, but it could also help understanding entanglement of PTI and ISR, a puzzle intriguing a fair part of the scientific community.

To tackle this important question, this thesis focuses on events underpinning ISR triggered by Srf as a model elicitor. In this study Srf was used as a mix of homologues slightly differing in the length of the fatty acid tail, to best mimic how it is produced by bacilli in nature.

Thus far, the mechanism behind Srf-triggered immunity remains mainly undeciphered. It is known that Srf triggers early immune events such as ROS production and medium alkalinization, however, perception by plant cell and important links between the perception and activation of these immune events are missing (Jourdan *et al*., 2009). Additionally, it is also known that further Srf triggered immune responses are in accordance with the phenomena of priming, where its pre-treatment upon pathogen attack enhances plant defense responses such as upregulation of lipoxygenase and phenylpropanoid pathway genes, whereas in the absence of the challenger these are not observed (Cawoy *et al*., 2014; Rodríguez *et al*., 2018).

Taking in consideration elusiveness of the topic, as the first approach the comparison of Srf to a well-known MAMP - flagellin (flg22) was used, due to its well described pathway for inducing immunity. The first part of this thesis focuses on Srf perception and mechanism underlying early immune events activation. Moreover, since the Srf's structure proved to be of great importance for its activity (Hoff *et al*., 2021), this work will also aim to evaluate the impact of structural changes on the plant immunization potential of CLPs.

In addition, this work gives clues for future research regarding mechanisms underpinning ISR following early immune event activation, such as signaling and activation of defense related pathways.

7. References

Abdel-Mawgoud AM, Lépine F, Déziel E. Rhamnolipids: Diversity of structures, microbial origins and roles. *Appl Microbiol Biotechnol*. 2010;86(5):1323-1336. doi:10.1007/s00253-010-2498-2

Aldon D, Mbengue M, Mazars C, Galaud J-P. Calcium Signalling in Plant Biotic Interactions. *Int J Mol Sci*. 2018;19(3): 665. doi:10.3390/ijms19030665

Ali R, Ma W, Lemtiri-Chlieh F, et al. Death Don't Have No Mercy and Neither Does Calcium: Arabidopsis CYCLIC NUCLEOTIDE GATED CHANNEL2 and Innate Immunity. *Plant Cell*. 2007;19(3):1081-1095. doi:10.1105/tpc.106.045096

Ali S, Ganai BA, Kamili AN, et al. Pathogenesis-related proteins and peptides as promising tools for engineering plants with multiple stress tolerance. *Microbiol Res*. 2 018;212-213(March):29-37. doi:10.1016/j.micres.2018.04.008

Altrão CS, Kaneko M, Shiina S, Kajikawa A, Shinohara H, Yokota K. Insights on suppression of bacterial leaf spot by Bacillus cyclic lipopeptides via induced resistance in Arabidopsis thaliana. *J Gen Plant Pathol*. 2022;88(4):259-263. doi:10.1007/s10327-022-01062-9

Andrić S, Meyer T, Rigolet A, et al. Lipopeptide Interplay Mediates Molecular Interactions between Soil Bacilli and Pseudomonads. Gralnick JA, ed. *Microbiol Spectr*. 2021;(December). doi:10.1128/spectrum.02038-21

Astier J, Besson-Bard A, Wawer I, et al. Nitric Oxide Signalling in Plants: Cross-Talk with Ca 2+ , Protein Kinases and Reactive Oxygen Species. In: *Annual Plant Reviews Online*. Vol 42. Chichester, UK: John Wiley & Sons, Ltd; 2018:147-170. doi:10.1002/9781119312994.apr0454

Astier J, Gross I, Durner J. Nitric oxide production in plants: an update. *J Exp Bot*. 2018;69(14):3401-3411. doi:10.1093/jxb/erx420

Audenaert K, Pattery T, Cornelis P, Höfte M. Induction of systemic resistance to Botrytis cinerea in tomato by Pseudomonas aeruginosa 7NSK2: Role of salicylic acid, pyochelin, and pyocyanin. *Mol Plant-Microbe Interact*. 2002;15(11):1147-1156 . doi:10.1094/MPMI.2002.15.11.1147

Avermaete T, Keulemans W, Honnay O, Govers G, De Coninck B, Zwart TA. *Food and Nutrition Security: Challenges for Farming, Procurement, and Consumption*. INC; 2023. doi:10.1016/b978-0-12-819470-6.00016-0

Basu D, Haswell ES. Plant mechanosensitive ion channels: an ocean of possibilities. *Curr Opin Plant Biol*. 2017;40:43-48 . doi:10.1016/j.pbi.2017.07.002

Berens ML, Berry HM, Mine A, Argueso CT, Tsuda K. Evolution of Hormone Signaling Networks in Plant Defense. *Annu Rev Phytopathol*. 2017;55:401-425. doi:10.1146/annurev-phyto-080516-035544

Boller T. Chemoperception of microbial signals in plant cells. *Annu Rev Plant Physiol Plant Mol Biol*. 1995;46:189-21 4. doi:10.1146/annurev.pp.46.060195.001201

Boller T, Felix G. A Renaissance of Elicitors: Perception of Microbe-Associated Molecular Patterns and Danger Signals by Pattern-Recognition Receptors. *Annu Rev Plant Biol*. 2009;60(1):379-406 . doi:10.1146/annurev.arplant.57.032905.105346

Bose J, Pottosin II, Shabala SS, Palmgren MG, Shabala S. Calcium Efflux Systems in Stress Signaling and Adaptation in Plants. *Front Plant Sci*. 2011;2(DEC):1-17. doi:10.3389/fpls.2011.00085

Boudsocq M, Droillard MJ, Regad L, Laurière C. Characterization of Arabidopsis calcium-dependent protein kinases: Activated or not by calcium? *Biochem J*. 2012;447(2):291-299. doi:10.1042/BJ20112072

Bücherl CA, Jarsch IK, Schudoma C, et al. Plant immune and growth receptors share common signalling components but localise to distinct plasma membrane nanodomains. *Elife*. 2017;6:1-28 . doi:10.7554/eLife.25114

Cacas J-L, Buré C, Grosjean K, et al. Revisiting Plant Plasma Membrane Lipids in Tobacco: A Focus on Sphingolipids. *Plant Physiol*. 2016;170(1):367-384. doi:10.1104/pp.15.00564

Cawoy H, Mariutto M, Henry G, et al. Plant defense stimulation by natural isolates of Bacillus depends on efficient surfactin production. *Mol Plant-Microbe Interact*. 2014;27(2):87-100. doi:10.1094/MPMI-09-13-0262-R

Cecchini NM, Steffes K, Schläppi MR, Gifford AN, Greenberg JT. Arabidopsis AZI1 family proteins mediate signal mobilization for systemic defence priming. *Nat Commun*. 2015;6(1):7658. doi:10.1038/ncomms8658

Chae D-H, Kim D-R, Cheong MS, Lee YB, Kwak Y-S. Investigating the Induced Systemic Resistance Mechanism of 2,4-Diacetylphloroglucinol (DAPG) using DAPG Hydrolase-Transgenic Arabidopsis. *Plant Pathol J*. 2020;36(3):255-266. doi:10.5423/PPJ.OA.02.2020.0031

Chen K, Tian Z, He H, Long C, Jiang F. Bacillus species as potential biocontrol agents against citrus diseases. *Biol Control*. 2020;151(January):104419. doi:10.1016/j.biocontrol.2020.104419

Choi HK, Song GC, Yi HS, Ryu CM. Field Evaluation of the Bacterial Volatile Derivative 3-Pentanol in Priming for Induced Resistance in Pepper. *J Chem Ecol*. 2014;40(8):882-892. doi:10.1007/s10886-014-0488-z

Chrzanowski Ł, Ławniczak Ł, Czaczyk K. Why do microorganisms produce rhamnolipids? *World J Microbiol Biotechnol*. 2012;28(2):401-419. doi:10.1007/s11274-011-0854-8

Conrath U, Beckers GJM, Flors V, et al. Priming: Getting ready for battle. *Mol Plant-Microbe Interact*. 2006;19(10):1062-1071. doi:10.1094/MPMI-19-1062

Cosse M, Seidel T. Plant Proton Pumps and Cytosolic pH-Homeostasis. *Front Plant Sci*. 2021;12(June):1-9. doi:10.3389/fpls.2021.672873

Cui B, Ma X, Li Y, et al. Perturbations in nitric oxide homeostasis promote Arabidopsis disease susceptibility towards Phytophthora parasitica. *Mol Plant Pathol*. 2021;22(9):1134-1148. doi:10.1111/mpp.13102

D'aes J, Hua GKH, De Maeyer K, et al. Biological control of rhizoctonia root rot on bean by phenazineand cyclic lipopeptide-producing Pseudomonas CMR12a. *Phytopathology*. 2011;101(8):996-1004. doi:10.1094/PHYTO-11-10-0315

D'Alessandro M, Erb M, Ton J, et al. Volatiles produced by soil-borne endophytic bacteria increase plant pathogen resistance and affect tritrophic interactions. *Plant Cell Environ*. 2014;37(4):813-826. doi:10.1111/pce.12220

Dame ZT, Rahman M, Islam T. Bacilli as sources of agrobiotechnology: recent advances and future directions. *Green Chem Lett Rev*. 2021;14(2):246-271. doi:10.1080/17518253.2021.1905080

David B V., Chandrasehar G, Selvam PN. Pseudomonas fluorescens : A Plant-Growth-Promoting Rhizobacterium (PGPR) With Potential Role in Biocontrol of Pests of Crops. In: *Crop Improvement Through Microbial Biotechnology*. Elsevier; 2018:221-243. doi:10.1016/B978-0-444-63987-5.00010-4

DeFalco TA, Zipfel C. Molecular mechanisms of early plant pattern-triggered immune signaling. *Mol Cell*. 2021;81(17):3449-3467 . doi:10.1016/j.molcel.2021.07.029

de Jong F, Munnik T. Attracted to membranes: lipid-binding domains in plants. *Plant Physiol*. 2021;185(3):707-723. doi:10.1093/plphys/kiaa100

De Vleesschauwer D, Djavaheri M, Bakker PAHM, Höfte M. Pseudomonas fluorescens WCS374r-induced systemic resistance in rice against Magnaporthe oryzae is based on pseudobactin-mediated priming for a salicylic acid-repressible multifaceted defense response. *Plant Physiol*. 2008;148(4):1996-2012. doi:10.1104/pp.108.127878

Demidchik V, Shabala S, Isayenkov S, Cuin TA, Pottosin I. Calcium transport across plant membranes: mechanisms and functions. *New Phytol*. 2018;220(1):49-69. doi:10.1111/nph.15266

Demidchik V, Shabala S. Mechanisms of cytosolic calcium elevation in plants: The role of ion channels, calcium extrusion systems and NADPH oxidase-mediated "ROS-Ca2+ Hub." *Funct Plant Biol*. 2018;45(1-2):9-27. doi:10.1071/FP16420

Dimopoulou A, Theologidis I, Varympopi A, et al. Shifting Perspectives of Translational Research in Bio-Bactericides: Reviewing the Bacillus amyloliquefaciens Paradigm. *Biology (Basel)*. 2021;10(11):1202. doi:10.3390/biology10111202

Estelle D, Laurence L, Marc O, Caroline DC, Magali D, Marie-Laure F. Linolenic fatty acid hydroperoxide acts as biocide on plant pathogenic bacteria: Biophysical investigation of the mode of action. *Bioorg Chem*. 2020;100(May):103877. doi:10.1016/j.bioorg.2020.103877

Falhof J, Pedersen JT, Fuglsang AT, Palmgren M. Plasma Membrane H+-ATPase Regulation in the Center of Plant Physiology. *Mol Plant*. 2016;9(3):323-337. doi:10.1016/j.molp.2015.11.002

Farace G, Fernandez O, Jacquens L, et al. Cyclic lipopeptides from Bacillus subtilis activate distinct patterns of defence responses in grapevine. *Mol Plant Pathol*. 2015;16(2):177-187 . doi:10.1111/mpp.12170

Farnese FS, Menezes-Silva PE, Gusman GS, Oliveira JA. When bad guys become good ones: The key role of reactive Oxygen species and Nitric Oxide in the plant responses to abiotic stress. *Front Plant Sci*. 2016;7(APR2016):1-15. doi:10.3389/fpls.2016.00471

Farzand A, Moosa A, Zubair M, et al. Suppression of sclerotinia sclerotiorum by the induction of systemic resistance and regulation of antioxidant pathways in tomato using fengycin produced by Bacillus amyloliquefaciens FZB42. *Biomolecules*. 2019;9(10) . doi:10.3390/biom9100613

Feng J, Chen L, Zuo J. Protein S -Nitrosylation in plants: Current progresses and challenges. *J Integr Plant Biol*. 2019;61(12):1206-1223. doi:10.1111/jipb.12780

Frerigmann H, Glawischnig E, Gigolashvili T. The role of MYB34, MYB51 and MYB122 in the regulation of camalexin biosynthesis in Arabidopsis thaliana. *Front Plant Sci*. 2015;6(AUG):1-11 . doi:10.3389/fpls.2015.00654

Freschi L. Nitric oxide and phytohormone interactions: current status and perspectives. *Front Plant Sci*. 2013;4(OCT):1-22 . doi:10.3389/fpls.2013.00398

Ganeshan G, Manoj Kumar A. Pseudomonas fluorescens , a potential bacterial antagonist to control plant diseases. *J Plant Interact*. 2005;1(3):123-134. doi:10.1080/17429140600907043

García-Gutiérrez L, Zeriouh H, Romero D, Cubero J, de Vicente A, Pérez-García A. The antagonistic strain Bacillus subtilis UMAF6639 also confers protection to melon plants against cucurbit powdery mildew by activation of jasmonate- and salicylic acid-dependent defence responses. *Microb Biotechnol*. 2013;6(3):264-274. doi:10.1111/1751-7915.12028

Geudens N, Martins JC. Cyclic lipodepsipeptides from Pseudomonas spp. - Biological Swiss-Army knives. *Front Microbiol*. 2018;9(AUG):1-18. doi:10.3389/fmicb.2018.01867

Gimenez-Ibanez S, Solano R. Nuclear jasmonate and salicylate signaling and crosstalk in defense against pathogens. *Front Plant Sci*. 2013;4(APR):1-11. doi:10.3389/fpls.2013.00072

Götze S, Stallforth P. Structure elucidation of bacterial nonribosomal lipopeptides. *Org Biomol Chem*. 2020;18(9):1710-1727. doi:10.1039/C9OB02539A

Han G. Origin and evolution of the plant immune system. *New Phytol*. 2019;222(1):70-83. doi:10.1111/nph.15596

Han Q, Wu F, Wang X, et al. The bacterial lipopeptide iturins induce Verticillium dahliae cell death by affecting fungal signalling pathways and mediate plant defence responses involved in pathogen-associated molecular pattern-triggered immunity. *Environ Microbiol* . 2015;17(4):1166-1188. doi:10.1111/1462-2920.12538

Han SH, Lee SJ, Moon JH, et al. GacS-dependent production of 2R, 3R-butanediol by Pseudomonas chlororaphis O6 is a major determinant for eliciting systemic resistance against Erwinia carotovora but not against Pseudomonas syringae pv. tabaci in tobacco. *Mol Plant-Microbe Interact*. 2006;19(8):924-930. doi:10.1094/MPMI-19-0924

Hao H, Fan L, Chen T, et al. Clathrin and Membrane Microdomains Cooperatively Regulate RbohD Dynamics and Activity in Arabidopsis. *Plant Cell*. 2014;26(4):1729-1745. doi:10.1105/tpc.113.122358

Harwood CR, Mouillon JM, Pohl S, Arnau J. Secondary metabolite production and the safety of industrially important members of the Bacillus subtilis group. *FEMS Microbiol Rev*. 2018;42(6):721-738 . doi:10.1093/femsre/fuy028

Henry G, Deleu M, Jourdan E, Thonart P, Ongena M. The bacterial lipopeptide surfactin targets the lipid fraction of the plant plasma membrane to trigger immune-related defence responses. *Cell Microbiol*. 2011;13(11):1824-1837. doi:10.1111/j.1462-5822.2011.01664.x

Hernández-Reyes C, Schenk ST, Neumann C, Kogel K-H, Schikora A. N - acyl-homoserine lactones-producing bacteria protect plants against plant and human pathogens. *Microb Biotechnol*. 2014;7(6):580-588. doi:10.1111/1751-7915.12177

Hoff G, Arguelles Arias A, Boubsi F, et al. Surfactin Stimulated by Pectin Molecular Patterns and Root Exudates Acts as a Key Driver of the Bacillus -Plant Mutualistic Interaction. Vidaver AK, ed. *MBio*. November 2021:2021.02.22.432335. doi:10.1128/mBio.01774-21

Huby E, Napier JA, Baillieul F, Michaelson L V., Dhondt-Cordelier S. Sphingolipids: towards an integrated view of metabolism during the plant

stress response. *New Phytol*. 2020;225(2):659-670 . doi:10.1111/nph.15997

Huot B, Yao J, Montgomery BL, He SY. Growth-defense tradeoffs in plants: A balancing act to optimize fitness. *Mol Plant*. 2014. doi:10.1093/mp/ssu049

Iavicoli A, Boutet E, Buchala A, Métraux JP. Induced systemic resistance in Arabidopsis thaliana in response to root inoculation with Pseudomonas fluorescens CHA0. *Mol Plant-Microbe Interact*. 2003;16(10):851-858. doi:10.1094/MPMI.2003.16.10.851

Jagodzik P, Tajdel-Zielinska M, Ciesla A, Marczak M, Ludwikow A. Mitogen-activated protein kinase cascades in plant hormone signaling. *Front Plant Sci*. 2018;9(October):1-26. doi:10.3389/fpls.2018.01387

Jaillais Y, Ott T. The Nanoscale Organization of the Plasma Membrane and Its Importance in Signaling: A Proteolipid Perspective. *Plant Physiol*. 2020;182(4):1682-1696. doi:10.1104/pp.19.01349

Janků, Luhová, Petřivalský. On the Origin and Fate of Reactive Oxygen Species in Plant Cell Compartments. *Antioxidants*. 2019;8(4):105. doi:10.3390/antiox8040105

Jarsch IK, Konrad SSA, Stratil TF, et al. Plasma Membranes Are Subcompartmentalized into a Plethora of Coexisting and Diverse Microdomains in Arabidopsis and Nicotiana benthamiana. *Plant Cell*. 2014;26(4):1698-1711. doi:10.1105/tpc.114.124446

Jeandet P, Hébrard C, Deville M-A, et al. Deciphering the Role of Phytoalexins in Plant-Microorganism Interactions and Human Health. *Molecules*. 2014;19(11):18033-18056. doi:10.3390/molecules191118033

Jedelská T, Sedlářová M, Lochman J, Činčalová L, Luhová L, Petřivalský M. Protein S-nitrosation differentially modulates tomato responses to infection by hemi-biotrophic oomycetes of Phytophthora spp. *Hortic Res*. 2021;8(1):34. doi:10.1038/s41438-021-00469-3

Jourdan E, Henry G, Duby F, et al. Insights into the defense-related events occurring in plant cells following perception of surfactin-type lipopeptide from Bacillus subtilis. *Mol Plant-Microbe Interact*. 2009;22(4):456-468. doi:10.1094/MPMI-22-4-0456

Jung HW, Tschaplinski TJ, Wang L, Glazebrook J, Greenberg JT. Priming in Systemic Plant Immunity. *Science (80-)*. 2009;324(5923):89-91. doi:10.1126/science.1170025

Kai M, Effmert U, Piechulla B. Bacterial-Plant-Interactions: Approaches to Unravel the Biological Function of Bacterial Volatiles in the Rhizosphere. *Front Microbiol*. 2016;7(FEB) . doi:10.3389/fmicb.2016.00108

Kapoor D, Singh S, Kumar V, Romero R, Prasad R, Singh J. Antioxidant enzymes regulation in plants in reference to reactive oxygen species (ROS) and reactive nitrogen species (RNS). *Plant Gene*. 2019;19(October 2018):100182. doi:10.1016/j.plgene.2019.100182

Kawagoe Y, Shiraishi S, Kondo H, Yamamoto S, Aoki Y, Suzuki S. Cyclic lipopeptide iturin A structure-dependently induces defense response in Arabidopsis plants by activating SA and JA signaling pathways. *Biochem Biophys Res Commun*. 2015;460(4):1015-1020 . doi:10.1016/j.bbrc.2015.03.143

Sayyed, R. Z. Plant Growth Promoting Rhizobacteria for Sustainable Stress Management: Volume 2: Rhizobacteria In Biotic Stress Management. 1st ed. 2019. doi:10.1007/978-981-13-6986-5

Kim DS, Hwang BK. An important role of the pepper phenylalanine ammonia-lyase gene (PAL1) in salicylic acid-dependent signalling of the defence response to microbial pathogens. *J Exp Bot*. 2014;65(9):2295-2306. doi:10.1093/jxb/eru109

Köhl J, Kolnaar R, Ravensberg WJ. Mode of Action of Microbial Biological Control Agents Against Plant Diseases: Relevance Beyond Efficacy. *Front Plant Sci*. 2019;10(July):1-19 . doi:10.3389/fpls.2019.00845

Kole RK, Roy K, Panja BN, Sankarganesh E, Manda T, Worede RE. Use of pesticides in agriculture and emergence of resistant pests. *Indian J Anim Heal*. 2019;58(2-SPL):53. doi:10.36062/ijah.58.2SPL.2019.53-70

Kong HG, Shin TS, Kim TH, Ryu CM. Stereoisomers of the bacterial volatile compound 2,3-butanediol differently elicit systemic defense responses of pepper against multiple viruses in the field. *Front Plant Sci*. 2018;9(February):1-13. doi:10.3389/fpls.2018.00090

Kong X, Xu L, Jamieson P. Plant Sense: The Rise of Calcium Channels. *Trends Plant Sci*. 2020;25(9):838-841. doi:10.1016/j.tplants.2020.06.002

Kramer J, Özkaya Ö, Kümmerli R. Bacterial siderophores in community and host interactions. *Nat Rev Microbiol*. 2020;18(3):152-163. doi:10.1038/s41579-019-0284-4

Krysan PJ, Colcombet J. Cellular complexity in MAPK signaling in plants: Questions and emerging tools to answer them. *Front Plant Sci.* 2018;871(November):1-14. doi:10.3389/fpls.2018.01674

Lam VB, Meyer T, Arias AA, Ongena M, Oni FE, Höfte M. Bacillus Cyclic Lipopeptides Iturin and Fengycin Control Rice Blast Caused by Pyricularia oryzae in Potting and Acid Sulfate Soils by Direct Antagonism and Induced Systemic Resistance. *Microorganisms*. 2021;9(7):1441. doi:10.3390/microorganisms9071441

Lawrence SR, Gaitens M, Guan Q, Dufresne C, Chen S. S-Nitroso-Proteome Revealed in Stomatal Guard Cell Response to Flg22. *Int J Mol Sci*. 2020;21(5):1688. doi:10.3390/ijms21051688

Le Mire G, Siah A, Brisset M-N, Gaucher M, Deleu M, Jijakli M. Surfactin Protects Wheat against Zymoseptoria tritici and Activates Both Salicylic Acid- and Jasmonic Acid-Dependent Defense Responses. *Agriculture*. 2018;8(1):11. doi:10.3390/agriculture8010011

Lee B, Farag MA, Park HB, Kloepper JW, Lee SH, Ryu C-M. Induced Resistance by a Long-Chain Bacterial Volatile: Elicitation of Plant Systemic Defense by a C13 Volatile Produced by Paenibacillus polymyxa.

Vinatzer BA, ed. *PLoS One*. 2012;7(11):e48744 . doi:10.1371/journal.pone.0048744

Lee D, Lal NK, Lin Z-JD, et al. Regulation of reactive oxygen species during plant immunity through phosphorylation and ubiquitination of RBOHD. *Nat Commun*. 2020;11(1):1838. doi:10.1038/s41467-020-15601-5

Leeman M, Den Ouden FM, Van Pelt JA, et al. Iron availability affects induction of systemic resistance to Fusarium wilt of radish by Pseudomonas fluorescens. *Phytopathology*. 1996;86(2):149-155. doi:10.1094/Phyto-86-149

Legrand A, Martinez D, Grélard A, et al. Nanodomain Clustering of the Plant Protein Remorin by Solid-State NMR. *Front Mol Biosci*. 2019;6(October):1-14. doi:10.3389/fmolb.2019.00107

Li P, Lu Y, Chen H, Day B. The Lifecycle of the Plant Immune System. *CRC Crit Rev Plant Sci*. 2020;39(1):72-100 . doi:10.1080/07352689.2020.1757829

Li Y, Héloir MC, Zhang X, et al. Surfactin and fengycin contribute to the protection of a Bacillus subtilis strain against grape downy mildew by both direct effect and defence stimulation. *Mol Plant Pathol*. 2019;20(8):1037-1050. doi:10.1111/mpp.12809

Liu X, Grabherr HM, Willmann R, et al. Host-induced bacterial cell wall decomposition mediates pattern-triggered immunity in Arabidopsis. Elife. 2014 Jun 23;3:e01990. doi: 10.7554/eLife.01990. PMID: 24957336; PMCID: PMC4103680.

Ma Z, Hoang Hua GKH, Ongena M, Höfte M. Role of phenazines and cyclic lipopeptides produced by pseudomonas sp. CMR12a in induced systemic resistance on rice and bean. *Environ Microbiol Rep*. 2016;8(5):896-904. doi:10.1111/1758-2229.12454

Ma Z, Hua GKH, Ongena M, Höfte M. Role of phenazines and cyclic lipopeptides produced by pseudomonas sp. CMR12a in induced systemic

resistance on rice and bean. *Environ Microbiol Rep*. 2016;8(5):896-904. doi:10.1111/1758-2229.12454

Ma Z, Ongena M, Höfte M. The cyclic lipopeptide orfamide induces systemic resistance in rice to Cochliobolus miyabeanus but not to Magnaporthe oryzae. *Plant Cell Rep*. 2017;36(11):1731-1746. doi:10.1007/s00299-017-2187-z

Maget-Dana R, Thimon L, Peypoux F, Ptak M. Surfactin/iturin A interactions may explain the synergistic effect of surfactin on the biological properties of iturin A. *Biochimie*. 1992;74(12):1047-1051. doi:10.1016/0300-9084(92)90002-V

Mahato DK, Lee KE, Kamle M, et al. Aflatoxins in Food and Feed: An Overview on Prevalence, Detection and Control Strategies. *Front Microbiol*. 2019;10(October):1-10. doi:10.3389/fmicb.2019.02266

Mamode Cassim A, Gouguet P, Gronnier J, et al. Plant lipids: Key players of plasma membrane organization and function. *Prog Lipid Res*. 2019;73(November 2018):1-27. doi:10.1016/j.plipres.2018.11.002

Marcec MJ, Gilroy S, Poovaiah BW, Tanaka K. Mutual interplay of Ca2+ and ROS signaling in plant immune response. *Plant Sci*. 2019;283(March):343-354. doi:10.1016/j.plantsci.2019.03.004

Martinez-Medina A, Flors V, Heil M, et al. Recognizing Plant Defense Priming. *Trends Plant Sci*. 2016;21(10):818-822 . doi:10.1016/j.tplants.2016.07.009

Mauch-Mani B, Baccelli I, Luna E, Flors V. Defense Priming: An Adaptive Part of Induced Resistance. *Annu Rev Plant Biol*. 2017;68(1):485-512. doi:10.1146/annurev-arplant-042916-041132

Maurhofer M. Induction of Systemic Resistance of Tobacco to Tobacco Necrosis Virus by the Root-Colonizing Pseudomonas fluorescens Strain CHA0: Influence of the gacA Gene and of Pyoverdine Production. *Phytopathology*. 1994;84(2):139. doi:10.1094/Phyto-84-139

Mejri S, Siah A, Coutte F, et al. Biocontrol of the wheat pathogen Zymoseptoria tritici using cyclic lipopeptides from Bacillus subtilis. *Environ Sci Pollut Res*. 2018;25(30):29822-29833. doi:10.1007/s11356-017-9241-9

Meng X, Zhang S. MAPK cascades in plant disease resistance signaling. *Annu Rev Phytopathol*. 2013;51:245-266. doi:10.1146/annurev-phyto-082712-102314

Meyer G De, Audenaert K, Monica H. Pseudomonas aeruginosa 7NSK2-induced systemic resistance in tobacco depends on in planta salicylic acid accumulation but is not associated with PR1a expression. 1999:513-517.

Meziane H, Van Der Sluis I, Van Loon LC, HÖfte M, Bakker PAHM. Determinants of Pseudomonas putida WCS358 involved in inducing systemic resistance in plants. *Mol Plant Pathol*. 2005;6(2):177-185. doi:10.1111/j.1364-3703.2005.00276.x

Møller IM, Sweetlove LJ. ROS signalling – specificity is required. *Trends Plant Sci*. 2010;15(7):370-374. doi:10.1016/j.tplants.2010.04.008

Monnier N, Cordier M, Dahi A, et al. Semipurified Rhamnolipid Mixes Protect Brassica napus Against Leptosphaeria maculans Early Infections. *Phytopathology*. 2020;110(4):834-842. doi:10.1094/PHYTO-07-19-0275-R

Monnier N, Furlan AL, Buchoux S, et al. Exploring the dual interaction of natural rhamnolipids with plant and fungal biomimetic plasma membranes through biophysical studies. *Int J Mol Sci*. 2019;20(5) . doi:10.3390/ijms20051009

Müller T, Behrendt U. Exploiting the biocontrol potential of plant-associated pseudomonads – A step towards pesticide-free agriculture? *Biol Control*. 2021;155(August 2020):104538 . doi:10.1016/j.biocontrol.2021.104538

Mur LAJ, Kumari A, Brotman Y, et al. Nitrite and nitric oxide are important in the adjustment of primary metabolism during the

hypersensitive response in tobacco. Foyer C, ed. *J Exp Bot*. 2019;70(17):4571-4582. doi:10.1093/jxb/erz161

Nguyen NH, Trotel-Aziz P, Clément C, Jeandet P, Baillieul F, Aziz A. Camalexin accumulation as a component of plant immunity during interactions with pathogens and beneficial microbes. *Planta*. 2022;255(6):116. doi:10.1007/s00425-022-03907-1

Nguyen NH, Trotel-Aziz P, Villaume S, et al. Priming of camalexin accumulation in induced systemic resistance by beneficial bacteria against Botrytis cinerea and Pseudomonas syringae pv. tomato DC3000. Höfte M, ed. *J Exp Bot*. 2022;73(11):3743-3757. doi:10.1093/jxb/erac070

Noack LC, Bayle V, Armengot L, et al. A nanodomain-anchored scaffolding complex is required for the function and localization of phosphatidylinositol 4-kinase alpha in plants. *Plant Cell*. 2022;34(1):302-332. doi:10.1093/plcell/koab135

Noctor G, Reichheld J-P, Foyer CH. ROS-related redox regulation and signaling in plants. *Semin Cell Dev Biol*. 2018;80:3-12 . doi:10.1016/j.semcdb.2017.07.013

Oelmüller R. Threat at One End of the Plant: What Travels to Inform the Other Parts? *Int J Mol Sci*. 2021;22(6):3152. doi:10.3390/ijms22063152

Olorunleke FE, Hua GKH, Kieu NP, Ma Z, Höfte M. Interplay between orfamides, sessilins and phenazines in the control of Rhizoctonia diseases by Pseudomonas sp. CMR12a. *Environ Microbiol Rep*. 2015;7(5):774-781. doi:10.1111/1758-2229.12310

Omoboye OO, Oni FE, Batool H, Yimer HZ, De Mot R, Höfte M. Pseudomonas Cyclic Lipopeptides Suppress the Rice Blast Fungus Magnaporthe oryzae by Induced Resistance and Direct Antagonism. *Front Plant Sci*. 2019;10(July). doi:10.3389/fpls.2019.00901

Ongena M, Jacques P. Bacillus lipopeptides: versatile weapons for plant disease biocontrol. *Trends Microbiol*. 2008;16(3):115-125 . doi:10.1016/j.tim.2007.12.009

Ongena M, Jourdan E, Adam A, et al. Surfactin and fengycin lipopeptides of Bacillus subtilis as elicitors of induced systemic resistance in plants. *Environ Microbiol*. 2007;9(4):1084-1090. doi: 10.1111/j.1462-2920.2006.01202.x

Ongena M, Jourdan E, Adam A, Schäfer M, Budzikiewicz H, Thonart P. Amino acids, iron, and growth rate as key factors influencing production of the Pseudomonas putida BTP1 benzylamine derivative involved in systemic resistance induction in different plants. *Microb Ecol*. 2008;55(2):280-292. doi:10.1007/s00248-007-9275-5

Ongena M, Jourdan E, Schäfer M, et al. Isolation of an N-alkylated benzylamine derivative from Pseudomonas putida BTP1 as elicitor of induced systemic resistance in bean. *Mol Plant-Microbe Interact*. 2005;18(6):562-569. doi:10.1094/MPMI-18-0562

Pande A, Mun BG, Lee DS, et al. NO Network for Plant–Microbe Communication Underground: A Review. *Front Plant Sci*. 2021;12(March):1-10. doi:10.3389/fpls.2021.658679

Park HB, Lee B, Kloepper JW, Ryu CM. One shot-two pathogens blocked: Exposure of Arabidopsis to hexadecane, a long chain volatile organic compound, confers induced resistance against both Pectobacterium carotovorum and Pseudomonas syringae. *Plant Signal Behav*. 2013;8(7). doi:10.4161/psb.24619

Park K, Park YS, Ahamed J, et al. Elicitation of induced systemic resistance of chili pepper by iturin a analogs derived from Bacillus vallismortis EXTN-1. *Can J Plant Sci*. 2016;96(4):564-570. doi:10.1139/cjps-2015-0199

Perneel M, D'hondt L, De Maeyer K, Adiobo A, Rabaey K, Höfte M. Phenazines and biosurfactants interact in the biological control of soil-borne diseases caused by Pythium spp. *Environ Microbiol*. 2008;10(3):778-788. doi: 10.1111/j.1462-2920.2007.01501.x

Pierre E, Marcelo P, Croutte A, et al. Impact of Rhamnolipids (RLs), Natural Defense Elicitors, on Shoot and Root Proteomes of Brassica napus

by a Tandem Mass Tags (TMTs) Labeling Approach. Int J Mol Sci. 2023;24(3). doi:10.3390/ijms24032390

Pieterse CMJ. Prime Time for Transgenerational Defense. *Plant Physiol*. 2012;158(2):545-545. doi:10.1104/pp.112.900430

Pieterse CMJ, Zamioudis C, Berendsen RL, Weller DM, Van Wees SCM, Bakker PAHM. Induced Systemic Resistance by Beneficial Microbes. *Annu Rev Phytopathol*. 2014;52(1):347-375. doi:10.1146/annurev-phyto-082712-102340

Platel R, Chaveriat L, Le Guenic S, et al. Importance of the C12 Carbon Chain in the Biological Activity of Rhamnolipids Conferring Protection in Wheat against Zymoseptoria tritici. *Molecules*. 2020;26(1):40. doi:10.3390/molecules26010040

Platel R, Lucau-Danila A, Baltenweck R, et al. Deciphering immune responses primed by a bacterial lipopeptide in wheat towards Zymoseptoria tritici. *Front Plant Sci.* 2023;13(January):1-19. doi:10.3389/fpls.2022.1074447

Pršić J, Ongena M. Elicitors of Plant Immunity Triggered by Beneficial Bacteria. *Front Plant Sci*. 2020;11(November):1-12 . doi:10.3389/fpls.2020.594530

Raaijmakers JM, De Bruijn I, De Kock MJD. Cyclic lipopeptide production by plant-associated Pseudomonas spp.: Diversity, activity, biosynthesis, and regulation. *Mol Plant-Microbe Interact*. 2006;19(7):699-710. doi:10.1094/MPMI-19-0699

Raaijmakers JM, de Bruijn I, Nybroe O, Ongena M. Natural functions of lipopeptides from Bacillus and Pseudomonas: More than surfactants and antibiotics. *FEMS Microbiol Rev*. 2010;34(6):1037-1062 . doi:10.1111/j.1574-6976.2010.00221.x

Raaijmakers JM, Mazzola M. Diversity and natural functions of antibiotics produced by beneficial and plant pathogenic bacteria. *Annu Rev Phytopathol*. 2012;50(1):403-424. doi:10.1146/annurev-phyto-081211-172908

Rahman A, Uddin W, Wenner NG. Induced systemic resistance responses in perennial ryegrass against Magnaporthe oryzae elicited by semi-purified surfactin lipopeptides and live cells of Bacillus amyloliquefaciens. *Mol Plant Pathol*. 2015;16(6):546-558. doi:10.1111/mpp.12209

Rajamanickam S, Nakkeeran S. Flagellin of Bacillus amyloliquefaciens works as a resistance inducer against groundnut bud necrosis virus in chilli (Capsicum annuum L.). *Arch Virol*. 2020;165(7):1585-1597 . doi:10.1007/s00705-020-04645-z

Ran LX, Li ZN, Wu GJ, Van Loon LC, Bakker PAHM. Induction of systemic resistance against bacterial wilt in Eucalyptus urophylla by fluorescent Pseudomonas spp. *Eur J Plant Pathol*. 2005;113(1):59-70. doi:10.1007/s10658-005-0623-3

Rodríguez J, Tonelli ML, Figueredo MS, Ibáñez F, Fabra A. The lipopeptide surfactin triggers induced systemic resistance and priming state responses in Arachis hypogaea L. *Eur J Plant Pathol*. 2018;152(3):845-851. doi:10.1007/s10658-018-1524-6

Romero-Puertas MC, Sandalio LM. Nitric Oxide Level Is Self-Regulating and Also Regulates Its ROS Partners. *Front Plant Sci*. 2016;7(MAR2016):1-5. doi:10.3389/fpls.2016.00316

Rondelli V, Koutsioubas A, Pršić J, et al. Sitosterol and glucosylceramide cooperative transversal and lateral uneven distribution in plant membranes. *Sci Rep*. 2021;11(1):21618. doi:10.1038/s41598-021-00696-7

Roongsawang N, Washio K, Morikawa M. Diversity of nonribosomal peptide synthetases involved in the biosynthesis of lipopeptide biosurfactants. *Int J Mol Sci*. 2011;12(1):141-172 . doi:10.3390/ijms12010141

Ryu C, Farag MA, Hu C, Reddy MS, Kloepper JW, Pare PW. Bacterial volatiles induced resistance in Arabidobsis. *Plant Physiol*. 2004;134(March):1017-1026. doi:10.1104/pp.103.026583.with

Salwan R, Sharma M, Sharma A, Sharma V. Insights into plant beneficial microorganism-triggered induced systemic resistance. *Plant Stress*. 2023;7(February):100140. doi:10.1016/j.stress.2023.100140

Sanchez L, Courteaux B, Hubert J, et al. Rhamnolipids Elicit Defense Responses and Induce Disease Resistance against Biotrophic, Hemibiotrophic, and Necrotrophic Pathogens That Require Different Signaling Pathways in Arabidopsis and Highlight a Central Role for Salicylic Acid. *Plant Physiol*. 2012;160(3):1630-164 1. doi:10.1104/pp.112.201913

Savary S, Willocquet L, Pethybridge SJ, Esker P, McRoberts N, Nelson A. The global burden of pathogens and pests on major food crops. *Nat Ecol Evol*. 2019;3(3):430-439. doi:10.1038/s41559-018-0793-y

Schenk ST, Stein E, Kogel KH, Schikora A. Arabidopsis growth and defense are modulated by bacterial quorum sensing molecules. *Plant Signal Behav*. 2012;7(2):178-181. doi:10.4161/psb.18789

Schikora A, Schenk ST, Hartmann A. Beneficial effects of bacteria-plant communication based on quorum sensing molecules of the N -acyl homoserine lactone group. *Plant Mol Biol*. 2016;90(6):605-612. doi:10.1007/s11103-016-0457-8

Schikora A, Schenk ST, Stein E, Molitor A, Zuccaro A, Kogel KH. N-acyl-homoserine lactone confers resistance toward biotrophic and hemibiotrophic pathogens via altered activation of AtMPK6. *Plant Physiol*. 2011;157(3):1407-1418. doi:10.1104/pp.111.180604

Schuhegger R, Ihring A, Gantner S, et al. Induction of systemic resistance in tomato by N-acyl-L-homoserine lactone-producing rhizosphere bacteria. *Plant Cell Environ*. 2006 May;29(5):909-18. doi: 10.1111/j.1365-3040.2005.01471.x. PMID: 17087474.

Shine MB, Xiao X, Kachroo P, Kachroo A. Signaling mechanisms underlying systemic acquired resistance to microbial pathogens. *Plant Sci*. 2019;279(January 2018):81-86. doi:10.1016/j.plantsci.2018.01.001

Shrestha A, Hernández-Reyes C, Grimm M, et al. AHL-Priming Protein 1 mediates N-3-oxo-tetradecanoyl-homoserine lactone priming in Arabidopsis. *BMC Biol*. 2022 Dec 5;20(1):268. doi: 10.1186/s12915-022-01464-3. PMID: 36464707; PMCID: PMC9721052

Siddiqui IA, Shaukat SS. Suppression of root-knot disease by Pseudomonas fluorescens CHA0 in tomato: Importance of bacterial secondary metabolite, 2,4-diacetylpholoroglucinol. *Soil Biol Biochem*. 2003;35(12):1615-1623. doi:10.1016/j.soilbio.2003.08.006

Soares C, Carvalho MEA, Azevedo RA, Fidalgo F. Plants facing oxidative challenges—A little help from the antioxidant networks. *Environ Exp Bot*. 2019;161(November 2018):4-25. doi:10.1016/j.envexpbot.2018.12.009

Song GC, Riu M, Ryu C-M. Beyond the two compartments Petri-dish: optimising growth promotion and induced resistance in cucumber exposed to gaseous bacterial volatiles in a miniature greenhouse system. *Plant Methods*. 2019;15(1):9. doi:10.1186/s13007-019-0395-y

Spoel SH, Dong X. How do plants achieve immunity? Defence without specialized immune cells. *Nat Rev Immunol*. 2012;12(2):89-100. doi:10.1038/nri3141

Stringlis IA, De Jonge R, Pieterse CMJ. The Age of Coumarins in Plant-Microbe Interactions. *Plant Cell Physiol*. 2019;60(7):1405-1419. doi:10.1093/pcp/pcz076

Stringlis IA, Proietti S, Hickman R, Van Verk MC, Zamioudis C, Pieterse CMJ. Root transcriptional dynamics induced by beneficial rhizobacteria and microbial immune elicitors reveal signatures of adaptation to mutualists. *Plant J*. 2018;93(1):166-180. doi:10.1111/tpj.13741

Süssmuth RD, Mainz A. Nonribosomal Peptide Synthesis—Principles and Prospects. *Angew Chemie - Int Ed*. 2017;56(14):3770-3821 . doi:10.1002/anie.201609079

Tada Y, Spoel SH, Pajerowska-Mukhtar K, et al. Plant Immunity Requires Conformational Charges of NPR1 via S-Nitrosylation and

Thioredoxins. *Science. 2008 Aug 15;321(5891):952-6. doi: 10.1126/science.1156970. Epub 2008 Jul 17*

Taj G, Agarwal P, Grant M, Kumar A. MAPK machinery in plants. *Plant Signal Behav*. 2010;5(11):1370-1378. doi:10.4161/psb.5.11.13020

Tanaka K, Amaki Y, Ishihara A, Nakajima H. Synergistic Effects of [Ile 7]Surfactin Homologues with Bacillomycin D in Suppression of Gray Mold Disease by Bacillus amyloliquefaciens Biocontrol Strain SD-32. *J Agric Food Chem*. 2015;63(22):5344-5353. doi:10.1021/acs.jafc.5b01198

Thakur M, Udayashankar AC. Lipoxygenases and Their Function in Plant Innate Mechanism. In: Jogaiah S, Abdelrahman M, eds. *Bioactive Molecules in Plant Defense*. Cham: Springer International Publishing; 2019:133-143. doi:10.1007/978-3-030-27165-7_8

Théatre A, Hoste ACR, Rigolet A, et al. Bacillus sp.: A Remarkable Source of Bioactive Lipopeptides. *Adv Biochem Eng Biotechnol*. 2022;181:123-179. doi: 10.1007/10_2021_182.

Théatre A, Cano-Prieto C, Bartolini M, et al. The Surfactin-Like Lipopeptides From Bacillus spp.: Natural Biodiversity and Synthetic Biology for a Broader Application Range. *Front Bioeng Biotechnol*. 2021;9(March). doi:10.3389/fbioe.2021.623701

Thor K, Jiang S, Michard E, et al. The calcium-permeable channel OSCA1.3 regulates plant stomatal immunity. *Nature* . 2020;585(7826):569-573. doi:10.1038/s41586-020-2702-1

Tian W, Hou C, Ren Z, et al. A calmodulin-gated calcium channel links pathogen patterns to plant immunity. *Nature*. 2019;572(7767):131-135. doi:10.1038/s41586-019-1413-y

Tomar RS, Kataria S, Jajoo A. Behind the scene: Critical role of reactive oxygen species and reactive nitrogen species in salt stress tolerance. *J Agron Crop Sci*. 2021;207(4):577-588. doi:10.1111/jac.12490

Tracanna V, de Jong A, Medema MH, Kuipers OP. Mining prokaryotes for antimicrobial compounds: from diversity to function. *FEMS Microbiol Rev*. 2017;41(3):417-429. doi:10.1093/femsre/fux014

Tran H, Ficke A, Asiimwe T, Höfte M, Raaijmakers JM. Role of the cyclic lipopeptide massetolide a in biological control of Phytophthora infestans and in colonization of tomato plants by Pseudomonas fluorescens. *New Phytol*. 2007;175(4):731-742. doi:10.1111/j.1469-8137.2007.02138.x

Turkan I. ROS and RNS: Key signalling molecules in plants. *J Exp Bot*. 2018;69(14):3313-3315. doi:10.1093/jxb/ery198

Tyagi S, Lee KJ, Shukla P, Chae JC. Dimethyl disulfide exerts antifungal activity against Sclerotinia minor by damaging its membrane and induces systemic resistance in host plants. *Sci Rep*. 2020;10(1):1-12. doi:10.1038/s41598-020-63382-0

Umetsu N, Shirai Y. Development of novel pesticides in the 21st century. *J Pestic Sci*. 2020;45(2):54-74. doi:10.1584/jpestics.D20-201

Varnier AL, Sanchez L, Vatsa P, et al. Bacterial rhamnolipids are novel MAMPs conferring resistance to Botrytis cinerea in grapevine. *Plant, Cell Environ*. 2009;32(2):178-193. doi:10.1111/j.1365-3040.2008.01911.x

Vatsa P, Sanchez L, Clement C, Baillieul F, Dorey S. Rhamnolipid biosurfactants as new players in animal and plant defense against microbes. *Int J Mol Sci*. 2010;11(12):5095-5108. doi:10.3390/ijms11125095

Verhagen BWM, Trotel-Aziz P, Couderchet M, Höfte M, Aziz A. Pseudomonas spp.-induced systemic resistance to Botrytis cinerea is associated with induction and priming of defence responses in grapevine. *J Exp Bot*. 2010;61(1):249-260. doi:10.1093/jxb/erp295

Vlot AC, Sales JH, Lenk M, et al. Systemic propagation of immunity in plants. *New Phytol*. 2021;229(3):1234-1250. doi:10.1111/nph.16953

Vos IA, Pieterse CMJ, van Wees SCM. Costs and benefits of hormone-regulated plant defences. *Plant Pathol*. 2013;62(S1):43-55 . doi:10.1111/ppa.12105

Wan WL, Zhang L, Pruitt R, et al. Comparing Arabidopsis receptor kinase and receptor protein-mediated immune signaling reveals BIK1-dependent differences. *New Phytol*. 2019;221(4):2080-2095. doi:10.1111/nph.15497

Wan J, He M, Hou Q, et al. Cell wall associated immunity in plants. *Stress Biol*. 2021;1(1):3. doi:10.1007/s44154-021-00003-4

Wang, H., Yang, X., Guo, L., Zeng, H., and Qiu, D. (2015). PeBL1, a novel protein elicitor from Brevibacillus laterosporus strain A60, activates defense responses and systemic resistance in Nicotiana benthamiana. *Appl. Environ. Microbiol*. 81, 2706–2716. doi: 10.1128/AEM.03586-14

Wang N, Liu M, Guo L, Yang X, Qiu D. A Novel Protein Elicitor (PeBA1) from Bacillus amyloliquefaciens NC6 Induces Systemic Resistance in Tobacco. *Int J Biol Sci*. 2016;12(6):757-767. doi:10.7150/ijbs.14333

Wang Y, Shimazaki K ichiro, Kinoshita T. Multiple Roles of the Plasma Membrane H+-ATPase and Its Regulation. Vol 35. 1st ed. Elsevier Inc.; 2014. doi:10.1016/B978-0-12-801922-1.00008-7

Wang Y, Chu C. S-Nitrosylation Control of ROS and RNS Homeostasis in Plants: The Switching Function of Catalase. *Mol Plant*. 2020;13(7):946-948. doi:10.1016/j.molp.2020.05.013

Wasternack C, Feussner I. The Oxylipin Pathways: Biochemistry and Function. *Annu Rev Plant Biol*. 2018;69(1):363-386. doi:10.1146/annurev-arplant-042817-040440

Wehner G, Kopahnke D, Richter K, Kecke S, Schikora A, Ordon F. Priming Is a Suitable Strategy to Enhance Resistance Towards Leaf Rust in Barley. *Phytobiomes J*. 2019;3(1):46-51. doi:10.1094/PBIOMES-09-18-0041-R

Weller DM, Mavrodi D V., Van Pelt JA, Pieterse CMJ, Van Loon LC, Bakker PAHM. Induced systemic resistance in Arabidopsis thaliana against Pseudomonas syringae pv. tomato by 2,4-diacetylphloroglucinol-producing Pseudomonas fluorescens. *Phytopathology*. 2012;102(4):403-412. doi:10.1094/PHYTO-08-11-0222

Wiesel L, Newton AC, Elliott I, et al. Molecular effects of resistance elicitors from biological origin and their potential for crop protection. *Front Plant Sci*. 2014;5(NOV):1-13. doi:10.3389/fpls.2014.00655

Wu G, Liu Y, Xu Y, Zhang G, Shen Q, Zhang R. Exploring Elicitors of the Beneficial Rhizobacterium Bacillus amyloliquefaciens SQR9 to Induce Plant Systemic Resistance and Their Interactions With Plant Signaling Pathways. *Mol Plant-Microbe Interact*. 2018;(January):MPMI-11-17-0273. doi:10.1094/MPMI-11-17-0273-R

Xu S, Guerra D, Lee U, Vierling E. S-nitrosoglutathione reductases are low-copy number, cysteine-rich proteins in plants that control multiple developmental and defense responses in Arabidopsis. *Front Plant Sci*. 2013;4(NOV):1-13. doi:10.3389/fpls.2013.00430

Yamamoto S, Shiraishi S, Suzuki S. Are cyclic lipopeptides produced by Bacillus amyloliquefaciens S13-3 responsible for the plant defence response in strawberry against Colletotrichum gloeosporioides? *Lett Appl Microbiol*. 2015;60(4):379-386. doi:10.1111/lam.12382

Yang T, Rao Z, Zhang X, Xu M, Xu Z, Yang ST. Improved Production of 2,3-Butanediol in Bacillus amyloliquefaciens by Over-Expression of Glyceraldehyde-3-Phosphate Dehydrogenase and 2,3-butanediol Dehydrogenase. *PLoS One*. 2013;8(10):1-9 . doi:10.1371/journal.pone.0076149

Yang P, Zhao Z, Fan J, et al. Bacillus proteolyticus OSUB18 triggers induced systemic resistance against bacterial and fungal pathogens in Arabidopsis. *Front Plant Sci*. 2023;14(January) . doi:10.3389/fpls.2023.1078100

Yu M, Lamattina L, Spoel SH, Loake GJ. Nitric oxide function in plant biology: a redox cue in deconvolution. *New Phytol*. 2014;202(4):1142-1156. doi:10.1111/nph.12739

Yu Y, Klauda JB. Symmetric and Asymmetric Models for the Arabidopsis thaliana Plasma Membrane: A Simulation Study. *J Phys Chem B*. 2021;125(41):11418-11431. doi:10.1021/acs.jpcb.1c04704

Yu Y, Gui Y, Li Z, Jiang C, Guo J, Niu D. Induced Systemic Resistance for Improving Plant Immunity by Beneficial Microbes. *Plants*. 2022;11(3):386. doi:10.3390/plants11030386

Yun B-W, Feechan A, Yin M, et al. S-nitrosylation of NADPH oxidase regulates cell death in plant immunity. *Nature*. 2011;478(7368):264-268. doi:10.1038/nature10427

Zamioudis C, Hanson J, Pieterse CMJ. β-Glucosidase BGLU42 is a MYB72-dependent key regulator of rhizobacteria-induced systemic resistance and modulates iron deficiency responses in Arabidopsis roots. *New Phytol*. 2014;204(2):368-379. doi:10.1111/nph.12980

Zamioudis C, Korteland J, Van Pelt JA, et al. Rhizobacterial volatiles and photosynthesis-related signals coordinate MYB 72 expression in Arabidopsis roots during onset of induced systemic resistance and iron-deficiency responses. *Plant J*. 2015;84(2):309-322. doi:10.1111/tpj.12995

Zarkani A, Stein E, Röhrich C, et al. Homoserine Lactones Influence the Reaction of Plants to Rhizobia. *Int J Mol Sci*. 2013;14(8):17122-17146. doi:10.3390/ijms140817122

Zeidler D, Zähringer U, Gerber I, et al. Innate immunity in Arabidopsis thaliana : Lipopolysaccharides activate nitric oxide synthase (NOS) and induce defense genes. *Proc Natl Acad Sci*. 2004;101(44):15811-15816. doi:10.1073/pnas.0404536101

Zhang Y, Yan X, Guo H, Zhao F, Huang L. A novel protein elicitor BAR11 from Saccharothrix yanglingensis Hhs.015 improves plant resistance to pathogens and interacts with catalases as targets. *Front Microbiol*. 2018;9(APR):1-12. doi:10.3389/fmicb.2018.00700

Zhang M, Zhang S. Mitogen-activated protein kinase cascades in plant signaling. *J Integr Plant Biol*. 2022;64(2):301-34 1. doi:10.1111/jipb.13215

Zhao X, Kuipers OP. Identification and classification of known and putative antimicrobial compounds produced by a wide variety of Bacillales species. *BMC Genomics*. 2016;17(1):1-18. doi:10.1186/s12864-016-3224-y

Zipfel C, Oldroyd GED. Plant signalling in symbiosis and immunity. *Nature*. 2017;543(7645):328-336. doi:10.1038/nature22009

Chapter 2

Perception of surfactin and activation of subsequent early immune events in plant root cells

1. Abstract

Root-associated rhizobacteria produce cyclic lipopeptides that activate induced systemic resistance (ISR) against microbial infection in various plants. However, how these molecules give rise to ISR remains elusive. Here, we reveal that immunity activation in *Arabidopsis thaliana* by the well-known lipopeptide elicitor surfactin (Srf) is mediated by docking into specific sphingolipid-enriched domains and relies on host membrane deformation and subsequent activation of mechanosensitive ion channels. This mechanism is distinct from host pattern recognition receptor-mediated immune activation described so far as the main mechanism for plant immunity activation. It represents a new aspect of plant immunization by mutualistic bacteria that will contribute to a rational implementation of these beneficials into crop disease management strategies.

2. Introduction

Induced systemic resistance (ISR) is a remarkable beneficial effect that PBB provide to their host plants, with high potential for implementation in sustainable agriculture (Dimopoulou *et al*., 2021). Among ISR elicitors produced by PBB, cyclic lipopeptides (CLPs) are considered as particularly important, especially surfactin (Srf; **Figure 9**). Srf is a CLP well conserved in plant beneficial bacilli (Harwood *et al*., 2018) and has a strong elicitor potential in a wide variety of plant species, such as bean, tomato, tobacco, and *Arabidopsis thaliana* (Ongena *et al*., 2007; García- Gutiérrez *et al*., 2013; Cawoy *et al*., 2014; Rodríguez *et al*., 2018; Hoff *et al*., 2021; Altrão *et al*., 2022).

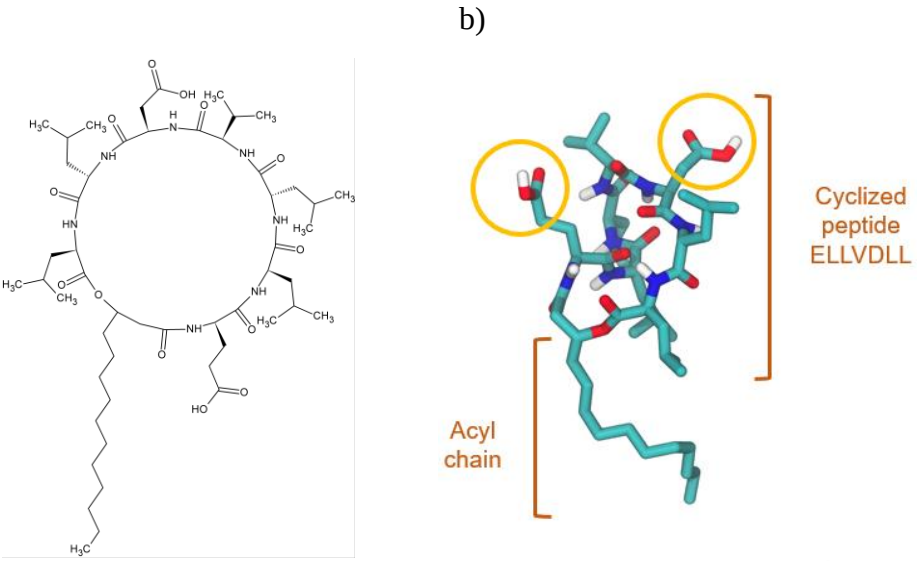

Figure 9 - Structure of Srf presented as **a)** 2D and **b)** 3D structural model of the heptapeptide Srf (C14 acyl chain homologue) in water (Gromacs v.4.5.4). Red: oxygen, white: hydrogen, dark blue: nitrogen, light blue: carbon. The polar amino acids are circled in yellow, other amino acids and the acyl chain constitute the non-polar part of the molecule.

However, intricate mechanisms of ISR, such as elicitor recognition at the plant plasma membrane (PPM) and the downstream molecular events underlying this phenomenon remain largely unknown. On the other hand,

tremendous advances have been done in the last decades on understanding how microbial pathogens are triggering immunity (DeFalco and Zipfel, 2021). Being in a constant vicinity of potentially harmful microorganisms, plants developed a surveillance system able to detect immune elicitors at nM concentrations and promptly activate immune responses (Han, 2019). Most commonly, these elicitors are classified as pathogen/microbe - associated molecular patterns (PAMPs/MAMPs, respectively), or as damage-associated molecular patterns (DAMPs) (Schellenberger *et al*., 2019). To successfully perceive these patterns, plants employ plethora of PPM embedded Pattern-Recognition Receptors (PRR). Upon association with co-receptors, PRRs activate receptor-like cytoplasmic kinases (RLCKs) such as BIK1 and its closest homolog PBL1 described as key convergent signaling hubs. This leads to phosphorylation of numerous substrate proteins and subsequent induction of a well-characterized immune response known as pattern triggered immunity (PTI) (DeFalco and Zipfel, 2021). Early hallmarks of PTI signaling in plants include apoplastic burst in reactive oxygen species ($[ROS]_{apo}$), calcium influx, medium alkalinization indicating H^+/K^+ exchange and membrane depolarization, or MAPK phosphorylation cascade (Meng *et al*., 2013; Falhof *et al*., 2016; Waszczak *et al*., 2018; Köster *et al*., 2022).

In this context, the aim of this work was to elucidate the mechanisms of perception and early immune events activation by Srf, used as a model ISR elicitor in this study. This elicitor was tested as a mix of homologues slightly differing in the length of the fatty acid tail (**Supplementary Figure 1**), as produced in nature by beneficial bacilli**.** Knowledge about ISR being sparse, the outset of this work relies on mechanisms of MAMP perception and activation of early immune events. In addition, a time-course RNAseq was conducted on *Arabidopsis thaliana* roots using the same setup previously reported for flg22 and the fungal MAMP chitin which enabled investigation of the differences between early transcriptional changes induced by Srf, as a priming agent, and the ones elicited by these MAMPs (Stringlis *et al*., 2018). Finally, a correlation of early immune responses to ISR effect of Srf was evaluated using the pathosystem *Arabidopsis thaliana* ecotype Col-0 (hereafter, *Arabidopsis*)/*Botrytis cinerea*.

3. Material and methods

3.1. Purification of surfactin, WLIP and orfamide B

Surfactin mix of homologues was purified from spent supernatant of *B. velezensis* liquid culture as previously described, with purity >99%, (Razafindralambo *et al*., 1993). The Srf mix contained C12/C13/C14/C15 homologues in the proportion 7/17/48/33%, respectively.

WLIP and orfamide B were produced using *P. putida* COW10 strain and *Pseudomonas sessilinigenes* CMR12a*Δsessilin* strain mutant (Andrić *et al*., 2021), respectively. For purification bacterial cultures were grown in casamino acid media (casamino acid 10 g/L, $MgSO_4$ 0.5 g/L, K_2HPO_4 0.3 g/L, pH 7) at 30°C for 48 h on 180 RPM continuous shaking.

After 48 h, cultures were centrifuged at 10 000 RPM for 1 h. CLPs were then extracted from cell-free supernatants by acid precipitation. To do so, supernatants were acidified to pH 2 with 4N HCl and incubated at 4°C overnight. The precipitate was collected by centrifugation (14 000 RPM, 1 h), resuspended in water and the pH was adjusted to 8 with NaOH. CLPs were extracted by liquid-liquid extraction (50:50 v/v) using butanol: ethyl acetate (30:70 v/v) as extraction solvent. The clear solvent phase was further evaporated using a rotary evaporator (water bath temperature 55°) and the dried material was resuspended in 100% ethanol. CLPs were purified by HPLC system (Agilent Series 1100; UV detector 214 nm) by collecting the peaks separated using a C18 column (Luna® Omega 5 µm, 250 x 10 mm) As mobile phase acetonitrile 80% (solution in water) acidified with trifluoroacetic acid (final concentration 0.1%), was used at 5 mL/min.

Srf was purified as a mix of homologues, whereas from orfamide only the major homologue B was purified.

Purity of the CLPs was checked by UPLC (Acquity H-class, Waters s.a., Zellik, Belgium) coupled to a single quadrupole mass spectrometer (Waters SQD mass analyzer) on an ACQUITY UPLC® BEH C_{18} 1.7 µm column. Elution was performed at 40°C with a constant flow rate of 0.6 mL/min using a gradient of acetonitrile in water both acidified with 0.1% formic acid as follows: one min at 30%, from 30% to 95% in 3.4 min and maintained at 95% for 2 min. Compounds were detected in electrospray positive ion mode by

setting SQD parameters as follows: cone voltage 120 V, source temperature 130°C; desolvation temperature 400°C, and nitrogen flow: 1000 $L.h^{-1}$.

All CLPs were conserved as powder (-20°C) and freshly prepared as a stock solution (10 mM) in 100% ethanol on the day of experiments. The 10 µM, concentration used in the experiments (with the exception of Evans blue experiment), was obtained by diluting stock solution in sterile water for plant roots, if not stated otherwise in the methods, and WI_{ca} solution (see protoplasts isolation) for protoplasts treatments. Consequently, the mock treatment contained 0.1 % of ethanol.

3.2. Plant material and growth condition

Arabidopsis thaliana ecotype Columbia (Col-0) was used as a wild-type control for all plant assays. For $[ROS]_{intra}$ and protoplasts isolation, *Arabidopsis* seeds were grown on half-strength Murashige and Skoog medium (M0222, Duchefa Biochimie; MS) medium with addition of 1% (w/v) sucrose and 14 g/L of agar, for 2 weeks.

For ISR experiments and conductivity measurements, one-week-old seedlings, germinated on half-strength MS medium containing 1% (w/v) sucrose and 14 g/L of agar, were transferred to Araponics systems containing growth solution (0.25% (v/v) FLORAMICRO®, 0.25% (v/v) FLORABLOOM®, 0.25% (v/v) FLORAGRO®; General Hydroponics®) (in ratio 1:1:1, at concentration recommended by the producer) where they were grown for four weeks.

Growth chamber conditions were constant throughout all experiments, with a photoperiod of 12 hours (100 µmol s^{-1} m^{-2}) and a temperature of 23°C.

Mutants of RKs and RLPs *fls2/efr1*, *bak1-5*, *bik1/pbl1*, *cerk1-2*, *sobir1-12*, *sobir1-13*, *lore-5*, and *rbohd*, *loh1*, *msl4/5/6/9/10*, *mca1/2* and Col-0^{aeq} mutants were described previously Nekrasov *et al*., 2009; Zhang *et al*., 2010; Schwessinger *et al*., 2011; Miya *et al*., 2007; Leslie *et al*., 2010; Ranf *et al*., 2015; Torres *et al*., 2002; Ternes *et al*., 2011; Haswell *et al*., 2008; Yamanaka *et al*., 2010; Knight *et al*., 1996; and Ranf *et al*., 2012, respectively. Additional

information about mutants can be found in the supplementary data section (**Supplementary table 1** and **8. Supplementary information**).

3.3. Root Protoplast isolation

The protoplast isolation procedure was adapted from (Yoo *et al*., 2007; Evrard *et al*., 2012). Roots from 12 to 15 days-old seedlings were cut into 1-2 mm segments and transferred to protoplasting solution (20 mM MES pH 5.7, 0.4 M mannitol, 20 mM KCl, 10 mM $CaCl_2$, 0.1 % (w/v) BSA, 1.5 % (w/v) cellulase R10 (Duchefa Chimie), 0.4 % macerozyme R10 (Duchefa Chimie)) for 4 hours at room temperature and in the dark. The suspension was then filtrated on gauze to remove root debris and the filtrate was centrifuged for 6 min at 800 RCF. The supernatant was discarded, and the pelleted protoplasts were rinsed once with W5 solution (4 mM MES pH 5.7, 154 mM NaCl, 125 mM $CaCl_2$, 5 mM KCl) before being resuspended in WI_{Ca} solution (2 mM MES pH 5.7, 0.5 M mannitol, 20 mM KCl, 2 mM $CaCl_2$) at a suitable concentration (Maintz *et al*., 2014). For experiments with surfactin, protoplasts were used right after their isolation. For experiments with flagellin, protoplasts rested overnight before being used, due to the lack of calcium response for both elicitors when treating protoplasts at the same age post isolation.

3.4. ISR evaluation

Plants grown for 4 weeks in Araponic systems were transferred in 10 mL vials. After 24 hours of rest, plants were transferred to the new vials containing 10 µM Srf or 0.1% ethanol (mock treatment) diluted in the hydroponics solution. After 24 h, plants were inoculated with *Botrytis cinerea* conidia solution. Spores were collected from *B. cinerea* strain B05.10, grown on PDA plates for 4 weeks using solution composed of 1,75 g/L KH_2PO_4; 0,74 g/L $MgSO_4$; 4 g/L glucose and 0.02% Tween 20. After spore collection the concentration was adjusted to $5x10^5$ spores per mL, and spores incubated (30° C, 180 RPM) for 8 hours. Inoculation was conducted by inoculating a drop of 3 µL of conidia solution onto seven leaves per plant, 15 plants per treatment (*loh1, mca1/2, msl 4/5/6/9/10* (experiment repeated two times) and for PRR

related mutants as indicated on the **Figure 21**). Number of spreading lesions was evaluated 96 h after post inoculation.

3.5. ROS measurements

Measurement of $[ROS]_{apo}$ in *Arabidopsis* roots was conducted according to Wyrsch *et al*., 2015. Briefly, *Arabidopsis* seedlings were allowed to germinate on half-strength MS medium for five days after which they were transferred to 24-well microplates containing liquid MS. After 10 days lower halves of the roots were isolated and two roots per well were placed in 0.1 mL of water in a microplate (96 Flat White – LumiNunc ™, ThermoFischer), and kept in the dark overnight. Before elicitation, horseradish peroxidase (Sigma-Aldrich) and luminol (Sigma-Aldrich) were added to a final concentration of 10 µg ml^{-1} and 100 µM, respectively. Luminescence measurement was conducted right upon adding the elicitor using the Spark® (Tecan) microplate reader. Measurement of $[ROS]_{apo}$ in *Arabidopsis* was conducted according to Bisceglia *et al*., 2015. The data in the graph represent value after subtraction of controls (each value = treated value - mean control).

For $[ROS]_{intra}$ measurement, 15 mm long *Arabidopsis* root segments, isolated from different plants, were placed in a well (one root/well) of a microplate (96 Flat Black – Greiner Bio-One™ CellStar™, Fischer Scientific) filled with sterile H_2O. After overnight incubation, roots were treated with 25 µM DCFH-DA (dichloro-dihydro-fluorescein diacetate; ACROS Organics) for 20 minutes, rinsed with PBS and next, wells were filled with CLP/mock solution. Experiments where $[ROS]_{intra}$ was measured after pre-treatment with the channel blocker or calcium chelator included an additional step where $LaCl_3$ (10 mM; Sigma-Aldrich) or EGTA (1mM; Sigma-Aldrich) respectively, were added three minutes before treatments. Fluorescence measurements (excitation wavelength 492 nm, emission wavelength 530 nm) were conducted by a Spark® (Tecan) microplate reader by using multiple readings (9) per well.

Data expressed as relative fluorescence increase were obtained by subtracting the fluorescence measured at the first time point from the fluorescence measured at each time points (the first time point taken as 0). The fluorescence fold increase was defined for each repeat as the ratio between the

fluorescence increase obtained at one time point in each treated repeat and the mean fluorescence increase obtained at the same time point in all mock treated repeats.

For $[ROS]_{intra}$ measurements in protoplasts, protoplasts isolated from roots of *Arabidopsis* Col-0 plants were incubated for 10 minutes with 5 µM of DCFH-DA. Then, wells of black 96-well microplates (96 Flat Black - Greiner Bio-One™ CellStar™, Fischer Scientific) were loaded with 150 µL of protoplasts solution per well. After the addition of 50 µL of four times concentrated treatment, the fluorescence was recorded every minute using Spark® microplate reader (Tecan) with an excitation filter at 485±20 nm and an emission filter at 535±25 nm. The data were processed as in roots.

3.6. Nitric oxide measurement

NO^- measurements, including measurements of NO in roots treated with NO scavenger, were conducted according to Zamioudis *et al*., 2015. Shortly, preparation of plant material was done as for the $[ROS]_{intra}$ measurements. After overnight rest, roots were incubated in a 5 µM DAF- FM DA diluted in buffered solution (10 mM Tris/HCl, pH 7.4) for 1 h in the dark. Upon this, roots were rinsed three times for 15 min each using fresh buffer (10 mM Tris/HCl, pH 7.4). The fluorescence was detected by Spark® microplate reader (Tecan), excitation 495 nm and emission at 515 nm, 9 points of measurement per well. For measurements of NO in scavenger treated plants, cPTIO (carboxy-PTIO, 2-(4-carboxyphenyl)-4,4,5,5-tetramethylimidazoline-1-oxyl-3-oxide; Sigma) was applied at 1 mM during the overnight rest after cutting the roots.

3.7. Calcium measurements with Fluo-4 AM on protoplasts

Protoplasts isolated from roots of *Arabidopsis* Col-0, *mca1/2* or *msl4/5/6/9/10* mutant were incubated for 1 hour with 5 µM of Fluo-4 AM (ThermoFischer) (from a 5 mM stock solution in DMSO). The suspension was

then centrifuged at 750 RCF and the supernatant was discarded to eliminate the remaining free fluo-4 AM. The protoplasts were resuspended in fresh WI_{Ca} solution and were incubated for 1 hour. Microplates (96 Flat Black – Greiner Bio-One™ CellStar™, Fischer Scientific) were loaded with 150 µL of protoplasts solution per well. For experiments with the channel blocker specific to mechanosensitive channels GsMTX-4 (Yoshimura *et al*., 2021; Tran *et al*., 2021), 7.5 µM of GsMTX-4 was added to protoplasts suspension 10 minutes before the loading in the wells. After the addition of 50 µL of 4 times concentrated treatment, the fluorescence was recorded every 15 seconds using a Spark® microplate reader (Tecan) with an excitation filter at 485±20 nm and an emission filter at 535±25 nm.

The values obtained were then converted as normalized fluorescence increase (F/F0) by dividing the fluorescence measured at each time points (F) by the fluorescence measured at the first time point (F0).

3.8. Medium alkalinization

Plants grown as described above were placed in 6 well microplates with roots submerged in the same hydroponic solution used in Araponics systems additionally containing Srf or mock treatment. The change in pH was measured with a pH microprobe (Jenco).

3.9. *Conductivity measurement in root medium*

Plants were grown similarly to the ones for the ISR experiments, but with prolonged growing time in Araponics (8 weeks). Next, plants were transferred in 10-times diluted Murashige and Skoog medium and rested overnight. For conductivity measurements, 35 mL of root medium was collected and supplemented with 10 µM of Srf, 0.9 % (v/v) Triton X-100 (positive control), or mock treatment. The root of one plant was then immersed in the measurement medium and conductivity was measured using a compact conductivity meter LAQUAtwin-EC-33 (HORIBA scientific). In each experiment conductivity was measured in the media of three plants per treatment separately, experiment was repeated three times.

3.10. Viability test in roots and root protoplasts

Effect of surfactin on root cells was assessed using Evan's Blue. Roots of six to eight-day-old seedlings were collected and incubated for 30 minutes in a solution containing 0.5 % of ethanol (mock treatment), 50 µM of surfactin or 0.9% of Triton X-100 (positive control). Next, roots were incubated with 0.25 % Evans blue (Sigma-Aldrich) solution for 10 min and rinsed twice with distilled water before microscopic observation.

Effect of surfactin concentration on protoplast viability was assessed with the fluorescent probe fluorescein diacetate (FDA). Protoplast suspensions were incubated with different concentrations of surfactin for 10 min and then incubated with 5µg/mL of FDA (from a stock solution of 5 mg/mL in acetone) for 10 min. Viability of protoplasts was determined with Bürker cell by counting the number of fluorescent protoplasts (viable protoplasts) divided by the total number of protoplasts.

3.11. RNAseq data analysis

Plants were grown and treated, and RNA was isolated according to Stringlis *et al*., 2018. Shortly, plant roots were treated for 0, 0.5, 1, 3 and 6 h, each treatment presented as three samples each containing eight roots from different plants. At the end of the treatment samples were flash-frozen in liquid nitrogen and stored at -80° C until the day of RNA extraction. Frozen tissue was homogenised using Eppendorf pestles, and following RNA extraction was conducted using Plant RNeasy Plant Mini Kit (Qiagen, Valencia, CA, USA).

The tool Trimmomatic v0.39 (Bolger *et al*., 2014) was used to trim the raw RNA-seq reads. Quality control on the trimmed reads was performed using FastQC v0.11.8 (Babraham Bioinformatics). We mapped the trimmed reads to the *Arabidopsis thaliana* reference genome (TAIR-10.1) using HISAT2 (Kim *et al*., 2015). The uniquely mapped reads to the annotated reference genome are estimated as 88.46%. SAMtools v1.9 (Li *et al*., 2009) was applied to generate the required BAM files and their indices. The command line tool featureCounts (Liao *et al*., 2014) was employed to calculate the read counts using the latest *Arabidospsis* genome annotation (Araport11_GTF_genes_transposons). Genes with few read counts (<20) were

filtered out before further analysis. DESeq2 pipeline (10.1186/s13059-014-0550-8) was used to conduct differential expression analysis with significance parameters set to $p<0.05$ and log2-fold-change > 2.

Genes identification was done using VirtualPlant (Katari *et al*., 2010), specificity of DEGs for certain treatments was done using conditional formatting in Excel.

3.12. Liposome preparation

1-palmitoyl-2-linoleoyl-sn-glycero-3-phosphocholine (PLPC), sitosterol (Sito) and D-glucosyl-ß-1,1'-N-palmitoyl-D-erythro-sphingosine (GluCer) were purchased from Avanti Polar Lipids and used without further purification.

Large unilamellar vesicles (LUVs, liposomes) were prepared for Isothermal titration calorimetry (ITC) and Laurdan generalized polarization experiments. The different lipid mixtures (PLPC (for ITC), PLPC-Sito (80-20 molar ratio) (for ITC), PLPC-GluCer (80-20 molar ratio) (for ITC) and PLPC-Sito-GluCer (60-20-20 molar ratio) (for ITC and Laurdan generalized polarization)) were dried from a chloroform/methanol (Scharlau Lab Co.) (2/1; v/v) solution under reduced pressure in a rotary evaporator at 30°C and then kept under vacuum overnight. The dried lipid films were then hydrated in Tris 10 mM NaCl 150 mM buffer at pH 8.5 or in MES 10 mM NaCl 150 mM buffer at pH 5.8 (to 1 mM of lipid for Laurdan analysis) during 1 h at 45°C with vortex mixing applied every 15 min and then subjected to five freeze/thaw cycles.

The dispersions were finally extruded fifteen times through two stacked Nuclepore 100 nm polycarbonate filters using a Lipex Biomembranes (Vancouver, BC) extruder to obtain LUVs (105.2 ± 5.1 nm). The average size of LUVs was determined at 25°C by dynamic light scattering (DLS) method using a Zetasizer nano ZS (Malvern instruments, UK) with a He–Ne laser source at a wavelength of 633 nm. The scattered light intensity was measured at a scattering angle of 173°.

3.13. ITC analysis

ITC analyses were performed with a VP-ITC Microcalorimeter (Microcal, Northampton, USA). The calorimeter cell (Volume of 1.4565 mL) was filled with a 10 µM (below the CMC concentration) surfactin solution in buffer (Tris 10 mM, NaCl 150 mM at pH 8.5). The syringe was filled with a suspension of LUVs at a lipid concentration of 5 mM. A series of 10 µL injections was performed at constant time intervals (6 min) at 25°C. The solution in the titration cell was stirred at 305 RPM. Prior to each analysis, all solutions were degassed using a sonicator bath. The heats of dilution of liposomes were determined by injecting liposomes in buffer and subtracted from the heats determined in the experiments. Data were processed by software Origin 7 (Originlab, Northampton, USA). All measurements were repeated at least three times with two different vesicle preparations.

3.14. Hypermatrix calculation

The Hypermatrix method (Lins *et al*., 1999; Brasseur *et al*., 1987) is a simple docking method that allows for the calculation of the interaction between a molecule and lipids. The molecule of interest (surfactin in this study) is fixed at the center of the system and oriented at a hydrophobic (pho)/hydrophilic (phi) interface using the TAMMO procedure (Brasseur *et al*., 1987). The lipid molecule is also oriented at the pho/phi interface and is positioned around the central molecule by rotations and translations (more than 10 million positions were tested). For each position, an energy value was calculated, according to a home-designed force field (Lins *et al*., 1995). The energy values together with the coordinates of all assemblies were stored in a matrix and classified, according to decreasing values.

The first stable match was considered as the best assembly between the two molecules.

3.15. Molecular dynamics simulation

Surfactin SC14 have been studied by molecular dynamics (MD) in presence of a membrane of PLPC and PLPC:GluCer:Sitosterol (60:20:20) with the

Gromacs v4.5.4 software (Hess *et al*., 2008). Coarse-grained simulations have been carried out first for peptide insertion and building of the lipid membrane. Models were converted to a CG representation suitable for the MARTINI 2.1 forcefield (Marrink *et al*., 2007) with the Martinize script and a coarse-grained peptide was placed over the membranes with the insane tool (Wassenaar *et al*., 2015). This first insertion was used to place afterwards 9 surfactins in both leaflets at the same membrane level. Water particles were then added as well as ions to neutralize the system. A 2000-steps steepest-descent energy minimization was performed to remove any steric clashes. An equilibration of 100 ns with a 20fs time step has been carried on. Temperature and pressure were coupled at 300 K and 1 bar using the weak coupling Berendsen algorithm (Berendsen *et al*., 1984) with $\tau T = 1$ ps and $\tau P = 1$ ps. Pressure was coupled semi-isotropically in XY and Z. Non-bonded interactions were computed up to 1.2 nm with the shift method. Electrostatics were treated with $\varepsilon = 15$. The compressibility was 10^{-5} (1/bars). The system was then transformed to an atomistic resolution with backwards (Wassenaar *et al*., 2014). Atomistic simulations have been performed with the GROMOS96 54a7 force field (Schmid *et al*., 2011; Poger *et al*., 2010a; Poger *et al*., 2010b). Parameters of the ester bond between the acyl and LEU7 residues and for the acyl chain were taken from the GROMOS96 54a7 force field (Oostenbrink *et al*., 2004). Parameters for the GluCer was taken from Lopez *et al*. 2013. All the systems studied were first minimized by steepest descent for 2000 steps. Then NVT and NPT equilibrations were carried on for 0.1 and 1 ns. The protein was under position restraints and periodic boundary conditions (PBC) were used with a 2 fs time step. Production runs were performed for 1µs. All the systems were solvated with SPC water (Berendsen *et al*., 1981) and the dynamics were carried out in the NPT conditions (300 K and 1 bar). Temperature was maintained by using the Nose-Hoover method (Nosé *et al*., 1984) with $\tau T = 0.5$ ps and a semiisotropic pressure was maintained by using the Parrinello-Rahman barostat (Parrinello *et al*., 1981) with a compressibility of 4.6×10^{-5} (1/bar) and $\tau P = 5$ ps. Nonbonded interactions were evaluated using a twin-range cutoff scheme. Interactions within the shorter range cutoff (0.8 nm) were calculated every step, whereas interactions within the longer cutoff (1.4 nm) were updated every 5 steps, together with the pair list. In all the simulations, a reaction-field correction was applied to the electrostatic interactions beyond the long-range cutoff (Tironi *et al*., 1995) using a relative dielectric permittivity constant εRF of 62. Bond lengths were maintained with the LINCS

algorithm (Hess *et al*., 1997). The trajectories were performed and analyzed with the GROMACS 4.5.4 tools as well as with homemade scripts and softwares, and 3D structures were analyzed with both PYMOL (DeLano Scientific, http://www.PyMOL.org) and VMD softwares (Humphrey *et al*., 1996).

3.16. Neutron Reflectivity (NR)

For deuterated surfactin production, *Bacillus velezensis* GA1 was cultured in 20 mL Liquid LB broth supplemented with 1g/L of deuterated Leucine (Cambridge isotope) for 24 h at 30°C under agitation. Extraction of surfactin was performed by liquid-liquid extraction using 20 mL of ethyl acetate/butanol (70:30 v/v). Solvents were evaporated under rotary evaporation and powder was resuspended in 2 mL of 100% ethanol prior to UPLC (Agilent 1290 Infinity II) purification by collecting each deuterated C15 surfactin peak. 10 µL extract was separated using C18 column (C18 Acquity UPLC BEH column; 2.1 × 50 mm × 1.7 µm; Waters) An isocratic 0.2 ml/min flow with 75% acetonitrile/water (acidified with 0.1% formic acid) was applied for 10 min before raising up to 100% acetonitrile for 5 min and going back to initial ratio before the next injection. Purified deuterated surfactin structure was confirmed by LC-MS/MS using the same LC method coupled with an accurate mass detector (Jet Stream ESI-Q-TOF 6530) in positive mode with parameter set up as follows : parameters: capillary voltage: 3.5 kV; nebulizer pressure: 35 psi; drying gas:8L/min; drying gastemperature:300°C; flow rate of sheath gas: 11 L/min; sheath gas temperature: 350°C; fragmentor voltage: 175 V; skimmer voltage: 65 V; octopole RF: 750 V. Collision energy 40V. Quantification was performed by comparing peak area of purified compound with the peak area of a commercial standard (Lipofabrik, Villeneuve d'Ascq). The relative amounts of the deuterated surfactin C15 is presented in **Table 2**. Lipid bilayer (ternary mixture of PLPC-Sito-Glucer – 60-20-20 molar ratio) depositions on silicon for NR measurements were obtained by injecting directly in the measuring cell (6 mL) at room temperature the extruded liposomes prepared as for x-ray investigation but to the final concentration of 0.5mg/ml, according to the procedures described in Rondelli *et al*., 2017.

Neutron reflectivity data were acquired at the MARIA neutron reflectometer (Mattauch *et al*., 2018) operated by Jülich Centre for Neutron Science at Heinz Maier-Leibnitz Zentrum in Garching (Germany), using custom temperature-regulated liquid cells (Koutsioubas *et al*., 2016). The measurements were performed using two different wavelengths, 10 Å for the low-q region and 5 Å for the high-q region up to 0.25 $Å^{-1}$, with a 10% wavelength spread.

Table 2 - Relative amounts of the deuterated Srf C15 variant isotopes produced, the molecular formula of their fatty acid chain and peptide cycle.

	1 deuterated entity		**2 deuterated entities**		**3 deuterated entities**		**Not deuterated**
	FA non deut + 1 Leu deut	***FA deut + 4 Leu non-deut.***	***FA not deut + 2 Leu deut***	***FA deut + 1 Leu deut***	***FA not deut + 3 Leu deut***	***FA deut + 2 Leu deut***	***FA not deut + Leu not deut***
Relative amount	0.261	0.100	0.260	0.077	0.222	0.047	0.034
FA	$C_{12}H_{25}$	$C_{12}H_{16}D_9$	$C_{12}H_{25}$	$C_{12}H_{16}D_9$	$C_{12}H_{25}$	$C_{12}H_{16}D_9$	$C_{12}H_{25}$
Cyclic peptide	$C_{41}H_{59}N_7O_{13}D_9$	$C_{41}H_{68}N_7O_{13}$	$C_{41}H_{50}N_7O_{13}D_{18}$	$C_{41}H_{59}N_7O_{13}D_9$	$C_{41}H_{41}N_7O_{13}D_{27}$	$C_{41}H_{50}N_7O_{13}D_{18}$	$C_{41}H_{68}N_7O_{13}$

The change of solvent contrast in the liquid cells was performed using a combination of valves and a peristaltic pump, at small flow rates ~ 0.5 ml/min. In a reflectivity experiment a grazing beam is sent to the sample and the reflected intensity is collected as a function of the reflection angle momentum transfer perpendicular to the interface qz ($qz = 4 \lambda \sin \vartheta /2$, where ϑ and λ are the angle of the incident beam and wavelength, respectively). The technique allows to get information about the sample cross structuring in a non-invasive way (Penfold *et al*., 1990; Rondelli *et al*., 2016). The silicon oxide layer, the water layer between the silicon oxide and the membrane and the different hydrophilic and hydrophobic layers of the lipid membranes have been modelled as defined layers with a proper thickness, compactness, and mean composition (and therefore contrast to neutrons). Reflectivity has been measured from the silicon supports and the samples in different water solutions (H_2O and D_2O - Sigma Chemical Co). After bare membrane characterization in two solvents, the Tris 10 mM NaCl 150 mM buffer at pH 8.5 solution was injected into the cell and NR measure was performed. Finally, 2 µg of surfactin in Tris HCl buffer at pH 8.5 have been injected into the cell, to the final 95:5 membrane:surfactin molar proportion. NR measurements have been performed on this system after 30 minutes incubation. Data have been analyzed by the

MotoFit program (Nelson *et al*., 2006). Data relative to the same system measured in different water contrasts have been analyzed by contemporary fits.

The scattering length density of the mixture used (**Supplementary Table 2**) has been calculated according to the table 2 accounting for relative molar proportions, by considering a volume of 1143 $Å^3$ for the hydrophilic portion and of 373 $Å^3$ for the fatty acid (FA) (Shen *et al*., 2010a; Shen *et al*., 2010b).

3.17. Laurdan polarization on root protoplasts and liposomes

Protoplasts suspension (1-2 10^5 protoplasts / mL) or 100 µM LUVs preparation was incubated with 2 µM of Laurdan (Sigma-Aldrich) for 1h. Then, wells of black 96-well microplates (Greiner Bio-One™ CellStar™, Fischer Scientific) were loaded with 100 µL of protoplasts or LUVs solution per well. The fluorescence was recorded using Spark® microplate reader (Tecan) by performing a fluorescence scan between 405 and 520 nm with an excitation wavelength at 360 nm. The fluorescence was recorded once before treatment and at 1, 6, 11, 16, 21 minutes after the addition of 25 µL (for protoplasts) or 100 µL (for LUVs) of treatment. The treatments were prepared in the buffer of protoplasts (WI_{Ca} solution) or LUV buffer respectively with a concentration taking into account the dilution factor occurring at the addition of treatment into 100 µL of protoplasts or LUVs solution (factor 5 for protoplasts, so concentration 5-times more concentrated than the final concentration and factor 2 for LUVs, so concentration 2-times more concentrated than the final concentration). The generalized polarization (GP) was defined as $GP = \frac{(I_{440nm} - I_{490nm})}{(I_{440nm} + I_{490nm})}$, were I_{440nm} and I_{490nm} represents the blank-subtracted fluorescence intensities at emission wavelengths of 440 nm and 490 nm respectively. Variation of GP (ΔGP) is defined as the subtraction of GP measured at each time point following treatment and GP measured before treatment.

3.18. Statistical methods

Statistical details of experiments are specified in the figure legends. All statistical analyses were performed in GraphPad Prism 8.0.1.

4. Results

4.1. ISR potential of Srf in Arabidopsis

In this study Srf was used as a mix of naturally produced homologues slightly differing in the length of the fatty acid tail (**Supplementary Figure 1**), at the minimal active concentration previously determined of 10 µM (Cawoy *et al*., 2014)**.** When applied as a root treatment on *Arabidopsis*, Srf successfully triggered ISR and significantly reduced leaf infection of *B. cinerea* (**Figure 9**). Therefore, we used Srf/*Arabidopsis* root cells as a model to further investigate the molecular mechanisms determining perception and immunity stimulation.

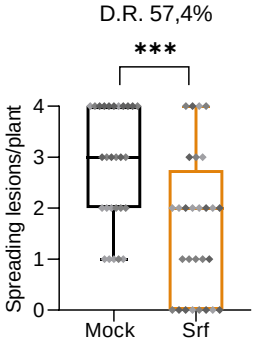

Figure 10 - Disease incidence caused by *Botrytis cinerea* in *Arabidopsis* Col-0 plants pre-treated with Srf (10 µM) compared to mock control (n=28 replicates from three independent experiments). The box plots encompass the 1st and 3rd quartiles, the horizontal line indicates the median, and error bars represent ± SD . Disease reduction (D.R.) is calculated from the mean values of both treatments. Significant difference ***P<0.001, two-tailed t-test.

4.2. Early immune events activated by Srf

In order to better understand the initial responses of the plant to Srf, a thorough investigation of the activated early immune events was firstly conducted.

4.2.1. *Srf triggered production of reactive oxygen species*

Even though a burst in apoplastic ROS ($[ROS]_{apo}$) is almost invariably associated with PTI (Waszczak *et al*., 2018), we did not observe it in *Arabidopsis* root cells treated with Srf (**Figure 10a**). Moreover, Srf-mediated ISR against *B. cinerea* was fully conserved in the *rbohD* mutant lacking functional plasma membrane NADPH oxidase (RBOHD) responsible for such $[ROS]_{apo}$ burst (**Figure 10b**) indicating that this enzyme is not required for Srf's activity (Torres *et al*., 2002; Morales *et al*., 2016).

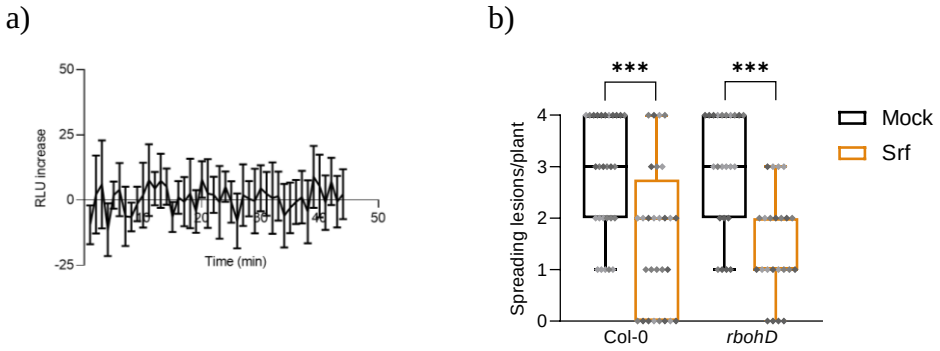

Figure 11 - Involvement of apoplastic ROS burst in Srf triggered immune responses. **a)** Kinetics of $[ROS]_{apo}$ burst measured in relative luminescence units (RLU) in *Arabidopsis* roots upon perception of Srf (10 µM). Means and SD were calculated from data obtained in two independent experiments (n=6). **b)** *Botrytis cinerea* disease incidence in *Arabidopsis* plants and *rbohD* mutant, mock or Srf pre-treated (10 µM) (n=28 for Col-0 and n=23 for *rbohD*). The box plots encompass the 1st and 3rd quartile, the whiskers extend to the minimum and maximum points, and the midline indicates the median. Asterisks indicate significant difference (***P<0.001, two-way ANOVA and Sidak's multiple-comparison post-hoc test).

On the other hand, Srf triggered a fast and consistent increase in intracellular ROS ($[ROS]_{intra}$) in *Arabidopsis* root tissues revealed by loading with the fluorescent probe DCFH-DA. The increase was significant at concentrations of 5, 10 and 20 µM, where the rapidity and intensity of the response increased with the increase of concentration (**Figure 12a**). This $[ROS]_{intra}$ burst is also observed in the *rbohD* mutant (**Figure 12b**), indicating that it is not caused by

the uptake of apoplastic ROS via aquaporins as it could be the case for the much lower response to flg22 (**Figure 12c**).

a)

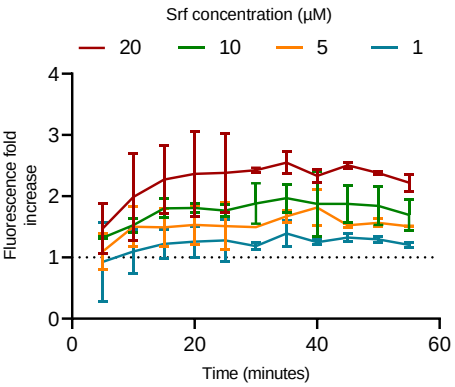

b)

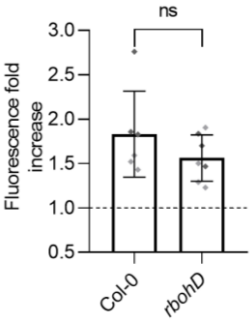

c)

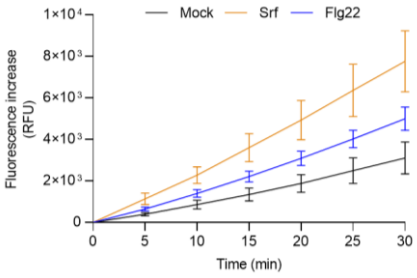

Figure 12 - Srf triggered production of intracellular ROS. **a)** Dose-dependent $[ROS]_{intra}$ production induced by Srf in *Arabidopsis* roots. Graph represents grouped data of two independent experiments (each n=3). **b)** $[ROS]_{intra}$ accumulation in Col-0 and *rbohD* roots following Srf (10 µM) treatment (30 minutes post treatment). Data are from two independent experiments (each n=3 or n=4) with differently shaded grey values of the symbols. ns indicates that there is no significant difference (two-tailed t-test). Values represented in **a)** and **b)** are obtained as fold increase in fluorescence values ± SD, after the addition of Srf compared to mock-treated. **c)** $[ROS]_{intra}$ accumulation in *Arabidopsis* roots following treatment with 10 µM Srf, 1µM flg22 or mock-treated measured with the fluorescent probe DCFH-DA. Data represents one (n=4) out of 2 independent experiments showing similar results.

Besides on *Arabidopsis*, Srf also induced only $[ROS]_{intra}$ in tomato roots with the same minimal active concentration of 5 µM (**Figure 13a,b**).

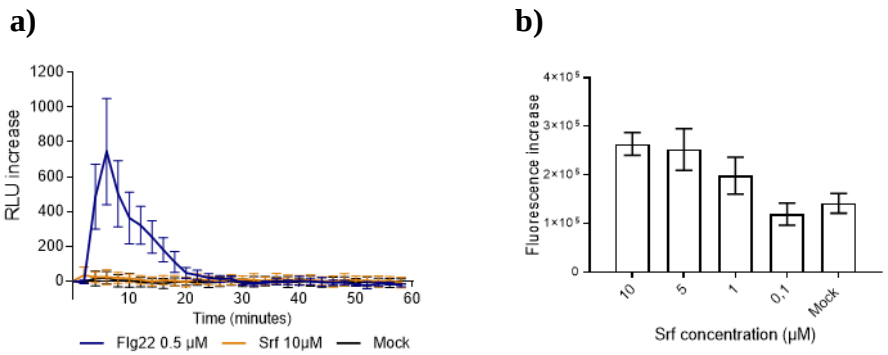

Figure 13 - Srf triggered ROS production in tomato roots. **a)** $[ROS]_{apo}$ measured in tomato roots upon the treatment flagellin 22 (Flg22) and surfactin (Srf) using luminol assay measuring relative luminescence units (RLU). **b)** Dose response of $[ROS]_{intra}$ triggered by Srf.

Interestingly, the data showed that the cell free supernatant of efficient Srf producer *Bacillus velezensis* GA1 elicits significantly higher $[ROS]_{apo}$ compared to a supernatant of its mutant not able to produce Srf (Δ*srf*) (**Figure 14a)**. This response is however restored to some extent by supplementing Δ*srf* supernatant with 10 µM of purified Srf (**Figure 14b)**. This suggests that even though it does not induce $[ROS]_{apo}$ (**Figure 13a**), Srf can enhance the burst induced by other elicitors.

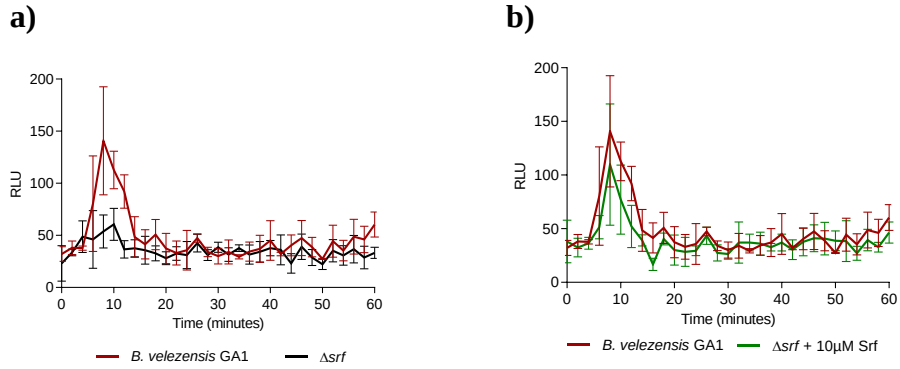

Figure 14 - Enhanced $[ROS]_{apo}$ burst in tomato roots in presence of Srf.

4.2.2. *Srf triggered production of reactive nitrogen species*

Production of intracellular nitrogen oxide (NO^-) by plant cells upon Srf treatment was detected using fluorescent probe DAF-FM DA, and the production was verified by using NO^- scavenger – cPTIO (Mur *et al*., 2011). In addition, to gain more information on the pathway of production *nia1nia2 Arabidopsis* mutant (lacking enzyme for reductive pathway intracellular synthesis; Chapter 1, section 3.2.2.) was used. The results showed a rapid NIA1NIA2 independent intracellular NO^- production upon Srf application successfully lowered by cPTIO (**Figure 15a-c**).

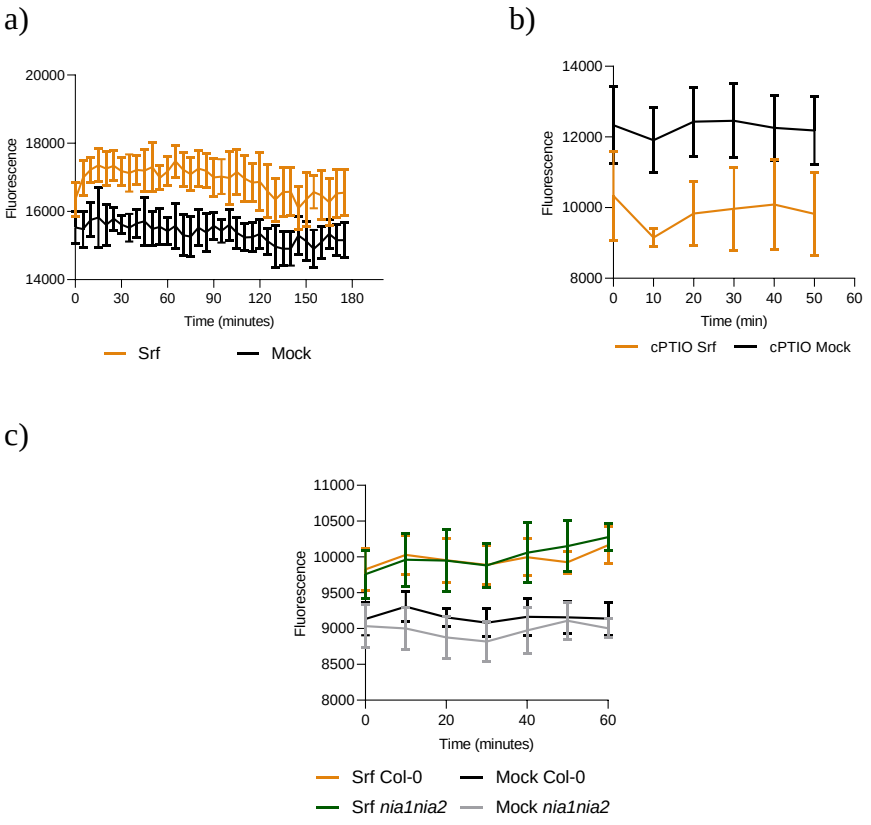

Figure 15 - Srf triggered production of NO^-. **a)** A rapid production of NO^- activated upon Srf treatment. **b)** Abolishment of Srf triggered NO^- burst in roots pretreated with NO^- scavenger cPTIO. **c)** Conserved production of NO^- in Arabidopsis mutant lacking NIA1NIA2 enzyme. **a, b, c** - each graph represents one out of three experiments (each n=4) showing similar results.

4.2.3. *Measurements of cytosolic calcium in Arabidopsis roots treated with Srf*

Besides oxidative burst, cytosolic Ca^{2+} ($[Ca^{2+}]_{cyt}$) spikes are also one of the early and key cellular events in immunity signaling in plants. Calcium elevations are deciphered in plant cells by sensor binding proteins which further activate downstream cascade leading to specific plant response (Köster *et al*., 2022). However, studies on roots of *Arabidopsis* line carrying the calcium reporter aequorin (Col-0^{AEQ}) have shown that Srf does not induce elevations in $[Ca^{2+}]_{cyt}$ (**Figure 16**).

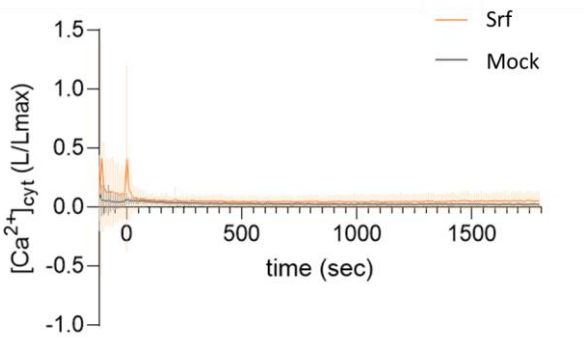

Figure 16 - $[Ca^{2+}]_{cyt}$ measured in Srf treated roots. Data of one representative experiment, out of two showing the same trend.

4.2.4. *Srf's influence on ion fluxes*

Being important indicators of plant immunity activation, Srf's impact on other ion fluxes was also tested. By following pH changes of *Arabidopsis* root media, we indeed observed medium alkalinization occurring within minutes upon Srf treatment (**Figure 17**). This possibly indicates activation of H^+ pumps leading to membrane depolarization (Falhof *et al*., 2016).

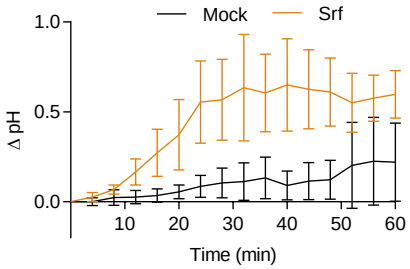

Figure 17 - pH of *Arabidopsis* root medium following mock treatment or addition of 10 µM Srf. Values on the graph are normalized to pH of the first time point ± SD and are from one representative experiment (n=4) out of 2 independent experiments showing similar results.

On the other hand, no significant increase in conductivity was measured in the medium following Srf treatment (**Figure 18**), indicating that the lipopeptide does not cause a massive electrolyte leakage that could be a sign of affected PPM integrity.

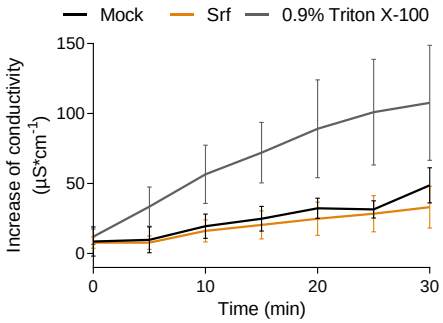

Figure 18 - Effect of Srf ion leakage in *Arabidopsis* roots. Conductivity variation in Col-0 root medium following Srf (10 µM) or mock treatment. The values represent eight biological replicates from three independent experiments.

4.3. Early root transcriptional changes induced by Srf

In addition to the studying early immune events, we also wanted to evaluate the initial transcriptional reprogramming occurring within hours in cells of *Arabidopsis* roots treated with Srf. Since Srf does not induce typical PTI-

associated $[ROS]_{apo}$ and $[Ca^{2+}]_{cyt}$ elevations, we postulated that the transcriptome analysis of roots treated with well-known MAMPs or Srf could help us to better understand to what extent plant responses to these elicitors differ. We explored these early changes via time course RNAseq analysis (30 min, 1h, 3h and 6h post treatment) using the same setup previously reported for flg22 and the fungal MAMP chitin (Stringlis et al., 2018). Data revealed a relatively low transcriptional response to Srf elicitation over all sampling times with a total of 564 differentially expressed genes (DEGs, Log_2 Fold Change > 2, $p<0.05$) compared to approximately 5000 DEGs and 2000 DEGs reported upon flg22 and chitin treatment respectively (Stringlis et al., 2018). While MAMPs mainly up-regulate early responsive genes, an almost equal number of up- and down-regulated DEGs were observed upon Srf treatment at all time points (**Figure 19**).

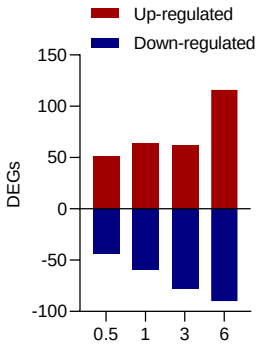

Figure 19 - Number of DEGs (Log_2 Fold Change > 2, P<0.05) in *Arabidopsis* root cells determined via RNAseq for each time point in response to Srf treatment (10µM).

Compared to flg22 and chitin, about half (47,9% and 58%, respectively) of the transcriptional changes are specific for Srf elicitation (**Figure 20a**; Stringlis et al., 2018). Strikingly, almost all of the downregulated genes that are not specific to Srf are oppositely – upregulated by flg22 and chitin (**Figure 20a)**.

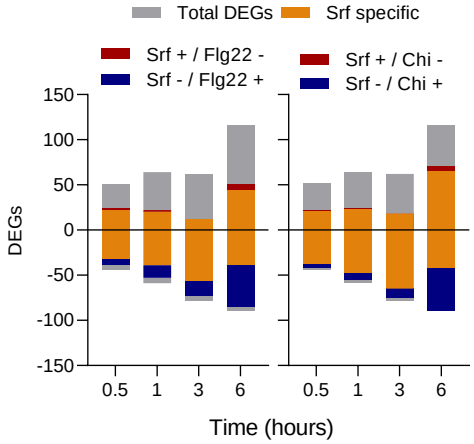

Figure 20 - Comparison of root transcriptional changes induced by Srf and well known MAMPs flg22 and chitin. The data was compared with those reported for DEGs in response to flg22 and chitin (Chi) using previously published data (Stringlis *et al*., 2018) and bars are subdivided by the number of genes specifically responding to Srf and by the number of genes differentially (oppositely) regulated by Srf and the two MAMPs (**Supplementary table 3 and 4** for the list of genes represented in the graphs).

Noteworthy is also that the most downregulated DEGs are usually Srf specific, which is not the case with highly upregulated DEGs, which are usually not Srf specific (**Figure 21a,b**).

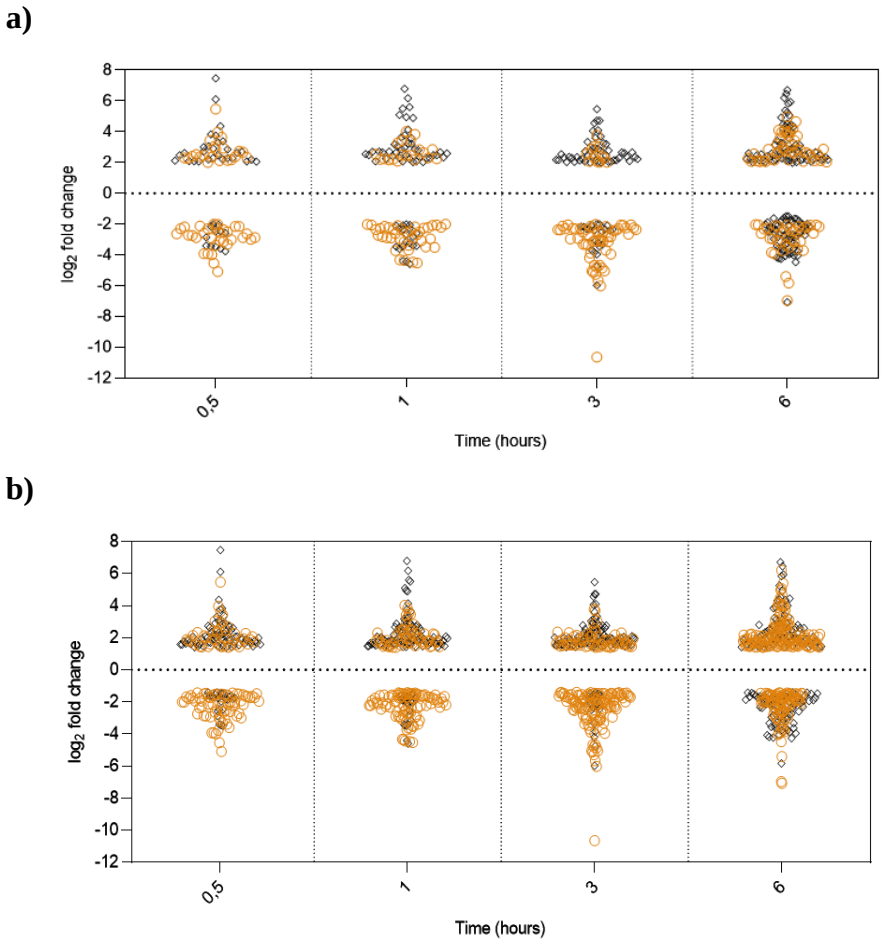

Figure 21 - Comparison of root transcriptional changes induced by Srf and well known MAMPs flg22 and chitin **a) flg22 b) chitin** Data obtained with the same comparison as in **Figure 20**, but represented only in terms of Srf specificity and log_2 fold changes values. Srf specific DEGs are represented as orange circles, DEGs found in chitin/flg22 treated roots as black rhombus.

Considering DEGs involved in immune signaling and defense mechanisms, additional differences can be observed between Srf and MAMP treatment. RNAseq data showed that genes related to calcium signaling, such as calcium binding hands/proteins, are at almost all instances downregulated upon Srf treatment throughout the time frame tested, whereas they are mostly upregulated by chitin and flg22 (Stringlis *et al.*, 2018; **Figure 22**). This possibly indicates that Srf could have an influence on downstream signaling

activated by $[Ca^{2+}]_{cyt}$ elevation. The expression of genes typically associated with $[ROS]_{apo}$ burst such as the *RBOHD* or some peroxidase genes are not as strongly modulated by Srf as with flg22 (**Figure 22**). Additionally, within the investigated time frame, Srf does not upregulate genes linked to MAPK (Meng et al., 2013) phosphorylation cascade nor other common defense-related markers, such as pathogenesis-related (PR) proteins or receptor-like kinases, and callose deposition and lignification genes (**Figure 22**). In summary, immunity stimulation by Srf does not lead to major changes in the expression of genes involved in signaling and defense by contrast to PTI, which is associated with substantial transcriptional reprogramming. **(Figure 22).**

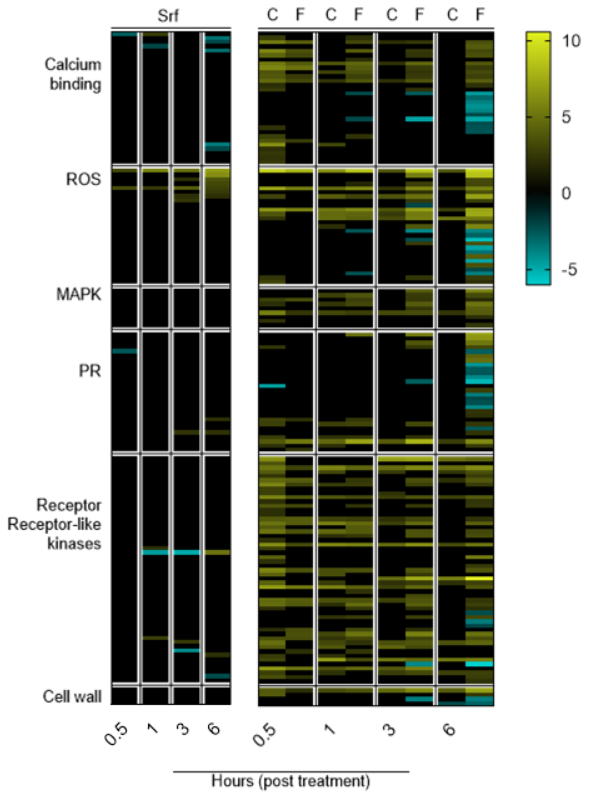

Figure 22 - Heatmap of the expression of genes putatively associated with plant immune responses (listed in **Supplementary Table 5**) that were modulated upon Srf treatment (S, left) (10 µM) and compared with their expression in response to flg22 and chitin (F and C respectively, right) based on published data (Stringlis *et al.*, 2018). Color scale represents Log_2 FC (> 2, P<0.005).

4.4. Perception of Srf by plant cells

4.4.1. Estimation of the involvement of well-known PRRs in Srf perception

So far, immunity elicitation was exclusively described as an elicitor/receptor dependent interaction (DeFalco and Zipfel, 2021). Therefore, to evaluate their involvement in the perception of Srf, we used a selected set of *Arabidopsis* mutants lacking receptors, coreceptors, and kinases commonly described as

key players in plant immunity (Chapter 1, section 3.7; **Supplementary table 1** for more information about the mutants).

First, considering that Srf has both a peptidic moiety and a fatty acid tail, the *Arabidopsis* mutants *fls2/efr1* and *lore-5* were tested. The *fls2/efr1* mutant lacks functional PRRs recognizing bacterial proteinaceous immunogenic patterns such as flg22, perceived by FLS2, and elf18, a peptide derived from its N-terminus Tu elongation factor, perceived by EFR (Jeworutzki *et al*., 2010). The *Arabidopsis lore-5* mutant on the other hand lacks functional PRR for recognition of acyl chain epitopes such as medium chain 3-hydroxy fatty acids (Ranf *et al*., 2015). In both cases Srf ISR-eliciting potential was fully conserved (**Figure 23**). Furthermore, Srf elicitation is also not significantly affected in mutants lacking co-receptors required for proper functioning of a wider range of PRRs detecting immunogenic peptides such as Pep1 (Liang *et al*., 2018), nlp20 (Albert *et al*., 2015) and IF1 (Fan *et al*., 2022) nor in the *bik1/pbl1* double mutant lacking RLCKs that act downstream of the PRR-co-receptor complexes (Blake *et al*., 2021) (**Figure 23**). Although we only tested a small subset of the multitude of PRRs potentially expressed in *Arabidopsis* and although early cellular signaling may be BIK1/PBL1-independent (Wan *et al*., 2019), these results strongly suggest that *Arabidopsis* does not sense Srf via PRR-type cell surface sentinels. This is in accordance with previous data from tobacco, which showed that Srf is still active on protease-treated cells and that there is no refractory state upon repeated Srf treatment unlike typically observed for PTI (Henry *et al*., 2011).

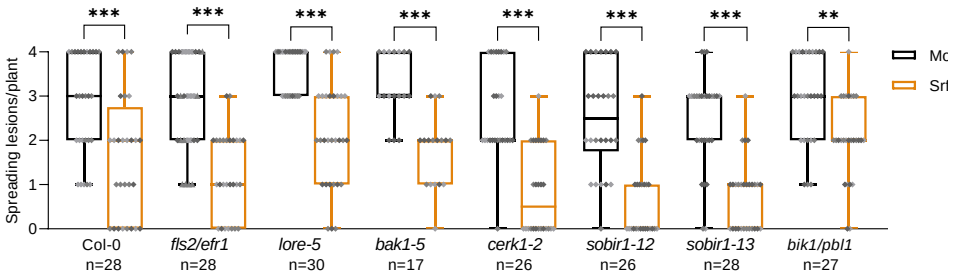

Figure 23- Disease incidence of *B. cinerea* in infected plants pre-treated with 10 µM Srf or mock-treated at the root level in *Arabidopsis* (Col-0 plants) or mutants lacking functional receptors required for the detection of bacterial proteinaceous immunogenic patterns (*fls2/efr*) or acyl chain epitopes (*lore*-5), co-receptors (*bak1*-5, *cerk1*-2, *sobir1*-12 and *sobir1*-13), or receptor-like cytoplasmic kinase (*bik1/pbl1*). Data are represented as in Figure 10. Asterisks indicate statistically significant differences to the mock treatment (***P*<0.01, ****P*< 0.001, two-way ANOVA and Sidak's multiple comparison test). Data presented are from three independent experiments (presented as differently shaded grey values).

4.4.2. *Potential of Srf to interact with PPM lipids*

As shown above, the molecular processes underlying immune activation by Srf are quite different from those described in the literature. Based on this, we postulated that the mechanism by which plant cells perceive the lipopeptide may differ from the PRR-based MAMP sensing.

Due to their amphipathicity (**Figure 9b**), CLPs readily interact with biological membranes, causing pore formation and membrane disruption responsible for their antimicrobial activities (Geudens and Martins, 2018; Zakharova et al., 2019; Gilliard *et al*., 2023). Considering that cell viability assays confirmed that Srf is not toxic for *Arabidopsis* root cells (**Supplementary Figure 2**), such an adverse effect on plant membranes is not expected, but we hypothesized that Srf perception by root cells might primarily rely on its interaction with the lipid phase of the PM.

Plant PM lipid phase is constituted out of three lipid classes laterally and transversally unevenly distributed within the two layers. Lipids dominating the cytosolic, inner layer are phospholipids, whereas sphingolipids are primarily located on the outer leaflet, where they assemble with sterols thus forming

nano-domains (**Figure 1**; Cacas *et al*., 2016; Rondeli *et al*., 2021; Yu and Klaud, 2021). In this study PLPC (1-Palmitoyl-2-linoleoyl-sn-glycero-3-phosphocholine) – ß-sitosterol – glucosylceramide (GluCer), were used as phospholipids – sterols – sphingolipids respective representatives. *In silico* docking simulation first revealed a more favorable interaction of Srf with GluCer and GIPCs than with the other typical PPM lipids PLPC and ß-sitosterol (**Figure 24**).

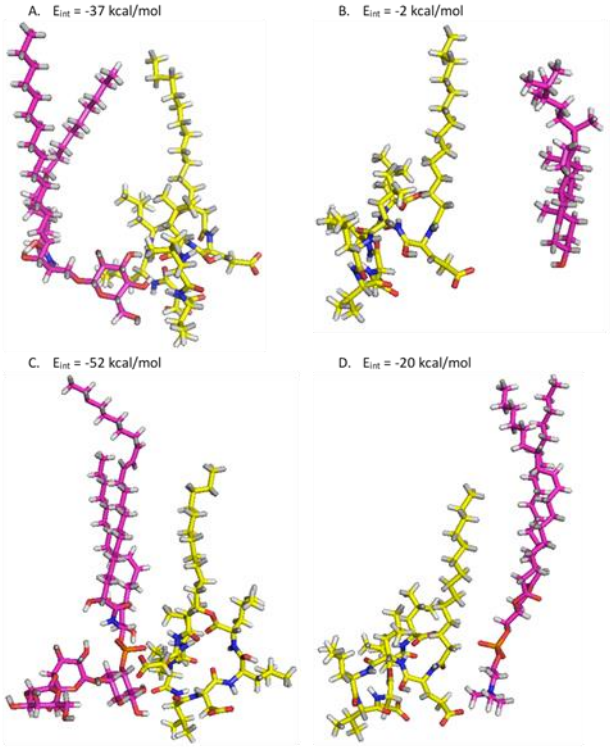

Figure 24 - Srf's potential to interact with lipids of PPM mimicking models: In silico docking simulation of the interaction between Srf and glucosylceramide (A), sitosterol (B), GIPC (C) and PLPC (D) lipids and their associated energy of interaction (Eint). A lower Eint value indicates a more favorable interaction. Hydrogen, oxygen and phosphate atoms are respectively represented in grey, red and blue. Carbon atoms of Srf are in yellow and carbon atoms of GluCer, Sito and PLPC are in pink.

In support of a preferential interaction with sphingolipids, molecular dynamic (MD) simulation on the same ternary lipid system showed the specific insertion of Srf in the vicinity of GluCer molecules or in GluCer-enriched areas

in the membrane (**Figure 25a**). To test this experimentally, we generated biomimetic liposomes using commercially available GluCer, PLPC and ß-sitosterol. Isothermal titration calorimetry performed on liposomes with increasing composition complexity in such lipids showed the highest binding affinity of Srf to model membranes containing GluCer (**Figure 25b**).

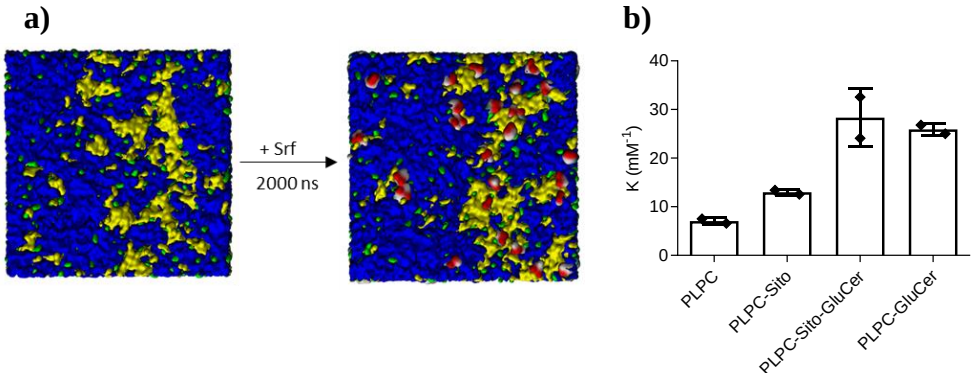

Figure 25 - Srf's potential to interact with lipids of PPM mimicking models. **a)** Molecular dynamics simulation of Srf insertion in GluCer-enriched domains of a PLPC-Sito-GluCer bilayer. Left: Top views of bilayers before (left, after 12.5µs of equilibration) and after Srf insertion (right). **b)** Binding coefficient (K) of Srf to liposomes with different lipid compositions. Graph presents values from two independent experiments (biophysical replicates), mean ± SD.

In light of these results, we tested Srf elicitor activity on the *Arabidopsis* ceramide synthase mutant *loh1* (LONGEVITY ASSURANCE 1 HOMOLOG1) and *fah1fah2* mutant (FATTY ACID HYDROXYLASE) both with significantly lower amount of these complex sphingolipids (Ternes *et al*., 2011; Lenarčič *et al*., 2017; see supplementary information for sphingolipids synthesis). A strongly reduced $[ROS]_{intra}$ response in *loh1* but not in *fah1fah2* was observed (**Figure 26a**). Based on the lack of $[ROS]_{intra}$ response in *loh1* an ISR experiment was conducted on this mutant. In accordance with ROS, a complete loss of Srf triggered ISR to *B. cinerea* infection was observed in the mutant compared to wild-type plants (**Figure 26b**).

a) b)

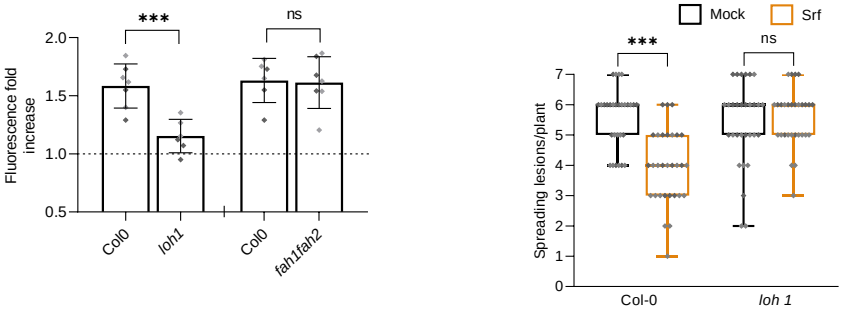

Figure 26 - Influence of sphingolipids on Srf triggered immune responses. **a)** $[ROS]_{intra}$ accumulation in roots of Col-0, *loh1* and *fah1fah2* mutants. Data represents fold increase in fluorescence values ± SD (n=6 from two independent experiments) at 30 min after Srf addition (10 µM) compared to values obtained for mock control. Significant difference ***P<0.001, two-tailed t-test. **b)** Disease incidence of *B. cinerea* in *Arabidopsis* Col-0 and *loh1* mutant plants, pre-treated with Srf (10 µM) compared with mock controls (n=30 from two independent experiments). Data are represented as in Figure 9. ns = not significant, ***P<0.001, two-way ANOVA and Sidak's multiple-comparison post-test.

To investigate further such lipid-dependent $[ROS]_{intra}$ elicitation we used other ISR-inducing CLPs, orfamide B, massetolide A and WLIP (Pršić and Ongena, 2020; **Figure 7** for structure) isolated from beneficial pseudomonads that resemble Srf in size and amphiphilic character. Each compound displayed a specific behavior regarding which type of altered sphingolipid content mutant is mostly affected in $[ROS]_{intra}$ response. Orfamide B showed similar results to Srf by losing the activity only in the *loh1*, WLIP lost the potential to trigger $[ROS]_{intra}$ production in both of the mutants tested, and massetolide A in *fah1fah2* (**Figure 27**). Thus, the CLP immunogenic activity thus relies on an intricate interaction with specific PPM sphingolipids as reported for other microbial compounds (Gerbeau-Pissot *et al.*, 2014; Sandor *et al.*, 2016; Lenarčič *et al.*, 2017).

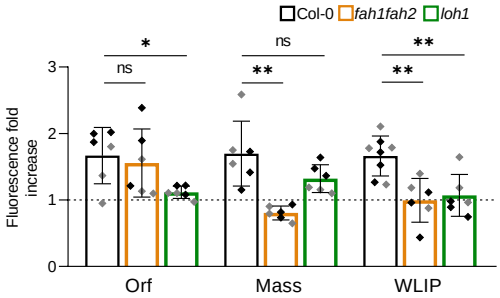

Figure 27 - $[ROS]_{intra}$ production in roots of Col-0, *loh1* and *fah1fah2* mutants following treatment with 10 µM orfamide B (Orf), massetolide A (Mass) or WLIP. Data represent fold increase in fluorescence values ± SD recorded at 30 min after the addition of these molecules compared to values obtained for mock-treated roots. Asterisks indicate significant difference (***P<0.001, two-tailed t-test).

4.4.3. *Influence of Srf on structural and rheological properties of the PPM mimicking models*

Our data emphasized the importance of lipids for the interaction of Srf with plants, therefore we wanted to further decipher the specificities of this interaction. In order to do so, various biophysical experiments were conducted on PPM mimicking models.

Neutron reflectometry (NR) is a powerful tool enabling measurements of thickness of one or several thin layers with the ability to distinguish structural features normal to the interface with sub-nanometer resolution. This technique involves shining a beam of neutrons onto the surface of study and once the beam hits the tested layer a reflection angle perpendicular to the interface is measured (Mattauch et al., 2018; Cousin and Fadda, 2020). Since this technique allows to measure the chemical composition of the different layers (distinguishing between lipid heads or tails, located in the outer or inner leaflet, but as well Srf) we used it to distinguish at what depth Srf inserts into the PPM mimicking bilayer. In addition, we used NR to measure the thickness of the PPM mimicking bilayer upon the interaction with Srf. These experiments showed that Srf inserts exclusively into the outer leaflet of PLPC-ß-sitosterol-GluCer model membranes (**Figure 28**). Moreover, NR data indicated that Srf insertion results in a decrease in membrane thickness (from 40 to 36Å), which

is more pronounced in ternary membranes than in membranes lacking GluCer (from 43 to 41Å) (**Supplementary Table 2**).

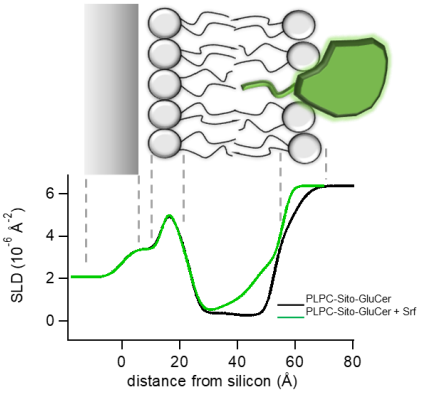

Figure 28 - Srf insertion in the bilayer and membrane thickness determined via neutron scattering length density (SLD) profiles of supported PLPC-Sito-GluCer membrane before (black) and after (green) Srf addition to the final 95:5 membrane: Srf molar proportion (0.24 mM) (below). Illustration (above) presents the correspondence between regions in the SLD profile and specific zones in the membrane.

To obtain information on the change in fluidity of the lipid phase, possibly caused by the insertion of Srf, a polarity sensitive probe – Laurdan, was furthermore used. When packing of the lipids increases, part of the water molecules is excluded from the bilayer which causes the emission spectral shift of Laurdan. By measuring the fluorescence at two different wavelengths, values are obtained for calculating the excitation Generalized Polarization (GP_{ex}) (calculation described in Materials and methods). The GP_{ex} value indicates the change in fluidity and increases with the increase of rigidification. The data revealed a significant increase in membrane lipid packing upon Srf addition observed on both PPM mimicking liposomes and protoplasts. Having the same trend in both of the systems suggests that the liposomes used in this study are suitable and promising tool for CLP/membrane lipids interaction studies when a more simplified model than a PPM is required (**Figure 29**, **Supplementary Figure 2 for time course**).

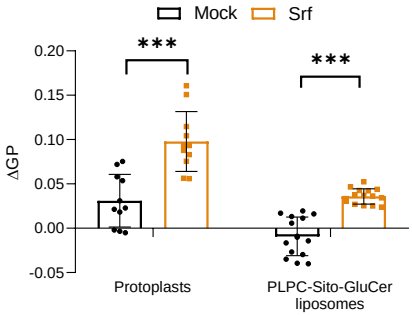

Figure 29 - Change of Laurdan generalized polarization (ΔGP) in Srf-treated (10 µM) Col-0 root protoplasts and in liposomes reflecting a change of membrane rigidity. Mean ± SD of 12 (for protoplasts) and 15 (for liposomes) replicates from 8 (for protoplasts) and 5 (for liposomes) independent experiments. ****P*<0.001, two-way ANOVA and Sidak's multiple comparison test.

Finally, a coarse-grained MD simulation was used to estimate the curvature that might occur due to insertion of Srf. Results suggested a strong curvature-inducing effect mediated by Srf docking as an additional impact on membrane physical properties (**Figure 30**).

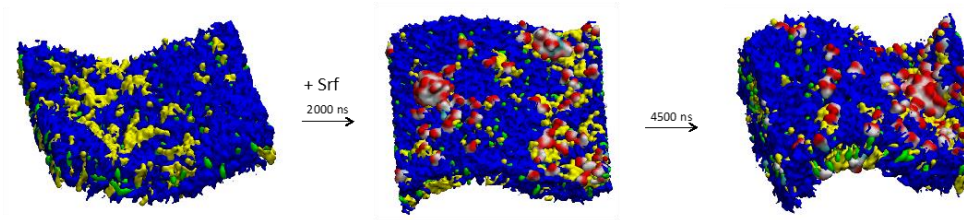

Figure 30 - Molecular dynamics modelling reveals a strong curvature of the plant plasma membrane model that may be induced by Srf. The lateral view shows the dynamic (ns, nanoseconds) of curving of a PLPC-Sito-GluCer bilayer upon docking of the lipopeptide into sphingolipid-enriched patches. PLPC in blue, sito in green, GluCer in yellow and Srf in red and white.

Altogether this data show that Srf preferentially inserts into the outer leaflet of the lipid bilayer in the vicinity of GluCer, and that this insertion causes structural and rheological changes of the membrane, such as thinning, rigidification, and curvature.

4.4.4. *Sensing mechanical stress induced by Srf*

4.4.4.1. Influence of mechanical stress induced by Srf on mechanosensitive ion channels activity

Srf's insertion resulting in structural and rheological changes of the bilayer, could represent a mechanical stress for the plasma membrane and be sensed via mechanosensitive ion channels (MSCs). Namely, MSCs are a group of mechanosensors whose gating depends on membrane fluidity, thickness, and curvature, due to their close interaction with the lipid bilayer. Gating of these channels is activated differently depending on the family of MSC in question. For instance, there are three proposed gating mechanisms for MSL channels. First, intrinsic bilayer model: This model suggests that MSC directly respond to external forces transmitted through the surrounding membrane. Second, tethered trapdoor model: In this model, external forces influence MSC gating through the tension applied to other cellular components like the cytoskeleton or extracellular matrix. The displacement of these components pulls on a tether, initiating channel opening. Third, hybrid model: According to this model, force-sensitive channels may be embedded within a cholesterol-rich platform, tethered to the cytoskeleton (Wilson *et al*., 2013; Monshausen and Haswell, 2013, Hamilton *et al*., 2014).

Generally, once activated MSCs conduct ions across the membrane, leading to osmoregulation, Ca^{2+} influx, membrane depolarization, and/or changes in extracellular ions pools (Codjoe *et al*., 2021). However, we did not observe Ca^{2+} influx, nor changes in medium conductivity, suggesting that major ion fluxes are not occurring in the cells of *Arabidopsis* roots. Given the role of the cell wall in maintaining membrane stability, we hypothesized that this mechanism could reduce the effect of Srf. Consequently, the influence of the cell wall could render the plant response very subtle, potentially falling below the threshold of detection. To test this, *Arabidopsis* root protoplasts were isolated to expose the plasma membrane and possibly obtain an emphasized response. Firstly, to rule out the possibility that Srf is toxic when acting directly on the PPM, a cell viability test was performed, which showed that Srf is not toxic for protoplasts at concentrations up to 25 µM (**Figure 31)**

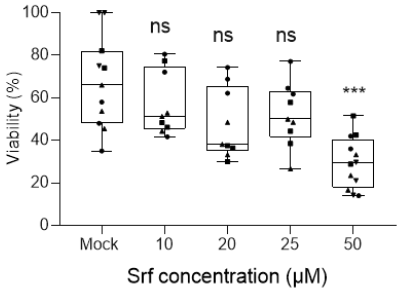

Figure 31 - Viability of root protoplasts measured with fluorescein diacetate in the presence of 10, 20, 25 and 50 µM Srf or 0.5% ethanol (negative control). Mean ± SD of 9 to 12 replicates (symbols on the graph) from three to four independent experiments (shown as different symbol shapes). Asterisks indicate statistically significant differences to the mock treatment (Brown-Forsythe and Welch ANOVA and Dunett's T3 multiple comparisons test; ns, not significant; ***P < 0.001).

Furthermore, we isolated protoplasts from the *Arabidopsis* Col-0^{AEQ} reporter line to measure calcium influx. A consistent calcium response triggered by Srf was observed, when treated with at least 5 µM (**Figure 32a)**, the threshold corresponding to the concentration needed for ROS burst in roots (**Figure 12**). This response was also successfully visualized by using a Fluo4-AM fluorescent probe in protoplasts isolated from the Col-0 *Arabidopsis* roots.

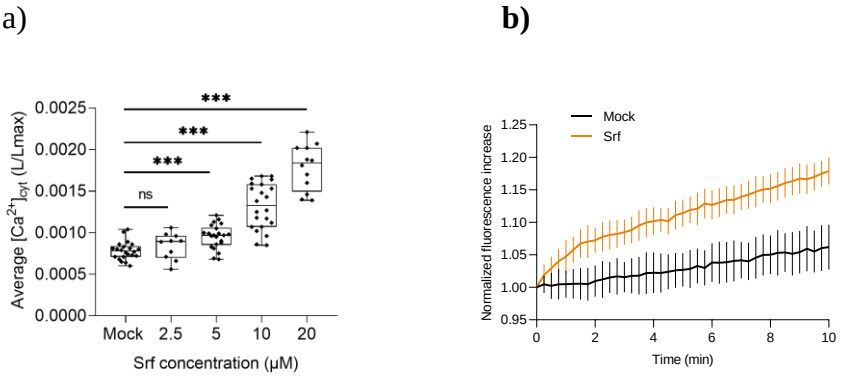

Figure 32 - Srf triggered calcium influx in *Arabidopsis* root protoplasts. **a)** Dose-dependent average $[Ca^{2+}]_{cyt}$ increase induced by Srf in root protoplasts of *Arabidopsis* Col-0^{AEQ}. Values are the average of L/Lmax values from 1.5 to 4 min after treatment corresponding to the top of the peak. Mean ± SD of at least 10 technical replicates from at least five independent experiments. Asterisks indicate statistically significant differences to the mock treatment (ns = no significant difference; **P*<0.05; ****P* < 0.001 Welch and Brown-Forsythe ANOVA); **b)** Kinetics of Srf-induced (at 10 µM) $[Ca^{2+}]_{cyt}$ increase as detected via Fluo-4 fluorescence in Col-0 root protoplasts. Data are represented as mean normalized fluorescence increase (± SD) of 14 replicates from four independent experiments.

Furthermore, we wanted to test the involvement of MSCs in Srf-triggered calcium influx using the same system. Among the MSCs, this study focused on two families, MCA and MSL, based on the ions they conduct and their location within the plant cells. MCAs are described as genuine transporters of calcium, while MSLs are considered as a non-selective ion transporters, but their indirect involvement in calcium signaling has been shown upon wounding and in response to cell swelling (Mori *et al*., 2018; Basu *et al*., 2020; Yoshimura *et al*., 2021; Moe-Lange *et al*., 2021). MCA family has two known members both located at the PPM, whereas MSL channels can be located at the plasma membrane but also on the membranes of certain organelles. Thus *msl4/5/6/9/10* and *mca1/2* mutants were chosen.

We measured calcium influx by using the Fluo4-AM probe in *msl4/5/6/9/10* and *mca1/2* mutants and observed a significantly lower response to Srf treatment as compared to Col-0 root protoplasts (**Figure 33**). This confirmed that Srf induces calcium influx, and that this influx is at least partially mediated via MSL 4/5/6/9/10 and MCA1/2.

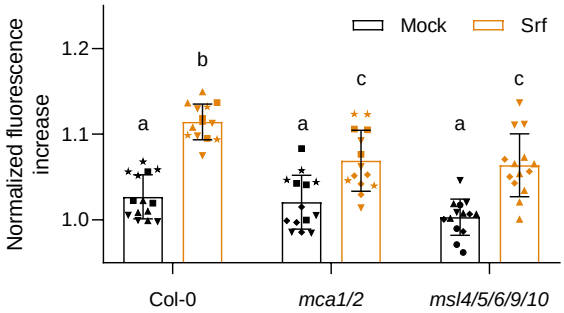

Figure 33 - $[Ca]_{cyt}$ detected with Fluo-4 in root protoplasts of Col-0, *mca1/2*, and *msl4/5/6/9/10*, mock- or Srf-treated (10 µM). Mean ± SD of 14 replicates from four independent experiments. Letters represent statistically different groups at $\alpha = 0.05$ (two-way ANOVA and Tukey's multiple-comparison post-test).

4.4.4.2. Effect of Srf activated MSCs dependent calcium influx on ROS in roots

Having in mind interplay of early immune events (Chapter 1, section 3.2.5.), we further wanted to test the influence of calcium and MSCs on $[ROS]_{intra}$ triggered by Srf in *Arabidopsis* roots. Firstly, pre-treatment with the Ca^{2+} channel blocker $LaCl_3$ or the chelator EGTA abolished the Srf-induced ROS burst (**Figure 34a,b**) confirming that calcium signaling acts upstream of $[ROS]_{intra}$ (Köster *et al.*, 2022). Furthermore, experiments on MSCs mutants showed an almost complete loss of $[ROS]_{intra}$ burst (**Figure 34c)**. In addition, pretreatment of roots with the MSCs blocker GsMTX-4 also resulted in a significant decrease in Srf triggered $[ROS]_{intra}$ confirming that activation of MSCs and subsequent ion fluxes act upstream of Srf-triggered ROS production (**data not shown**).

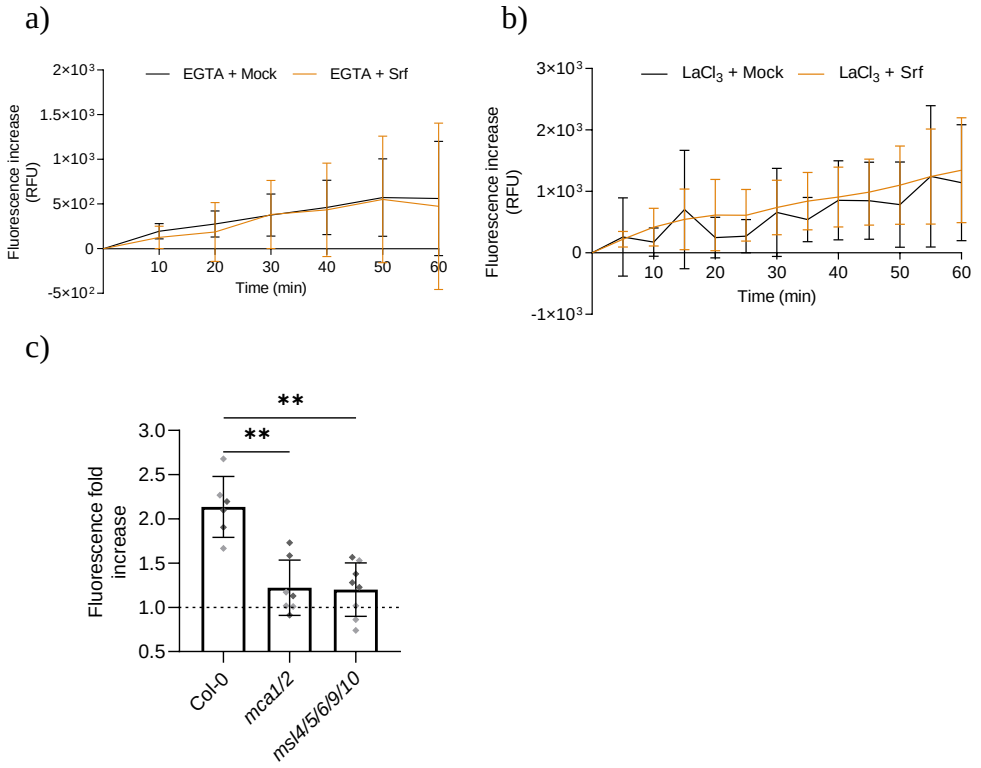

Figure 34 – Involvement of mechanosensitive ion channels in Srf triggered immune responses. **a)** $[ROS]_{intra}$ accumulation in Arabidopsis Col-0 (n=6), *mca1/2* (n=7), and *msl4/5/6/9/10* (n=8) roots following Srf treatment (10 µM). Data represent fold increase in fluorescence values 30 mins after Srf addition compared to mock-treated roots. Mean ± SD from two independent experiments. **P<0.01, two-tailed t-test. b**)** the non-selective Ca^{2+} channel blocker $LaCl_3$ **(**10 mM) and c**)** the Ca^{2+} chelator EGTA (1mM)**.** Graphs represent mean fluorescence increase observed ± SD of 7 replicates from 2 independent experiments.

4.4.4.3. Effect of MSC absence on Srf triggered ISR

Finally, to confirm that the lack of early immune responses in the MSC mutants is correlated with the ISR effect of Srf on plants, an ISR experiment was performed. Results showed that *mca1/2* and *msl4/5/6/9/10* plants were strongly impaired in mounting systemic resistance upon Srf treatment confirming their enrollment in the Srf-triggered ISR (**Figure 35**).

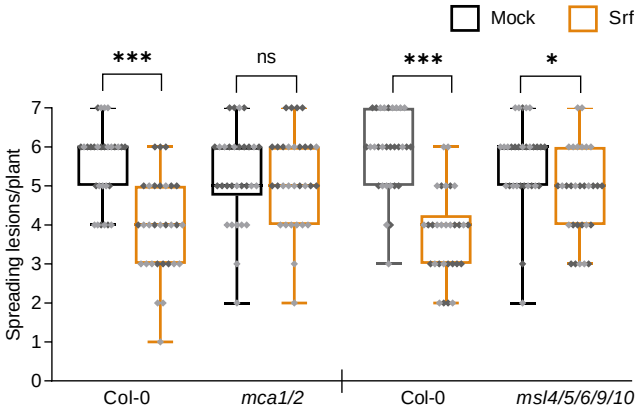

Figure 35 - Disease incidence of *B. cinerea* in *Arabidopsis* Col-0, *mca1/2*, and *msl4/5/6/9/10* mutant plants, mock- or Srf pre-treated (10 µM; each n=30 from two independent experiments represented as differently shaded grey values). Data are represented as in **Figure 10**.

Collectively, although contributions of other mechanosensitive proteins and channels cannot be ruled out (Thor *et al*., 2020; Goodman et al., 2023), our data provide evidence for a key role of these channels in Srf-induced plant defenses. Both mutants being affected in mounting ISR possibly suggests that these channels may act in a coordinated manner to tailor specific ion fluxes leading to plant immune response.

In addition to $[ROS]_{intra}$ and calcium influx, we also tested NO^- accumulation in these mutants. Interestingly, not only was NO^- production independent of these channels, but it was also slightly elevated (with the statistical significance) (**Figure 36**). This suggests that although crucial for Srf triggered ISR, Srf might still induce plant responses that are independent of these MSCs.

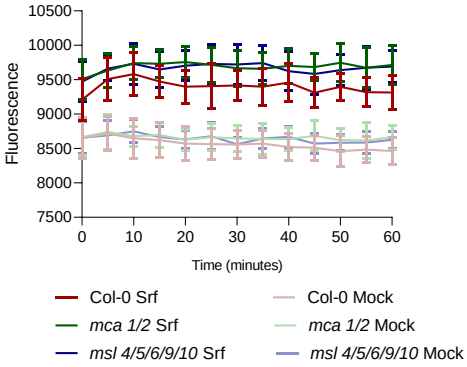

Figure 36 - Accumulation of NO^- in the wild type (Col-0) *Arabidopsis* roots, and *mca1/2*, *msl4/5/6/9/10* mutants roots. Graph represents grouped data from three independent experiments, each n=4.

5. Discussion

As previously reported for other plant species (Pršić and Ongena, 2020), treatment with Srf prepares *Arabidopsis* to mount defense responses culminating in the systemically expressed ISR phenotype. We provide new insights into the molecular basis of the well-known long-standing process of CLP-triggered plant immunity activation by unveiling a new lipid-mediated mechanism for the detection of these molecules at the cell surface. The CLP inserts into sphingolipid-enriched domains acting as docking platforms in the PPM, causing membrane deformation. Such membrane changes have been described in the literature to be perceived via MSC, and this work shows that representatives of these channels are required for early immune responses activation and induction of ISR by Srf. Clearly, this process differs from the receptor-based surveillance system engaged in the recognition of MAMPs by plant cells or in the perception of other lipopeptides as agonists of TLR-type PRRs in metazoans (Mohammad *et al*., 2022) and therefore reflects a new aspect of plant-microbe communication mediated by small chemicals from beneficial bacteria. Collectively, our data show that Srf perception leads to a quite specific immune activation signature regarding the type, timing and amplitude of early defense-related events and the weak transcriptional reprogramming as compared to PTI. This may explain why elicitation by Srf is cost-effective for the host plant as it does not result in growth-defense trade-off (Debois *et al*., 2015; He *et al*., 2022) nor does it cause a strong response associated with the alertness state or a hypersensitive reaction leading to cell death.

In addition to conducting ions, certain MSCs have been suggested to have the ability to activate plant responses independently of their gating. For instance, it has been documented that the soluble N-terminus of MSL 8, 9, and 10 contains intrinsically disordered regions, that have been described in plant biology for their putative roles in myriad functions, such as transcription, scaffolding, and stress responses (Flynn *et al*., 2022)

Besides the MSCs tested in this study, a possible role of other MSCs in harmonizing ion fluxes, such as OSCA, cannot be ruled out. Moreover, a protein receptor FERONIA may also play an important role. In *Arabidopsis* seedlings, it has been shown that mutants lacking this receptor show severely altered Ca^{2+} signaling induced by different forms of mechanical perturbation.

In addition, this receptor is also involved in plant responses such as Ca^{2+} signaling, medium alkalization, ROS burst, to numerous biotic and abiotic stresses (Shih et al., 2014; Ji et al., 2020).

When examining the rise in $[ROS]_{intra}$, it can be observed that the increase follows consistent rather than the transient trend, as frequently described in the literature for other elicitors. This behavior may be attributed to the presence of Srf in the media during ROS measurements. Namely, when recognized by a high affinity receptor, too high concentration of an elicitor can cause saturation of the receptor and subsequently the end of the signal as well. As Srf is not recognized by a receptor, saturation is not expected, and the signal might be prolongated as long as Srf continues to insert in the PPM. A potential method to verify this theory is treating plant roots with Srf, followed by thorough rinsing of the treatment, and subsequently quantifying $[ROS]_{intra}$ levels in roots resuspended exclusively in a buffer solution.

The MSC-independent intracellular NO^{-} burst triggered by Srf, suggests that Srf may activate other proteins by affecting membrane properties. A possible explanation is that this is because Srf preferentially inserts within the lipids located in the microdomains, described as protein-rich signaling platforms (Huby *et al*., 2020). However, since the plasma membrane properties are not only influenced locally where Srf inserts, the involvement of proteins that are not located in microdomains cannot be excluded.

The phytopathosystem used in this study having a high variability is not suitable for studying at what extent different players are influencing the final ISR. Possible solution would be using a phytopathosystem with higher precision of disease incident estimation, such as *Arabidopsis*/*Pseudomonas syringae pv. maculicola* in which Srf is already reported as active in triggering ISR (Altrão *et al*., 2022).

Further investigations are needed for a comprehensive understanding of the whole process from perception to systemic signaling leading to CLP-induced plant resistance. While this is challenging due to a lack of knowledge about mechanisms underlying ISR, it is mandatory to rationally implement the use of these compounds or their producers as bio-sourced alternatives to plant-protective chemicals in sustainable agriculture.

6. Data authorship

This work is a result of collaboration with different colleagues, which helped in realizing/providing the work presented in following figures:

- Fig 10, 11b, 23 Patricio Luzuriaga-Loaiza
- Fig 18, 29, 32, 33, Supp fig 2; 3 Guillaume Gilliard
- Fig 24 Manon Genva
- Fig 25b Magali Deleu
- Fig 25a, 30 Jean-Marc Crowet
- Fig 28 in collaboration with Magali Deleu and Valeria Rondelli

Additionally, the raw RNAseq data was processed by Heba Ibrahim.

7. Supplementary data

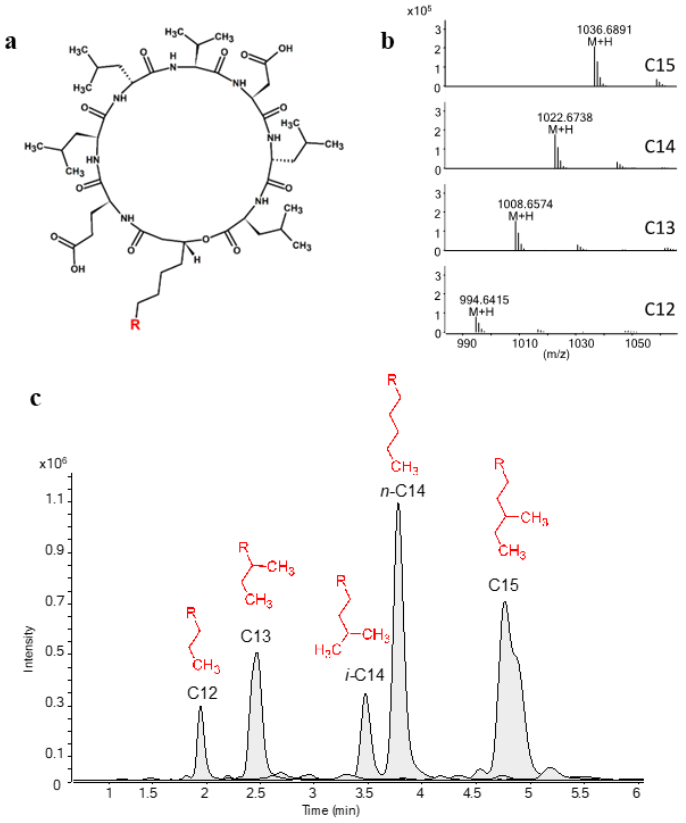

Supplementary Figure 1 - *Bacillus velezensis* produces surfactin as a mixture of structural variants differing in length and branching type of the fatty acid chain (R in the structure presented in (a) that are identified on the basis of the exact mass of their molecular ion (b) upon UPLC-MS profiling (c). This diversity is due to the low selectivity of the first C-domain of the multi-modular enzymatic machinery responsible for the synthesis of the compound. It allows using diverse fatty acids from the intracellular pool for binding to the first amino acid of the nascent peptide (Duban *et al* 2022).

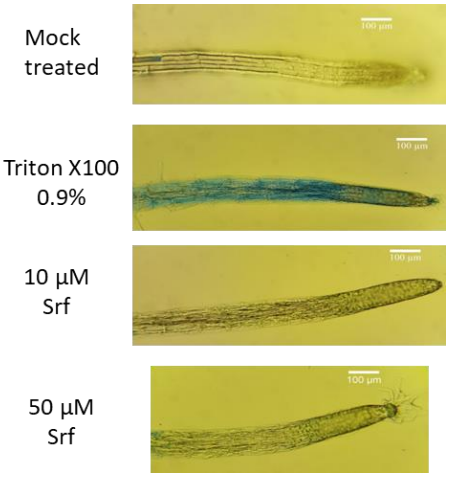

Supplementary Figure 2 - Root cell viability visualized with Evan's blue following treatment with different Srf concentrations, 0.5% ethanol (negative control) or 0.9% Triton X100 (positive control). Experiments were performed on three different individuals for each treatment with similar results.

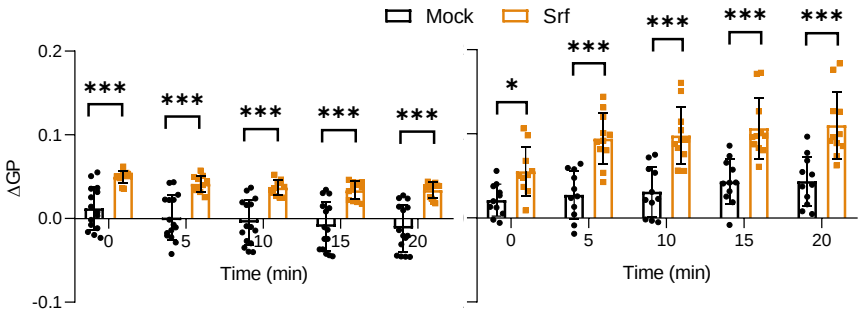

Supplementary Figure 3 – Rigidification of PPM mimicking liposomes (left) and root protoplasts plasma membrane (right).

Supplementary table 1. Description of *Arabidopsis* mutants used in ISR experiment represented in **Figure 23**

fls2/efr1	*Arabidopsis* mutant lacking functional leucine-rich repeat receptor kinases FLS2 and EFR, PRRs for bacterial flagellin and EF-Tu, respectively, recognition (Nekrasov *et al*., 2009)
lore-5	*Arabidopsis* mutant lacking receptor–like kinase LORE, a receptor for recognition of acyl chain epitopes such as medium chain 3-hydroxy fatty acids (Ranf *et al*., 2015)
bak1-5	*Arabidopsis* mutant lacking leucine-rich repeat receptor like kinases BAK 1-5 acting as a signaling partner of different receptor like kinases (Schwessinger *et al*., 2011)
cerk1-2	*Arabidopsis* mutant lacking functional receptor-like kinases CERK1 and 2, a common co-receptor for lysin motif carrying receptors, such as receptors for chitin and peptidoglycan (Miya *et al*., 2007; Zipfel and Oldroyd, 2017)
sobir1-12, sobir1-13	*Arabidopsis* mutant lacking leucine-rich repeat receptor-like kinases SOBIR with which leucine-rich repeat-receptor-like proteins lacking an intracellular kinase domain are forming receptor complexes to achieve immune signaling (Leslie *et al*., 2010; Van der Burgh *et al*., 2019)
bik1/pbl1	*Arabidopsis* mutant lacking central immune regulator BOTRYTIS-INDUCED KINASE1 (BIK1), and its closest homologue PBL1, the PM-associated cytosolic kinases acting downstream of multiple immune receptors and coordinating multiple plant immune responses (Zhang *et al*., 2010; Oelmüller 2021)

Supplementary Table 2 - Structural parameters used to fit the Neutron reflectivity spectra relative to the **(a)** PLPC-Sito-GluCer bilayer and **(b)** PLPC-Sito bilayer before (left) and after (right) Srf addition. A contemporary fitting of data collected from the membranes in H_2O and D_2O has been performed. SLD: Scattering length density ($\pm 0.05*10^{-6}Å^{-2}$), FA: fatty acid chain.

a)

	PLPC-Sito-GluCer bilayer			**PLPC-Sito-GluCer bilayer + Srf**		
	Thickness (±1Å)	SLD	Solvent penetration (±5%vol)	Thickness (±1Å)	SLD	Solvent penetration (±5%vol)
Heads in	6	1.93	25	6	1.93	25
Chains in	14	-0.28	10	14	-0.28	10
Chains out	14	-0.41	10	10	-0.38	20
Heads out	6	1.98	25	6	2	30

b)

	PLPC-Sito bilayer			**PLPC-Sito bilayer + Srf**		
	Thickness (±1Å)	SLD	Solvent penetration (±5%vol)	Thickness (±1Å)	SLD	Solvent penetration (±5%vol)
Heads in	8	1.93	15	7	1.93	15
Chains in	14	-0.34	3	14	-0.34	3
Chains out	15	-0.34	3	13	-0.32	7
Heads out	6	1.93	15	7	1.83	25

Supplementary table 3: List of Srf induced genes represented in the **Figure 20**. Genes in gray highlighted cells are also induced by flg22, genes in black letters have same regulation, the ones in red are oppositely regulated by the two elicitors. Genes and their fold changes (log2 FC) in transparent cells are Srf specific.

Srf 0,5 h vs flg22 all time points					
		continued		continued	
gene	log2 FC	gene	log2 FC	gene	log2 FC
At3g12910	**7,473559**	At1g75945	3,029064	At4g11870	-3,92481
At5g37840	**6,117427**	At1g09240	2,923564	At5g51990	-3,93327
At1g26410	**4,369326**	At1g07400	2,874274	At2g40080	-3,98872
At4g22030	**3,82961**	At1g02450	2,733618	At5g20630	-4,54421
At1g26380	**3,747453**	At4g15248	2,671774	At1g12610	-5,08698
At2g15780	**3,379899**	At4g27310	2,530284		
At1g14540	**3,307229**	At3g16930	2,455706		
At2g04515	**3,062422**	At2g46670	2,404239		
At1g14550	**3,002402**	At3g12580	2,380407		
At2g37810	**2,911863**	At5g54470	2,374722		
At3g13433	**2,858845**	At4g24700	2,348208		
At2g23270	**2,716883**	At2g31380	2,324851		
At2g31335	**2,687301**	At3g46230	2,303751		
At5g11140	**2,634364**	At1g51330	2,258325		
At5g04120	**2,613871**	At2g32130	2,185557		
At1g53625	**2,482979**	At1g52827	2,145669		
At2g36800	**2,467183**	At5g27765	2,132396		
At2g28270	**2,295063**	At5g15960	2,011502		
At3g62950	**2,28742**	At5g48250	-2,00151		
At1g09350	**2,276943**	At1g17665	-2,01483		
At5g37490	**2,215372**	At5g03204	-2,1245		
At1g26420	**2,200292**	At1g31580	-2,14961		
At1g51920	**2,18718**	At1g09950	-2,15309		
At1g51915	**2,133084**	At3g29798	-2,17392		
At1g07160	**2,104725**	At2g05915	-2,23037		
At1g51913	**2,092822**	At5g42800	-2,29523		
At4g03480	**2,078219**	At3g23637	-2,30011		
At5g57123	**2,076965**	At1g05800	-2,36585		
At4g23810	**2,060013**	At2g02120	-2,49948		
At1g47400	**-2,00188**	At1g43590	-2,5414		
At4g27654	**-2,03683**	At1g05136	-2,59304		
At3g56970	**-2,15861**	At3g62550	-2,6357		
At2g24850	**-2,47365**	At1g09030	-2,63955		
At4g12360	**-2,4752**	At1g76640	-2,70956		
At1g72910	**-2,57861**	At5g23115	-2,74482		
At3g44870	**-2,86237**	At4g25490	-2,87028		
At3g20395	**-3,40401**	At3g63160	-2,87542		
At3g44860	**-3,44493**	At4g34410	-2,87918		
At1g17420	**-3,48538**	At5g64770	-2,93266		
At3g22830	**-3,58863**	At3g32090	-2,99243		
At1g30135	**-3,7722**	At4g01535	-3,012		
At3g01345	5,475234	At1g06135	-3,07581		
At1g73220	3,962332	At4g35655	-3,14491		
At2g25990	3,646777	At2g11205	-3,31166		
At3g55790	3,433336	At5g08760	-3,38634		

Srf 1h vs flg22 all time points					
		continued		continued	
gene	log2 FC	gene	log2 FC	gene	log2 FC
At3g12910	**6,793469**	**At2g21040**	**-2,11589**	At2g37805	-2,22462
At5g37840	**6,176578**	**At2g31335**	**-2,26417**	At2g34430	-2,25869
At1g14550	**5,612086**	**At1g52890**	**-2,26781**	At4g12500	-2,28904
At4g22030	**5,519853**	**At5g26070**	**-2,32755**	At3g44950	-2,32677
At3g44860	**5,101099**	**At1g65500**	**-2,59205**	ATCg01070	-2,35692
At1g22810	**4,958329**	**At1g60050**	**-2,65654**	At1g19150	-2,35756
At2g24850	**4,894403**	**At2g02990**	**-2,81372**	At1g67860	-2,45043
At5g11140	**4,140115**	**At2g15780**	**-3,14193**	At2g04070	-2,50098
At1g71520	**3,780336**	**At3g54040**	**-3,23107**	At1g02450	-2,53856
At2g44840	**3,640064**	**At1g05680**	**-3,39558**	ATCG00690	-2,60584
At3g44870	**3,583021**	**At5g36140**	**-3,42572**	At1g29910	-2,68983
At2g38240	**3,242899**	**At5g24180**	**-3,4611**	At5g43290	-2,73081
At4g23810	**3,217715**	**At5g04120**	**-3,47853**	At2g37800	-2,81593
At5g24110	**3,174264**	**At5g44575**	**-3,60656**	At4g12470	-2,89057
At4g17090	**3,066164**	**At5g42530**	**-4,40922**	At5g35830	-2,89235
At3g23230	**2,962362**	**At1g08090**	**-4,42682**	At2g11205	-2,9047
At1g07160	**2,871242**	**At2g36800**	**-4,59623**	At1g23130	-2,94832
At5g01380	**2,856913**	At4g35655	4,021319	At1g29920	-2,9514
At1g70130	**2,796518**	At3g07522	3,829014	At2g05070	-3,07244
At5g48540	**2,715679**	At1g05800	3,448349	At5g20630	-3,1584
At1g17420	**2,709011**	At3g01345	3,417784	At1g69730	-3,38283
At4g22105	**2,696576**	At1g12610	3,268518	At5g36130	-3,48051
At1g56250	**2,676876**	At5g27765	2,840305	At5g08760	-3,50976
At1g51920	**2,657298**	At5g03204	2,829422	At3g05730	-3,68822
At1g79130	**2,638326**	At1g20310	2,64908	At3g60415	-3,72891
At1g21110	**2,594641**	At1g76640	2,539243	At4g12480	-4,32107
At5g37490	**2,559807**	At2g22760	2,480155	At1g09240	-4,34826
At1g78230	**2,485908**	At4g25433	2,468891	At4g23300	-4,47191
At1g14540	**2,48308**	At2g13275	2,447871	At1g08100	-4,5324
At1g72520	**2,480358**	At4g22620	2,297497		
At4g13420	**2,469162**	At3g09863	2,248725		
At1g51915	**2,426056**	At5g12030	2,244007		
At3g28360	**2,35899**	At3g25770	2,223889		
At4g18195	**2,337573**	At2g17660	2,208588		
At5g64905	**2,31605**	At4g34410	2,197603		
At1g30135	**2,275016**	At4g05095	2,179598		
At4g28460	**2,271498**	At3g22275	2,082589		
At2g26380	**2,264127**	At3g02480	-2,00959		
At3g48520	**2,253075**	At3g51644	-2,01926		
At4g18197	**2,080274**	At2g34320	-2,05994		
At5g01550	**2,078076**	At1g73000	-2,06184		
At4g22710	**2,076803**	At5g55620	-2,09221		
At1g32970	**2,032566**	At4g33735	-2,09519		
At1g56240	**2,027209**	At4g35400	-2,1419		
At3g47480	**-2,02043**	At4g16880	-2,17369		
At2g28850	**-2,0574**	At3g55790	-2,2086		
At4g12360	**-2,08344**	At1g32080	-2,21687		

Srf 3h vs flg22 all time points					
		continued		continued	
gene	log2 FC	gene	log2 FC	gene	log2 FC
At3g12910	**5,475559**	**At1g66600**	**2,039335**	At3g55330	-2,24068
At4g22030	**4,727409**	**At3g03670**	**2,034062**	At1g67740	-2,24786
At1g14550	**4,723695**	**At4g23550**	**2,008118**	At3g62550	-2,25186
At1g26410	**4,568594**	**At4g28350**	**2,001531**	At2g30570	-2,27694
At1g26380	**4,101143**	**At3g46080**	**-2**	At1g55670	-2,2812
At1g14540	**4,056904**	**At3g62410**	**-2,00457**	At2g35370	-2,29524
At4g13420	**3,702604**	**At1g47400**	**-2,04763**	At4g33560	-2,30057
At1g02920	**3,601576**	**At3g25760**	**-2,10652**	At2g10975	-2,31123
At2g37810	**3,346524**	**At1g47395**	**-2,17001**	At4g09900	-2,34473
At1g26240	**3,254935**	**At4g17090**	**-2,18027**	At1g65190	-2,35978
At5g48430	**3,212726**	**At3g46090**	**-2,29685**	At1g20340	-2,37209
At1g53625	**2,923441**	**At1g22630**	**-2,32402**	At3g48200	-2,38494
At2g26560	**2,918878**	**At3g44860**	**-2,32757**	At5g55450	-2,40478
At5g37490	**2,877739**	**At1g21250**	**-2,34**	At3g26650	-2,43262
At4g10530	**2,781812**	**At4g21445**	**-2,40571**	At5g38980	-2,46819
At3g16150	**2,767581**	**At1g10640**	**-2,41681**	At1g76900	-2,52173
At2g38240	**2,755965**	**At4g13500**	**-2,48183**	At1g32060	-2,52227
At4g10520	**2,724789**	**At1g68520**	**-3,04986**	At1g42970	-2,6603
At2g43570	**2,664998**	**At5g52780**	**-3,21397**	At4g12470	-2,69001
At3g15500	**2,654063**	**At5g42530**	**-3,3462**	At3g60415	-2,81793
At2g23270	**2,625882**	**At5g13730**	**-3,44661**	At1g27480	-2,82413
At1g63590	**2,546492**	**At5g44575**	**-3,69078**	At2g21530	-2,93634
At5g11140	**2,468767**	**At5g44580**	**-3,85218**	At4g12320	-2,94832
At4g01250	**2,457816**	**At5g38990**	**-3,96954**	At5g45680	-2,9704
At3g48850	**2,393394**	**At1g72910**	**-4,749**	At5g51720	-3,04603
At3g54040	**2,375344**	**At2g36800**	**-5,97907**	At3g55800	-3,08678
At1g13520	**2,372811**	At2g13810	3,78199	At4g16880	-3,09952
At1g75490	**2,360429**	At1g53610	3,051095	At3g46780	-3,10864
At5g64110	**2,354189**	At5g63250	3,034441	At4g12480	-3,12911
At1g36622	**2,331951**	At1g58320	2,892654	At5g36120	-3,15573
At1g64160	**2,305762**	At5g52400	2,564752	At5g55620	-3,31099
At1g19020	**2,294078**	At4g27310	2,379136	At1g15980	-3,31195
At1g36640	**2,234644**	At2g44220	2,314316	At5g17220	-3,37056
At2g43590	**2,229178**	At2g18680	2,302762	At1g09240	-3,7038
At1g30730	**2,184768**	At2g07642	2,086801	At3g51420	-3,88695
At5g43520	**2,16761**	At1g80440	2,081466	At1g31580	-3,95567
At3g13433	**2,157832**	At3g01175	2,018622	At1g75460	-4,19778
At1g76410	**2,156819**	At4g34410	2,015607	At3g63160	-4,67032
At2g44370	**2,154294**	At1g06830	-2,02636	At5g43290	-4,67902
At3g62950	**2,134555**	At5g07990	-2,04342	At1g23130	-4,80604
At2g02990	**2,099164**	At1g07400	-2,05027	At4g23300	-4,86102
At5g24180	**2,096187**	At4g28750	-2,06636	At1g32080	-5,04108
At2g46750	**2,075397**	At3g48420	-2,08198	At1g69730	-5,04859
At1g13480	**2,064966**	At3g22210	-2,12913	At5g08760	-5,11524
At5g25250	**2,0518**	ATCG00020	-2,13369	At1g19150	-5,27998
At1g49570	**2,046155**	At4g14090	-2,14913	At3g16250	-5,6545
				At3g05730	-6,01342
				At5g20630	-10,6434

Srf 6h vs flg22 all time points					
		continued		continued	
gene	log2 FC	gene	log2 FC	gene	log2 FC
At1g14550	6,710334	At5g62420	2,32036	At5g38700	-2,754
At1g26380	6,457278	At3g28740	2,311467	At5g52050	-2,77555
At5g05340	6,200332	At3g59900	2,278871	At1g27730	-2,82782
At2g30750	5,937335	At3g54040	2,255285	At2g40000	-2,84704
At5g04120	5,841164	At2g05540	2,235479	At5g17350	-2,91433
At4g13420	5,397059	At3g60270	2,233001	At1g72520	-2,9519
At3g49620	5,26201	At3g20340	2,231099	At1g35210	-2,99952
At1g08090	5,0749	At5g48430	2,229856	At5g40000	-3,04361
At2g36800	4,920397	At5g43580	2,202274	At3g29000	-3,14116
At1g69920	4,539671	At1g06160	2,199317	At3g50930	-3,26596
At5g44575	4,478185	At3g01970	2,195341	At4g27280	-3,32333
At1g64160	4,44795	At1g57630	2,19355	At5g57560	-3,32437
At1g26240	4,384731	At5g20230	2,169483	At4g30430	-3,42308
At3g25760	4,354679	At3g05950	2,166782	At5g64870	-3,54774
At2g15780	4,324564	At1g69930	2,166133	At5g42380	-3,58843
At2g37810	4,180726	At1g69490	2,155807	At1g22810	-3,60534
At4g13500	4,010568	At2g15960	2,154615	At3g10930	-3,64476
At2g26560	3,93115	At5g24180	2,144484	At4g17090	-3,74702
At2g43510	3,844345	At3g54420	2,133862	At3g02840	-3,78287
At1g49570	3,546595	At2g43590	2,106875	At3g44260	-3,87809
At5g60770	3,418143	At3g03670	2,083661	At4g11280	-3,89223
At4g22030	3,291473	At1g22630	2,064999	At1g07135	-3,95687
At1g26410	3,243538	At2g29460	2,03817	At1g15010	-4,03921
At1g44010	3,159306	At2g26740	2,035162	At2g46400	-4,0474
At1g66600	3,155896	At1g65500	2,023942	At4g29780	-4,07944
At5g64120	3,129211	At5g61600	-2,0147	At2g44840	-4,1811
At3g16150	2,91882	At5g57510	-2,02576	At4g24570	-4,22418
At5g42530	2,898749	At1g32920	-2,0367	At1g80840	-4,25947
At3g12910	2,897725	At1g56240	-2,08711	At4g27654	-4,47942
At1g52890	2,826866	At5g39670	-2,08716	At4g25470	-7,06845
At1g14540	2,807897	At4g25480	-2,12619	At4g23300	4,982655
At5g44580	2,796335	At2g20150	-2,14857	At1g08100	4,66307
At5g36140	2,754876	At2g32140	-2,17662	At3g12900	4,189698
At5g61890	2,679414	At1g56250	-2,23321	At5g06905	4,103862
At2g39980	2,639485	At4g17490	-2,30387	At3g02100	4,091242
At3g13433	2,610475	At5g10380	-2,32161	At4g12470	4,012501
At2g28850	2,608662	At4g22710	-2,36188	At4g12480	3,993874
At3g18250	2,6025	At1g72920	-2,38609	At1g09240	3,983156
At2g02990	2,584704	At3g56790	-2,3877	At1g73000	3,902054
At5g19890	2,541034	At1g30370	-2,48176	At3g48740	3,754099
At3g15440	2,518993	At5g47850	-2,51004	At5g23660	3,725837
At1g05680	2,518976	At1g60190	-2,53583	At1g32080	3,600657
At3g62950	2,508061	At4g13395	-2,55125	At5g39520	3,43349
At1g26420	2,47745	At5g22250	-2,59021	At4g12320	3,19938
At1g24145	2,404436	At1g17420	-2,66302	At5g06900	3,102982
At5g52350	2,336202	At1g30135	-2,68958	At1g23130	2,992269
At4g08380	2,331093	At5g58680	-2,71031	At2g44581	2,879949

continued		continued	
gene	log2 FC	gene	log2 FC
At2g34430	2,876135	At1g20823	-2,27467
At3g62550	2,863347	At1g74450	-2,32795
At4g33070	2,808146	At1g18740	-2,3861
At4g33560	2,805796	At3g27540	-2,39517
At4g16880	2,769694	At4g33970	-2,40894
At5g08760	2,729478	At1g47130	-2,44085
At1g52790	2,675137	At1g61470	-2,54169
At4g03540	2,647115	At1g35140	-2,59029
At5g12030	2,637871	At2g35290	-2,60434
At5g36130	2,576161	At1g74930	-2,92355
At4g10270	2,572875	At2g14290	-2,96153
At1g43800	2,542251	At4g27657	-3,03519
At1g12805	2,536726	At4g27652	-3,04616
At4g12500	2,366412	At1g19210	-3,13648
At5g16970	2,268586	At3g50060	-3,15667
At2g37805	2,217082	At5g11070	-3,16423
At5g43290	2,173882	At2g30020	-3,34201
At5g17220	2,147222	At1g73540	-3,50543
ATCG00700	2,131379	At1g18300	-3,63193
At5g50660	2,126946	At1g50750	-3,71581
At1g73120	2,110174	At4g01360	-3,72279
At3g20760	2,10715	At2g22760	-3,84517
At1g77120	2,077898	At1g50745	-3,94452
At2g04070	2,074504	At4g25490	-5,40969
At3g48920	2,055227	At4g34410	-5,83936
At1g63580	2,054911	At1g12610	-6,96068
At1g52800	2,026842		
At3g28340	-2,02847		
At1g77640	-2,04563		
At5g57010	-2,05942		
At5g43620	-2,07116		
At4g15150	-2,07462		
At5g42325	-2,09581		
At1g09950	-2,15817		
At2g33580	-2,1604		
At2g34600	-2,16484		
At3g56400	-2,17761		
At5g42965	-2,19173		
At1g66500	-2,24582		

Supplementary table 4: List of Srf induced genes represented in the **Figure 20**. Genes in gray highlighted cells are induced also by chitin, genes in black letters have same regulation, the ones in red are oppositely regulated by the two elicitors. Genes and their fold changes (log2 FC) in transparent cells are Srf specific.

Srf 0,5 h vs chi all time points					
		continued		continued	
gene	log2 FC	gene	log2 FC	gene	log2 FC
At3g12910	**7,473559**	At4g15248	2,671774	At4g11870	-3,92481
At5g37840	**6,117427**	At4g27310	2,530284	At5g51990	-3,93327
At1g26410	**4,369326**	At3g16930	2,455706	At2g40080	-3,98872
At4g22030	**3,82961**	At2g46670	2,404239	At5g20630	-4,54421
At1g26380	**3,747453**	At5g54470	2,374722	At1g12610	-5,08698
At2g15780	**3,379899**	At2g31380	2,324851		
At1g14540	**3,307229**	At3g46230	2,303751		
At2g04515	**3,062422**	At1g09350	2,276943		
At1g14550	**3,002402**	At1g51330	2,258325		
At2g37810	**2,911863**	At1g52827	2,145669		
At1g07400	**2,874274**	At5g27765	2,132396		
At3g13433	**2,858845**	At5g57123	2,076965		
At1g02450	**2,733618**	At5g15960	2,011502		
At2g23270	**2,716883**	At5g48250	-2,00151		
At5g11140	**2,634364**	At1g47400	-2,00188		
At5g04120	**2,613871**	At1g17665	-2,01483		
At1g53625	**2,482979**	At4g27654	-2,03683		
At2g36800	**2,467183**	At5g03204	-2,1245		
At3g12580	**2,380407**	At1g31580	-2,14961		
At4g24700	**2,348208**	At1g09950	-2,15309		
At2g28270	**2,295063**	At3g56970	-2,15861		
At3g62950	**2,28742**	At3g29798	-2,17392		
At5g37490	**2,215372**	At2g05915	-2,23037		
At1g26420	**2,200292**	At5g42800	-2,29523		
At1g51920	**2,18718**	At3g23637	-2,30011		
At2g32130	**2,185557**	At1g05800	-2,36585		
At1g51915	**2,133084**	At2g02120	-2,49948		
At1g07160	**2,104725**	At1g43590	-2,5414		
At1g51913	**2,092822**	At1g05136	-2,59304		
At4g03480	**2,078219**	At3g62550	-2,6357		
At4g23810	**2,060013**	At1g09030	-2,63955		
At2g24850	**-2,47365**	At1g76640	-2,70956		
At4g12360	**-2,4752**	At5g23115	-2,74482		
At1g72910	**-2,57861**	At3g44870	-2,86237		
At4g34410	**-2,87918**	At4g25490	-2,87028		
At3g20395	**-3,40401**	At3g63160	-2,87542		
At3g44860	**-3,44493**	At5g64770	-2,93266		
At1g17420	**-3,48538**	At3g32090	-2,99243		
At3g01345	5,475234	At4g01535	-3,012		
At1g73220	3,962332	At1g06135	-3,07581		
At2g25990	3,646777	At4g35655	-3,14491		
At3g55790	3,433336	At2g11205	-3,31166		
At1g75945	3,029064	At5g08760	-3,38634		
At1g09240	2,923564	At3g22830	-3,58863		
At2g31335	2,687301	At1g30135	-3,7722		

Srf 1 h vs chi all time points					
		continued		continued	
gene	log2 FC	gene	log2 FC	gene	log2 FC
At3g12910	**6,793469**	**At2g37800**	**-2,81593**	At1g52890	-2,26781
At5g37840	**6,176578**	**At2g15780**	**-3,14193**	At4g12500	-2,28904
At1g14550	**5,612086**	**At1g05680**	**-3,39558**	At3g44950	-2,32677
At4g22030	**5,519853**	**At5g36140**	**-3,42572**	At5g26070	-2,32755
At3g44860	**5,101099**	**At5g24180**	**-3,4611**	ATCG01070	-2,35692
At1g22810	**4,958329**	**At5g04120**	**-3,47853**	At1g19150	-2,35756
At2g24850	**4,894403**	**At5g42530**	**-4,40922**	At1g67860	-2,45043
At5g11140	**4,140115**	**At2g36800**	**-4,59623**	At2g04070	-2,50098
At1g71520	**3,780336**	At4g35655	4,021319	At1g65500	-2,59205
At2g44840	**3,640064**	At3g07522	3,829014	ATCG00690	-2,60584
At2g38240	**3,242899**	At3g44870	3,583021	At1g60050	-2,65654
At4g23810	**3,217715**	At1g05800	3,448349	At1g29910	-2,68983
At5g24110	**3,174264**	At3g01345	3,417784	At5g43290	-2,73081
At4g17090	**3,066164**	At1g12610	3,268518	At2g02990	-2,81372
At3g23230	**2,962362**	At5g27765	2,840305	At4g12470	-2,89057
At1g07160	**2,871242**	At5g03204	2,829422	At5g35830	-2,89235
At5g01380	**2,856913**	At1g76640	2,539243	At2g11205	-2,9047
At1g70130	**2,796518**	At1g78230	2,485908	At1g23130	-2,94832
At5g48540	**2,715679**	At2g22760	2,480155	At1g29920	-2,9514
At1g17420	**2,709011**	At4g13420	2,469162	At2g05070	-3,07244
At4g22105	**2,696576**	At4g25433	2,468891	At5g20630	-3,1584
At1g56250	**2,676876**	At2g13275	2,447871	At3g54040	-3,23107
At1g51920	**2,657298**	At3g28360	2,35899	At1g69730	-3,38283
At1g20310	**2,64908**	At4g22620	2,297497	At5g36130	-3,48051
At1g79130	**2,638326**	At1g30135	2,275016	At5g08760	-3,50976
At1g21110	**2,594641**	At3g48520	2,253075	At5g44575	-3,60656
At5g37490	**2,559807**	At3g09863	2,248725	At3g05730	-3,68822
At1g14540	**2,48308**	At5g12030	2,244007	At3g60415	-3,72891
At1g72520	**2,480358**	At3g25770	2,223889	At4g12480	-4,32107
At1g51915	**2,426056**	At4g05095	2,179598	At1g09240	-4,34826
At4g18195	**2,337573**	At3g22275	2,082589	At1g08090	-4,42682
At5g64905	**2,31605**	At3g02480	-2,00959	At4g23300	-4,47191
At4g28460	**2,271498**	At3g51644	-2,01926	At1g08100	-4,5324
At2g26380	**2,264127**	At3g47480	-2,02043		
At2g17660	**2,208588**	At1g73000	-2,06184		
At4g34410	**2,197603**	At5g55620	-2,09221		
At4g18197	**2,080274**	At4g33735	-2,09519		
At5g01550	**2,078076**	At2g21040	-2,11589		
At4g22710	**2,076803**	At4g35400	-2,1419		
At1g32970	**2,032566**	At4g16880	-2,17369		
At1g56240	**2,027209**	At3g55790	-2,2086		
At2g28850	**-2,0574**	At1g32080	-2,21687		
At2g34320	**-2,05994**	At2g37805	-2,22462		
At4g12360	**-2,08344**	At2g34430	-2,25869		
At1g02450	**-2,53856**	At2g31335	-2,26417		

Srf 3 h vs chi all time points					
		continued		continued	
gene	log2 FC	gene	log2 FC	gene	log2 FC
At3g12910	**5,475559**	**At1g21250**	**-2,34**	At3g48200	-2,38494
At4g22030	**4,727409**	**At1g10640**	**-2,41681**	At5g55450	-2,40478
At1g14550	**4,723695**	**At4g13500**	**-2,48183**	At4g21445	-2,40571
At1g26410	**4,568594**	**At5g42530**	**-3,3462**	At3g26650	-2,43262
At1g26380	**4,101143**	**At5g44580**	**-3,85218**	At5g38980	-2,46819
At1g14540	**4,056904**	**At1g75460**	**-4,19778**	At1g76900	-2,52173
At1g02920	**3,601576**	**At1g72910**	**-4,749**	At1g32060	-2,52227
At2g37810	**3,346524**	**At2g36800**	**-5,97907**	At1g42970	-2,6603
At1g26240	**3,254935**	At2g13810	3,78199	At4g12470	-2,69001
At5g48430	**3,212726**	At4g13420	3,702604	At3g60415	-2,81793
At1g53610	**3,051095**	At5g63250	3,034441	At1g27480	-2,82413
At1g53625	**2,923441**	At1g58320	2,892654	At2g21530	-2,93634
At2g26560	**2,918878**	At5g52400	2,564752	At4g12320	-2,94832
At5g37490	**2,877739**	At4g27310	2,379136	At5g45680	-2,9704
At4g10530	**2,781812**	At3g54040	2,375344	At5g51720	-3,04603
At3g16150	**2,767581**	At5g64110	2,354189	At1g68520	-3,04986
At2g38240	**2,755965**	At2g44220	2,314316	At3g55800	-3,08678
At4g10520	**2,724789**	At2g18680	2,302762	At4g16880	-3,09952
At2g43570	**2,664998**	At2g43590	2,229178	At3g46780	-3,10864
At3g15500	**2,654063**	At1g30730	2,184768	At4g12480	-3,12911
At2g23270	**2,625882**	At1g76410	2,156819	At5g36120	-3,15573
At1g63590	**2,546492**	At2g02990	2,099164	At5g52780	-3,21397
At5g11140	**2,468767**	At2g07642	2,086801	At5g55620	-3,31099
At4g01250	**2,457816**	At1g80440	2,081466	At1g15980	-3,31195
At3g48850	**2,393394**	At1g49570	2,046155	At5g17220	-3,37056
At1g13520	**2,372811**	At3g01175	2,018622	At5g13730	-3,44661
At1g75490	**2,360429**	At3g46080	-2	At5g44575	-3,69078
At1g36622	**2,331951**	At3g62410	-2,00457	At1g09240	-3,7038
At1g64160	**2,305762**	At1g06830	-2,02636	At3g51420	-3,88695
At1g19020	**2,294078**	At5g07990	-2,04342	At1g31580	-3,95567
At1g36640	**2,234644**	At1g47400	-2,04763	At5g38990	-3,96954
At5g43520	**2,16761**	At4g28750	-2,06636	At3g63160	-4,67032
At3g13433	**2,157832**	At3g48420	-2,08198	At5g43290	-4,67902
At2g44370	**2,154294**	At3g22210	-2,12913	At1g23130	-4,80604
At3g62950	**2,134555**	ATCG00020	-2,13369	At4g23300	-4,86102
At5g24180	**2,096187**	At4g14090	-2,14913	At1g32080	-5,04108
At2g46750	**2,075397**	At1g47395	-2,17001	At1g69730	-5,04859
At1g13480	**2,064966**	At3g55330	-2,24068	At5g08760	-5,11524
At5g25250	**2,0518**	At1g67740	-2,24786	At1g19150	-5,27998
At1g66600	**2,039335**	At3g62550	-2,25186	At3g16250	-5,6545
At3g03670	**2,034062**	At2g30570	-2,27694	At3g05730	-6,01342
At4g34410	**2,015607**	At1g55670	-2,2812	At5g20630	-10,6434
At4g23550	**2,008118**	At2g35370	-2,29524		
At4g28350	**2,001531**	At3g46090	-2,29685		
At1g07400	**-2,05027**	At4g33560	-2,30057		
At3g25760	**-2,10652**	At2g10975	-2,31123		
At4g17090	**-2,18027**	At4g09900	-2,34473		
At1g22630	**-2,32402**	At1g65190	-2,35978		
At3g44860	**-2,32757**	At1g20340	-2,37209		

Srf 6 h vs chi all time points					
		continued		continued	
gene	log2 FC	gene	log2 FC	gene	log2 FC
At1g14550	6,710334	At5g24180	2,144484	At3g44260	-3,87809
At1g26380	6,457278	At3g54420	2,133862	At4g11280	-3,89223
At2g30750	5,937335	At3g03670	2,083661	At1g07135	-3,95687
At5g04120	5,841164	At1g22630	2,064999	At2g46400	-4,0474
At3g49620	5,26201	At1g63580	2,054911	At4g29780	-4,07944
At2g36800	4,920397	At2g29460	2,03817	At2g44840	-4,1811
At1g69920	4,539671	At5g57510	-2,02576	At4g24570	-4,22418
At1g64160	4,44795	At1g32920	-2,0367	At1g80840	-4,25947
At1g26240	4,384731	At5g57010	-2,05942	At4g34410	-5,83936
At3g25760	4,354679	At1g56240	-2,08711	At5g05340	6,200332
At2g15780	4,324564	At5g39670	-2,08716	At4g13420	5,397059
At2g37810	4,180726	At4g25480	-2,12619	At1g08090	5,0749
At4g13500	4,010568	At2g20150	-2,14857	At4g23300	4,982655
At2g26560	3,93115	At2g32140	-2,17662	At1g08100	4,66307
At2g43510	3,844345	At1g56250	-2,23321	At5g44575	4,478185
At3g48740	3,754099	At4g17490	-2,30387	At3g12900	4,189698
At5g60770	3,418143	At5g10380	-2,32161	At5g06905	4,103862
At4g22030	3,291473	At4g22710	-2,36188	At3g02100	4,091242
At1g26410	3,243538	At1g72920	-2,38609	At4g12470	4,012501
At1g44010	3,159306	At3g56790	-2,3877	At4g12480	3,993874
At1g66600	3,155896	At1g30370	-2,48176	At1g09240	3,983156
At3g16150	2,91882	At5g47850	-2,51004	At1g73000	3,902054
At5g42530	2,898749	At5g22250	-2,59021	At5g23660	3,725837
At3g12910	2,897725	At1g35140	-2,59029	At1g32080	3,600657
At1g14540	2,807897	At1g17420	-2,66302	At1g49570	3,546595
At5g44580	2,796335	At5g58680	-2,71031	At5g39520	3,43349
At5g36140	2,754876	At1g27730	-2,82782	At4g12320	3,19938
At5g61890	2,679414	At2g40000	-2,84704	At5g64120	3,129211
At3g13433	2,610475	At5g17350	-2,91433	At5g06900	3,102982
At2g28850	2,608662	At1g72520	-2,9519	At1g23130	2,992269
At3g18250	2,6025	At2g14290	-2,96153	At2g44581	2,879949
At3g15440	2,518993	At1g35210	-2,99952	At2g34430	2,876135
At1g05680	2,518976	At5g40000	-3,04361	At3g62550	2,863347
At3g62950	2,508061	At3g29000	-3,14116	At1g52890	2,826866
At1g26420	2,47745	At3g50930	-3,26596	At4g33070	2,808146
At1g24145	2,404436	At4g27280	-3,32333	At4g33560	2,805796
At5g52350	2,336202	At5g57560	-3,32437	At4g16880	2,769694
At4g08380	2,331093	At4g30430	-3,42308	At5g08760	2,729478
At5g62420	2,32036	At5g64870	-3,54774	At1g52790	2,675137
At3g60270	2,233001	At5g42380	-3,58843	At4g03540	2,647115
At5g48430	2,229856	At1g22810	-3,60534	At2g39980	2,639485
At1g57630	2,19355	At1g18300	-3,63193	At5g12030	2,637871
At5g20230	2,169483	At3g10930	-3,64476	At2g02990	2,584704
At1g69930	2,166133	At4g17090	-3,74702	At5g36130	2,576161
At1g69490	2,155807	At3g02840	-3,78287	At4g10270	2,572875

continued		continued	
gene	log2 FC	gene	log2 FC
At1g43800	2,542251	At1g09950	-2,15817
At5g19890	2,541034	At2g33580	-2,1604
At1g12805	2,536726	At2g34600	-2,16484
At4g12500	2,366412	At3g56400	-2,17761
At3g28740	2,311467	At5g42965	-2,19173
At3g59900	2,278871	At1g66500	-2,24582
At5g16970	2,268586	At1g20823	-2,27467
At3g54040	2,255285	At1g74450	-2,32795
At2g05540	2,235479	At1g18740	-2,3861
At3g20340	2,231099	At3g27540	-2,39517
At2g37805	2,217082	At4g33970	-2,40894
At5g43580	2,202274	At1g47130	-2,44085
At1g06160	2,199317	At1g60190	-2,53583
At3g01970	2,195341	At1g61470	-2,54169
At5g43290	2,173882	At4g13395	-2,55125
At3g05950	2,166782	At2g35290	-2,60434
At2g15960	2,154615	At1g30135	-2,68958
At5g17220	2,147222	At5g38700	-2,754
ATCG00700	2,131379	At5g52050	-2,77555
At5g50660	2,126946	At1g74930	-2,92355
At1g73120	2,110174	At4g27657	-3,03519
At3g20760	2,10715	At4g27652	-3,04616
At2g43590	2,106875	At1g19210	-3,13648
At1g77120	2,077898	At3g50060	-3,15667
At2g04070	2,074504	At5g11070	-3,16423
At3g48920	2,055227	At2g30020	-3,34201
At2g26740	2,035162	At1g73540	-3,50543
At1g52800	2,026842	At1g50750	-3,71581
At1g65500	2,023942	At4g01360	-3,72279
At5g61600	-2,0147	At2g22760	-3,84517
At3g28340	-2,02847	At1g50745	-3,94452
At1g77640	-2,04563	At1g15010	-4,03921
At5g43620	-2,07116	At4g27654	-4,47942
At4g15150	-2,07462	At4g25490	-5,40969
At5g42325	-2,09581	At1g12610	-6,96068
		At4g25470	-7,06845

Supplementary table 5: Genes putatively related to plant immunity presented in the **Figure 22**.

Category	Accession n°
Calcium binding	At1g76640
	At4g27280
	At5g39670
	At3g47480
	At3g29000
	At1g73805
	At2g41090
	At2g41100
	At3g01830
	At1g76650
	At4g20780
	At4g33050
	At1g21550
	At3g51920
	At1g29025
	At1g29020
	At1g24620
	At1g05990
	At3g59370
	At2g24300
	At2g17890
	At1g61950
	At4g04710
	At2g35890
	At4g04700
	At5g66210
	At5g42380
	At5G57010
	At2g26190
	At3g25600
	At3g57530
ROS	AT1G14550
	AT5G05340
	AT1G49570
	AT5G64120
	AT1G14540
	AT5G19890
	AT3G03670
	AT5G64110
	AT2G41480
	AT5G39580
	AT3G49110
	AT5G19880
	AT4g11290
	AT4g08780
	AT5g15180
	AT1g30870
	AT2g39040
	AT4g08770
	AT3g49960
	AT1g34510
	AT1g71695
	AT2g43480
	AT4g37520
	AT2g18980
	AT4g16270
	AT5G07390
	AT5G47910

continued

Category	Accession n°
MAPK	At1g18350
	At1g73500
	At5g55090
	At5g67080
	At3g50310
	At1g01560
	At2g46070
	At3g45640
	At1g07150
PR	AT1g75830
	AT5g44420
	AT2g26020
	AT1g19610
	AT2g02120
	AT5g26130
	AT4g33710
	AT4g25790
	AT5g57625
	AT4g30320
	AT4g31470
	AT5g66590
	AT2g19980
	AT3g04720
	AT1g73620
	AT4g38660
	AT2g28790
	AT2g19990
	AT3g12500
	AT5g24090
	AT3g54420
	AT4g01700
	AT1g56680
	AT2g43590
	AT1g02360
	AT2g43620
	AT2g43580
	AT3g47540
Receptor, receptor-like related	At1g65790
	At1g65800
	At4g21380
	At5g48400
	At5g48410
	At5g11210
	At2g29110
	At5g11180
	At2g29120
	At2g29100
	At3g59700
	At4g23190
	At5g58940
	At4g00330
	At4g23180
	At4g23220
	At4g23230
	At4g23250
	At4g23260
	At4g23270
	At4g23280

continued

Category	Accession n°
Receptor, receptor-like related	At5g01550
	At4g23300
	At4g23320
	At4g38830
	At4g21400
	At4g11470
	At4g11480
	At4g04540
	At4g04570
	At4g00970
	At4g23130
	At4g23140
	At4g23170
	At5g01540
	At5g01560
	At4g20940
	At2g24130
	At3g28040
	At5g01890
	At5g46330
	At2g19190
	At5g48540
	At1g63590
	At1g63570
	At5g38990
	At1g63580
	At1g63560
	At1g63600
	At4g11521
	At5g60900
	At2g32140
	At3g05360
cell wall related	AT1g67980
	AT1G80820
	AT4G36220
	AT5g36870

8. Supplementary information

Sphingolipids synthesis pathway in plants

Sphingolipids are involved in the regulation of membrane fluidity and biophysical order, and also play important roles in vesicle trafficking, plant development and defense (Huby *et al*., 2020). They are divided into four classes: glycosyl inositol phosphoceramides (GIPCs), glucosylceramides (GluCer), ceramides (Cer), and free long-chain bases (LCBs) (Pata *et al*., 2010). This class represents up to 40% of the PPM lipidome, whereas in the sphingolipid-enriched outer leaflet, GIPCs solely constitute more than 50% (Markham *et al*., 2013; Mortimer and Scheller, 2020). It is suspected that there are more than 500 different sphingolipids, with 168 reported in Arabidopsis alone. Even though their profile varies depending on the plant species/tissue, GIPCs and GluCers constitute the majority of the sphingolipidomes (Markham and Jaworski, 2007; Pata *et al*., 2010; Michaelson *et al*., 2016).

The *de novo* biosynthesis of these lipids starts in the endoplasmic reticulum (ER), where the synthesis of various Long Chain Bases (LCB) occurs. Furthermore, LCBs are linked to fatty acids (FAs) by sphingosine N-acyltransferases (Cer synthases: LOH1, LOH2, and LOH3) to form Cer. The structure of Cer depends on the activated Cer synthases, LOH1 and LOH3 resulting in very long-chain FA (VLCFA) (C20–C28) trihydroxy LCBs Cers, whereas Cers composed of both dihydroxy LCBs (d18:0) and trihydroxy LCBs (t18:0) with shorter (C16) FA chain LCBs are synthetized by LOH2 (Berkey *et al*., 2012). VLCFA-ceramides are considered to be selectively involved in lipid microdomains formation and as well as in vesicle trafficking, therefore lack of LOH1 and LOH3 causes serious defect in membrane organization. Due to its severe mutation *loh 1* accumulates free LCBs (d18:0 and t18:0) and/or ceramide species with C (16) FA, and it is characterized by reduced growth compared to the wild type (Berkey *et al*., 2012). For the synthesis of more complex sphingolipids, GluCers and GIPCs, Cers are used as basic building blocks. The process of GluCer biosynthesis is catalyzed by glucosylceramide synthase and it occurs in the ER and/or PPM (Pata *et al*., 2010; Ali *et al*., 2018). On the other hand, for biosynthesis of GIPCs, Cers are transferred to the Golgi, and in the first step a phosphorylinositol head group is added, to form an inositol phosphorylceramide (IPC) by IPC synthase. IPCs are further

glycosylated by various glycosyltransferases, resulting in the formation of GIPCs (Fang *et al*., 2016).

Even though the majority of Cers, GluCers and GIPCs contain mainly α-hydroxylated FAs, the FAs used to synthesize the basic building blocks Cers are without these moieties, suggesting that FA hydroxylation is likely to be downstream of ceramide formation, and dependent on the activity of fatty acid hydroxylases 1 and 2 (FAH1, FAH2) (Pata *et al*., 2010). Mutants deprived of these two enzymes logically display low level of α-hydroxylated sphingolipids and higher level of trihydroxylated LCBs and ceramides (König *et al*., 2012).

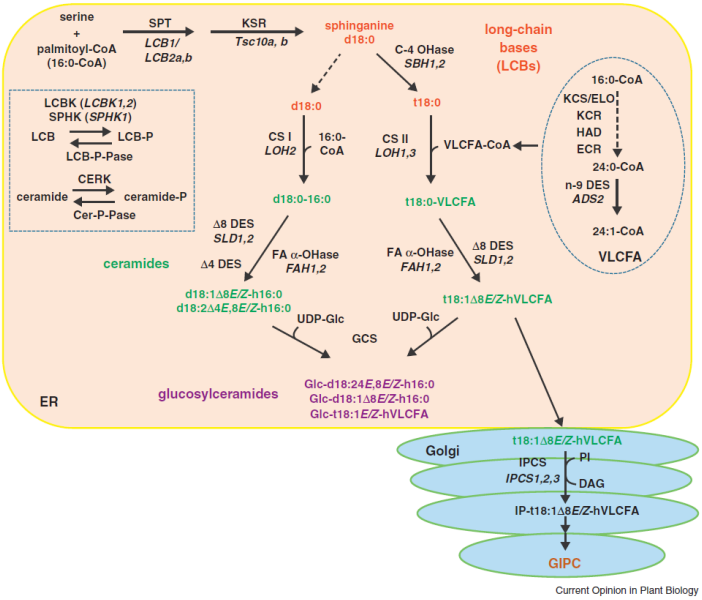

Supplementary figure 4. Simplified sphingolipid biosynthesis pathway (Markham *et al*., 2013).

9. References

Albert I, Böhm H, Albert M, et al. An RLP23–SOBIR1–BAK1 complex mediates NLP-triggered immunity. *Nat Plants*. 2015;1(10):15140. doi:10.1038/nplants.2015.140

Ali U, Li H, Wang X, Guo L. Emerging Roles of Sphingolipid Signaling in Plant Response to Biotic and Abiotic Stresses. *Mol Plant*. 2018;11(11):1328-1343. doi:10.1016/j.molp.2018.10.001

Altrão CS, Kaneko M, Shiina S, Kajikawa A, Shinohara H, Yokota K. Insights on suppression of bacterial leaf spot by Bacillus cyclic lipopeptides via induced resistance in Arabidopsis thaliana. *J Gen Plant Pathol*. 2022;88(4):259-263. doi:10.1007/s10327-022-01062-9

Andrić S, Meyer T, Rigolet A, et al. Lipopeptide Interplay Mediates Molecular Interactions between Soil Bacilli and Pseudomonads. Gralnick JA, ed. *Microbiol Spectr*. 2021;(December). doi:10.1128/spectrum.02038-21

Basu D, Shoots JM, Haswell ES. Interactions between the N- and C-termini of the mechanosensitive ion channel At MSL10 are consistent with a three-step mechanism for activation. Napier R, ed. *J Exp Bot*. 2020;71(14):4020-4032. doi:10.1093/jxb/eraa192

Berkey R, Bendigeri D, Xiao S. Sphingolipids and Plant Defense/Disease: The "Death" Connection and Beyond. *Front Plant Sci*. 2012;3(April):1-22. doi:10.3389/fpls.2012.00068

Berendsen HJC, Postma JPM, Van Gunsteren WF, Dinola A, Haak JR. Molecular dynamics with coupling to an external bath. *J Chem Phys*. 1984;81(8):3684-3690. doi:10.1063/1.448118

Berendsen, H. J. C., Postma, J. P. M., van Gunsteren, W. F. & Hermans, J. Interaction models for water in relation to protein hydration. Book chapter: Intermolecular forces, pp 331–342 (1981).

Bisceglia N, Gravino M, Savatin D. Luminol-based Assay for Detection of Immunity Elicitor-induced Hydrogen Peroxide Production in Arabidopsis thaliana Leaves. *BIO-PROTOCOL*. 2015;5(24). doi:10.21769/bioprotoc.1685

Blake C, Christensen MN, Kovács ÁT. Molecular Aspects of Plant Growth Promotion and Protection by Bacillus subtilis. *Mol Plant Microbe Interact*. 2021;34(1):15-25. doi:10.1094/MPMI-08-20-0225-CR

Bolger AM, Lohse M, Usadel B. Trimmomatic: A flexible trimmer for Illumina sequence data. *Bioinformatics*. 2014;30(15):2114-2120. doi:10.1093/bioinformatics/btu170

Brasseru R, Killian JA, De Kruijff B, Ruysschaert JM. Conformational analysis of gramicidin-gramicidin interactions at the air/water interface suggests that gramicidin aggregates into tube-like structures similar as found in the gramicidin-induced hexagonal HII phase. *BBA - Biomembr*. 1987;903(1):11-17. doi:10.1016/0005-2736(87)90150-7

Cacas J-L, Buré C, Grosjean K, et al. Revisiting Plant Plasma Membrane Lipids in Tobacco: A Focus on Sphingolipids. *Plant Physiol*. 2016;170(1):367-384. doi:10.1104/pp.15.00564

Codjoe JM, Miller K, Haswell ES. Plant cell mechanobiology: greater than the sum of its parts. *Plant Cell*. 2021;(1):1-17. doi:10.1093/plcell/koab230

Cawoy H, Mariutto M, Henry G, et al. Plant defense stimulation by natural isolates of Bacillus depends on efficient surfactin production. *Mol Plant-Microbe Interact*. 2014;27(2):87-100. doi:10.1094/MPMI-09-13-0262-R

Cousin F, Fadda G. An introduction to neutron reflectometry. *EPJ Web Conf*. 2020;236:04001. doi:10.1051/epjconf/202023604001

Davis BM, Jensen R, Williams P, O'Shea P. The interaction of N-acylhomoserine lactone quorum sensing signaling molecules with biological membranes: Implications for inter-kingdom signaling. *PLoS One*. 2010;5(10):1-10. doi:10.1371/journal.pone.0013522

Debois D, Fernandez O, Franzil L, et al. Plant polysaccharides initiate underground crosstalk with bacilli by inducing synthesis of the immunogenic lipopeptide surfactin. *Environ Microbiol Rep*. 2015;7(3):570-582. doi:10.1111/1758-2229.12286

DeFalco TA, Zipfel C. Molecular mechanisms of early plant pattern-triggered immune signaling. *Mol Cell*. 2021;81(17):3449-3467. doi:10.1016/j.molcel.2021.07.029

De Kesel J, Conrath U, Flors V, et al. The Induced Resistance Lexicon: Do's and Don'ts. *Trends Plant Sci*. 2021;(January). doi:10.1016/j.tplants.2021.01.001

Demidchik V, Shabala S, Isayenkov S, Cuin TA, Pottosin I. Calcium transport across plant membranes: mechanisms and functions. *New Phytol*. 2018;220(1):49-69. doi:10.1111/nph.15266

Dimopoulou A, Theologidis I, Varympopi A, et al. Shifting Perspectives of Translational Research in Bio-Bactericides: Reviewing the Bacillus amyloliquefaciens Paradigm. *Biology (Basel)*. 2021;10(11):1202. doi:10.3390/biology10111202

Evrard A, Bargmann BOR, Birnbaum KD, Tester M, Baumann U, Johnson AAT. Fluorescence-activated cell sorting for analysis of cell type-specific responses to salinity stress in arabidopsis and rice. *Methods Mol Biol*. 2012;913:265-276. doi:10.1007/978-1-61779-986-0_18

Falhof J, Pedersen JT, Fuglsang AT, Palmgren M. Plasma Membrane H+-ATPase Regulation in the Center of Plant Physiology. *Mol Plant*. 2016;9(3):323-337. doi:10.1016/j.molp.2015.11.002

Fan L, Fröhlich K, Melzer E, et al. Genotyping-by-sequencing-based identification of Arabidopsis pattern recognition receptor RLP32 recognizing proteobacterial translation initiation factor IF1. *Nat Commun*. 2022;13(1). doi:10.1038/s41467-022-28887-4

Fang L, Ishikawa T, Rennie EA, et al. Loss of Inositol Phosphorylceramide Sphingolipid Mannosylation Induces Plant Immune

Responses and Reduces Cellulose Content in Arabidopsis. *Plant Cell*. 2016;28(12):2991-3004. doi:10.1105/tpc.16.00186

Flynn AJ, Miller K, Codjoe JM, King MR, Posey AE, Haswell ES. The soluble N-termini of mechanosensitive ion channels MSL8, MSL9, and MSL10 are environmentally sensitive intrinsically disordered regions with distinct biophysical characteristics. *bioRxiv*. January 2022:2022.10.14.512244. doi:10.1101/2022.10.14.512244

García-Gutiérrez L, Zeriouh H, Romero D, Cubero J, de Vicente A, Pérez-García A. The antagonistic strain Bacillus subtilis UMAF6639 also confers protection to melon plants against cucurbit powdery mildew by activation of jasmonate- and salicylic acid-dependent defence responses. *Microb Biotechnol*. 2013;6(3):264-274. doi:10.1111/1751-7915.12028

Geudens N, Martins JC. Cyclic lipodepsipeptides from Pseudomonas spp. - Biological Swiss-Army knives. *Front Microbiol*. 2018;9(AUG):1-18. doi:10.3389/fmicb.2018.01867

Gerbeau-Pissot P, Der C, Thomas D, et al. Modification of plasma membrane organization in tobacco cells elicited by cryptogein. *Plant Physiol*. 2014;164(1):273-286. doi:10.1104/pp.113.225755

Gilliard G, Furlan AL, Smeralda W, Pršić J, Deleu M. Added Value of Biophysics to Study Lipid-Driven Biological Processes: The Case of Surfactins, a Class of Natural Amphiphile Molecules. *Int J Mol Sci*. 2022;23(22):13831. doi:10.3390/ijms232213831

Girard L, Höfte M, Mot R De. Lipopeptide families at the interface between pathogenic and beneficial Pseudomonas -plant interactions. *Crit Rev Microbiol*. 2020;46(4):397-419. doi:10.1080/1040841X.2020.1794790

Glazebrook J, Ausubel FM. Isolation of phytoalexin-deficient mutants of Arabidopsis thaliana and characterization of their interactions with bacterial pathogens. *Proc Natl Acad Sci U S A*. 1994;91(19):8955-8959. doi:10.1073/pnas.91.19.8955

Goodman MB, Haswell ES, Vásquez V. Mechanosensitive membrane proteins: Usual and unusual suspects in mediating mechanotransduction. *J Gen Physiol*. 2023;155(3):1-11. doi:10.1085/jgp.202213248

Hamant O, Haswell ES. Life behind the wall: Sensing mechanical cues in plants. *BMC Biol*. 2017;15(1):1-9. doi:10.1186/s12915-017-0403-5

Hamilton ES, Schlegel AM, Haswell ES. United in Diversity: Mechanosensitive Ion Channels in Plants. *Annu Rev Plant Biol*. 2014;66(1):113-137. doi:10.1146/annurev-arplant-043014-114700

Harwood CR, Mouillon JM, Pohl S, Arnau J. Secondary metabolite production and the safety of industrially important members of the Bacillus subtilis group. *FEMS Microbiol Rev*. 2018;42(6):721-738. doi:10.1093/femsre/fuy028

Haslam TM, Feussner I. Diversity in sphingolipid metabolism across land plants. *J Exp Bot*. 2022;73(9):2785-2798. doi:10.1093/jxb/erab558

Haswell ES, Peyronnet R, Barbier-Brygoo H, Meyerowitz EM, Frachisse JM. Two MscS Homologs Provide Mechanosensitive Channel Activities in the Arabidopsis Root. *Curr Biol*. 2008;18(10):730-734. doi:10.1016/j.cub.2008.04.039

Henry G, Deleu M, Jourdan E, Thonart P, Ongena M. The bacterial lipopeptide surfactin targets the lipid fraction of the plant plasma membrane to trigger immune-related defence responses. *Cell Microbiol*. 2011;13(11):1824-1837. doi:10.1111/j.1462-5822.2011.01664.x

Hess B, Bekker H, Berendsen HJC, Fraaije JGEM. LINCS: A linear constraint solver for molecular simulations. *J Comput Chem*. 1997;18(12):1463-1472. doi:10.1002/(SICI)1096-987X(199709)18:12<1463::AID-JCC4>3.0.CO;2-H

Hess B, Kutzner C, Van Der Spoel D, Lindahl E. GRGMACS 4: Algorithms for highly efficient, load-balanced, and scalable molecular simulation. *J Chem Theory Comput*. 2008;4(3):435-447. doi:10.1021/ct700301q

Hoff G, Arguelles Arias A, Boubsi F, et al. Surfactin Stimulated by Pectin Molecular Patterns and Root Exudates Acts as a Key Driver of the Bacillus -Plant Mutualistic Interaction. Vidaver AK, ed. *MBio*. November 2021:2021.02.22.432335. doi:10.1128/mBio.01774-21

Huby E, Napier JA, Baillieul F, Michaelson L V., Dhondt-Cordelier S. Sphingolipids: towards an integrated view of metabolism during the plant stress response. *New Phytol*. 2020;225(2):659-670 . doi:10.1111/nph.15997

Humphrey W, Dalke A, Schulten K. VMD: Visual molecular dynamics. *J Mol Graph*. 1996;14(1):33-38. doi:10.1016/0263-7855(96)00018-5

Jeworutzki E, Roelfsema MRG, Anschütz U, et al. Early signaling through the arabidopsis pattern recognition receptors FLS2 and EFR involves Ca^{2+}-associated opening of plasma membrane anion channels. Plant J. 2010;62(3):367-378. doi:10.1111/j.1365-313X.2010.04155.x

Ji D, Chen T, Zhang Z, Li B, Tian S. Versatile roles of the receptor-like kinase feronia in plant growth, development and host-pathogen interaction. *Int J Mol Sci*. 2020;21(21):1-16. doi:10.3390/ijms21217881

Katari MS, Nowicki SD, Aceituno FF, et al. VirtualPlant: A software platform to support systems biology research. *Plant Physiol*. 2010;152(2):500-515. doi:10.1104/pp.109.147025

Kim D, Langmead B, Salzberg SL. HISAT: a fast spliced aligner with low memory requirements. *Nat Methods*. 2 015;12(4):357-360. doi:10.1038/nmeth.3317

Knight H, Trewavas AJ, Knight MR. Cold calcium signaling in arabidopsis involves two cellular pools and a change in calcium signature after acclimation. *Plant Cell*. 1996;8(3):489-503. doi:10.2307/3870327

König S, Feussner K, Schwarz M, et al. Arabidopsis mutants of sphingolipid fatty acid α-hydroxylases accumulate ceramides and salicylates. *New Phytol*. 2012;196(4):1086-1097. doi:10.1111/j.1469-8137.2012.04351.x

Köster P, DeFalco TA, Zipfel C. Ca 2+ signals in plant immunity. *EMBO J*. 2022:1-18. doi:10.15252/embj.2022110741

Koutsioubas A. Combined coarse-grained molecular dynamics and neutron reflectivity characterization of supported lipid membranes. *J Phys Chem B*. 2016;120(44):11474-11483. doi:10.1021/acs.jpcb.6b05433

Lenarčič T, Albert I, Böhm H, et al. Eudicot plant-specific sphingolipids determine host selectivity of microbial NLP cytolysins. *Science (80-)*. 2017;358(6369):1431-1434. doi:10.1126/science.aan6874

Leslie ME, Lewis MW, Youn JY, Daniels MJ, Liljegren SJ. The EVERSHED receptor-like kinase modulates floral organ shedding in Arabidopsis. *Development*. 2010;137(3):467-476. doi:10.1242/dev.041335

Li H, Handsaker B, Wysoker A, et al. The Sequence Alignment/Map format and SAMtools. *Bioinformatics*. 2009;25(16):2078-2079. doi:10.1093/bioinformatics/btp352

Liang X, Zhou JM. Receptor-Like Cytoplasmic Kinases: Central Players in Plant Receptor Kinase-Mediated Signaling. *Annu Rev Plant Biol*. 2018;69(1):267-299. doi:10.1146/annurev-arplant-042817-040540

Liao Y, Smyth GK, Shi W. FeatureCounts: An efficient general purpose program for assigning sequence reads to genomic features. *Bioinformatics*. 2014;30(7):923-930. doi:10.1093/bioinformatics/btt656

Lins L, Brasseur R. Pp. 1879-1884, 1995. 1995;50(Il):1879-1884.

Lins L, Thomas-Soumarmon A, Pillot T, Vandekerckhove J, Rosseneu M, Brasseur R. Molecular determinants of the interaction between the C-terminal domain of Alzheimer's β-amyloid peptide and apolipoprotein E α-helices. *J Neurochem*. 1999;73(2):758-769. doi:10.1046/j.1471-4159.1999.0730758.x

López CA, Sovova Z, Van Eerden FJ, De Vries AH, Marrink SJ. Martini force field parameters for glycolipids. *J Chem Theory Comput*. 2013;9(3):1694-1708. doi:10.1021/ct3009655

Maintz J, Cavdar M, Tamborski J, et al. Comparative analysis of MAMP-induced calcium influx in arabidopsis seedlings and protoplasts. *Plant Cell Physiol*. 2014;55(10):1813-1825. doi:10.1093/pcp/pcu112

Markham JE, Jaworski JG. Rapid measurement of sphingolipids from Arabidopsis thaliana by reversed-phase high-performance liquid chromatography coupled to electrospray ionization tandem mass spectrometry. *Rapid Commun Mass Spectrom*. 2007;21(7):1304-1314. doi:10.1002/rcm.2962

Markham JE, Lynch D V., Napier JA, Dunn TM, Cahoon EB. Plant sphingolipids: function follows form. *Curr Opin Plant Biol*. 2013;16(3):350-357. doi:10.1016/j.pbi.2013.02.009

Marrink SJ, Risselada HJ, Yefimov S, Tieleman DP, De Vries AH. The MARTINI force field: Coarse grained model for biomolecular simulations. *J Phys Chem B*. 2007;111(27):7812-7824. doi:10.1021/jp071097f

Martinac B, Adler J, Kung C. Mechanosensitive ion channels of E. coli activated by amphipaths. *Nature*. 1990;348(6298):261-263. doi:10.1038/348261a0

Martinez-Medina A, Flors V, Heil M, et al. Recognizing Plant Defense Priming. *Trends Plant Sci*. 2016;21(10):818-822. doi:10.1016/j.tplants.2016.07.009

Mattauch S, Koutsioubas A, Rücker U, et al. The high-intensity reflectometer of the jülich centre for neutron science: MARIA. *J Appl Crystallogr*. 2018;51:546-654. doi:10.1107/S1600576718006994

Meng X, Zhang S. MAPK cascades in plant disease resistance signaling. *Annu Rev Phytopathol*. 2013;51:245-266. doi:10.1146/annurev-phyto-082712-102314

Michaelson L V., Napier JA, Molino D, Faure J-D. Plant sphingolipids: Their importance in cellular organization and adaption. *Biochim Biophys Acta - Mol Cell Biol Lipids*. 2016;1861(9):1329-1335. doi:10.1016/j.bbalip.2016.04.003

Miya A, Albert P, Shinya T, et al. CERK1, a LysM receptor kinase, is essential for chitin elicitor signaling in Arabidopsis. *Proc Natl Acad Sci U S A*. 2007;104(49):19613-19618. doi:10.1073/pnas.0705147104

Moe-Lange J, Gappel NM, Machado M, et al. Interdependence of a mechanosensitive anion channel and glutamate receptors in distal wound signaling. *Sci Adv*. 2021;7(37). doi:10.1126/sciadv.abg4298

Mohammad M, Ali A, Nguyen MT, Götz F, Pullerits R, Jin T. Staphylococcus aureus lipoproteins in infectious diseases. *Front Microbiol*. 2022;13(October):1-17. doi:10.3389/fmicb.2022.1006765

Monshausen GB, Haswell ES. A force of nature: Molecular mechanisms of mechanoperception in plants. *J Exp Bot*. 2013;64(15):4663-4680. doi:10.1093/jxb/ert204

Morales J, Kadota Y, Zipfel C, Molina A, Torres MA. The Arabidopsis NADPH oxidases RbohD and RbohF display differential expression patterns and contributions during plant immunity. *J Exp Bot*. 2016;67(6):1663-1676. doi:10.1093/jxb/erv558

Mori K, Renhu N, Naito M, et al. Ca2+-permeable mechanosensitive channels MCA1 and MCA2 mediate cold-induced cytosolic Ca2+ increase and cold tolerance in Arabidopsis. *Sci Rep*. 2018;8(1):550. doi:10.1038/s41598-017-17483-y

Mortimer JC, Scheller HV. Synthesis and Function of Complex Sphingolipid Glycosylation. *Trends Plant Sci*. 2020;25(6):522-524. doi:10.1016/j.tplants.2020.03.007

Mur LAJ, Mandon J, Cristescu SM, Harren FJM, Prats E. Methods of nitric oxide detection in plants: A commentary. Plant Sci. 2011;181(5):509-519. doi:10.1016/j.plantsci.2011.04.003

Nekrasov V, Li J, Batoux M, et al. Control of the pattern-recognition receptor EFR by an ER protein complex in plant immunity. *EMBO J*. 2009;28(21):3428-3438. doi:10.1038/emboj.2009.262

Nelson A. Co-refinement of multiple-contrast neutron/X-ray reflectivity data using MOTOFIT. *J Appl Crystallogr*. 2006;39(2):273-276. doi:10.1107/S0021889806005073

Nosé S. A unified formulation of the constant temperature molecular dynamics methods. *J Chem Phys*. 1984;81(1):511-519. doi:10.1063/1.447334

Ongena M, Jourdan E, Adam A, et al. Surfactin and fengycin lipopeptides of Bacillus subtilis as elicitors of induced systemic resistance in plants. *Environ Microbiol*. 2007;9(4):1084-10 90. doi:10.1111/j.1462-2920.2006.01202.x

Oostenbrink C, Villa A, Mark AE, Van Gunsteren WF. A biomolecular force field based on the free enthalpy of hydration and solvation: The GROMOS force-field parameter sets 53A5 and 53A6. *J Comput Chem*. 2004;25(13):1656-1676. doi:10.1002/jcc.20090

Parrinello M, Rahman A. Polymorphic transitions in single crystals: A new molecular dynamics method. *J Appl Phys*. 1981;52(12):7182-7190. doi:10.1063/1.328693

Pata MO, Hannun YA, Ng CKY. Plant sphingolipids: decoding the enigma of the Sphinx. *New Phytol*. 2010;185(3):611-630. doi:10.1111/j.1469-8137.2009.03123.x

Penfold J, Thomas RK. The application of the specular reflection of neutrons to the study of surfaces and interfaces. *J Phys Condens Matter*. 1990;2(6):1369-1412. doi:10.1088/0953-8984/2/6/001

Pieterse CMJ, Zamioudis C, Berendsen RL, Weller DM, Van Wees SCM, Bakker PAHM. Induced Systemic Resistance by Beneficial Microbes. *Annu Rev Phytopathol*. 2014;52(1):347-375. doi:10.1146/annurev-phyto-082712-102340

Poger D, Mark AE. On the Validation of Molecular Dynamics Simulations of Saturated and cis-Monounsaturated Phosphatidylcholine Lipid Bilayers: A Comparison with Experiment. *J Chem Theory Comput*. 2010;6(1):325-336. doi:10.1021/ct900487a

Poger D, Van Gunsteren WF, Mark AE. A new force field for simulating phosphatidylcholine bilayers. *J Comput Chem*. 2010;31(6):1117-1125. doi:10.1002/jcc.21396

Pršić J, Ongena M. Elicitors of Plant Immunity Triggered by Beneficial Bacteria. *Front Plant Sci*. 2020;11(November):1-12. doi:10.3389/fpls.2020.594530

Ranf S, Gisch N, Schäffer M, et al. A lectin S-domain receptor kinase mediates lipopolysaccharide sensing in Arabidopsis thaliana. *Nat Immunol*. 2015;16(4):426-433. doi:10.1038/ni.3124

Ranf S, Grimmer J, Pöschl Y, et al. Defense-related calcium signaling mutants uncovered via a quantitative high-throughput screen in arabidopsis thaliana. *Mol Plant*. 2012;5(1):115-130. doi:10.1093/mp/ssr064

Razafindralambo H, Paquot M, Hbid C, Jacques P, Destain J, Thonart P. Purification of antifungal lipopeptides by reversed-phase high-performance liquid chromatography. *J Chromatogr A*. 1993;639(1):81-85. doi:10.1016/0021-9673(93)83091-6

Rodríguez J, Tonelli ML, Figueredo MS, Ibáñez F, Fabra A. The lipopeptide surfactin triggers induced systemic resistance and priming state responses in Arachis hypogaea L. *Eur J Plant Pathol*. 2018;152(3):845-851. doi:10.1007/s10658-018-1524-6

Rondelli V, Koutsioubas A, Pršić J, et al. Sitosterol and glucosylceramide cooperative transversal and lateral uneven distribution in plant membranes. *Sci Rep*. 2021;11(1):21618. doi:10.1038/s41598-021-00696-7

Rondelli V, Brocca P, Motta S, et al. Amyloidβ Peptides in interaction with raft-mime model membranes: A neutron reflectivity insight. *Sci Rep*. 2016;6(February). doi:10.1038/srep20997

Rondelli V, Brocca P, Tranquilli N, Fragneto G, Del Favero E, Cantù L. Building a biomimetic membrane for neutron reflectivity investigation: Complexity, asymmetry and contrast. *Biophys Chem*. 2017;229(March):135-141. doi:10.1016/j.bpc.2017.04.011

Sandor R, Der C, Grosjean K, et al. Plasma membrane order and fluidity are diversely triggered by elicitors of plant defence. *J Exp Bot*. 2016;67(17):5173-5185. doi:10.1093/jxb/erw284

Schellenberger R, Crouzet J, Nickzad A, et al. Bacterial rhamnolipids and their 3-hydroxyalkanoate precursors activate Arabidopsis innate immunity through two independent mechanisms. *Proc Natl Acad Sci U S A*. 2021;118(39):1-10. doi:10.1073/PNAS.2101366118

Schellenberger R, Touchard M, Clément C, et al. Apoplastic invasion patterns triggering plant immunity: plasma membrane sensing at the frontline. *Mol Plant Pathol*. 2019;20(11):1602-1616. doi:10.1111/mpp.12857

Schikora A, Schenk ST, Hartmann A. Beneficial effects of bacteria-plant communication based on quorum sensing molecules of the N -acyl homoserine lactone group. *Plant Mol Biol*. 2016;90(6):605-612. doi:10.1007/s11103-016-0457-8

Schmid N, Eichenberger AP, Choutko A, et al. Definition and testing of the GROMOS force-field versions 54A7 and 54B7. *Eur Biophys J*. 2011;40(7):843-856. doi:10.1007/s00249-011-0700-9

Schwessinger B, Roux M, Kadota Y, et al. Phosphorylation-dependent differential regulation of plant growth, cell death, and innate immunity by the regulatory receptor-like kinase BAK1. *PLoS Genet*. 2011;7(4). doi:10.1371/journal.pgen.1002046

Shen H-H, Thomas RK, Penfold J, Fragneto G. Destruction and solubilization of supported phospholipid bilayers on silica by the biosurfactant surfactin. *Langmuir*. 2010;26(10):7334-7342. doi:10.1021/la904212x

Shen H-H, Thomas RK, Taylor P. The location of the biosurfactant surfactin in phospholipid bilayers supported on silica using neutron reflectometry. *Langmuir*. 2010;26(1):320-327. doi:10.1021/la9034936

Shih H-W, Miller ND, Dai C, Spalding EP, Monshausen GB. The Receptor-like Kinase FERONIA Is Required for Mechanical Signal

Transduction in Arabidopsis Seedlings. *Curr Biol*. 2014;24(16):1887-1892. doi:10.1016/j.cub.2014.06.064

Stringlis IA, Proietti S, Hickman R, Van Verk MC, Zamioudis C, Pieterse CMJ. Root transcriptional dynamics induced by beneficial rhizobacteria and microbial immune elicitors reveal signatures of adaptation to mutualists. *Plant J*. 2018;93(1):166-180. doi:10.1111/tpj.13741

Ternes P, Feussner K, Werner S, et al. Disruption of the ceramide synthase LOH1 causes spontaneous cell death in Arabidopsis thaliana. *New Phytol*. 2011;192(4):841-854. doi:10.1111/j.1469-8137.2011.03852.x

Thor K, Jiang S, Michard E, et al. The calcium-permeable channel OSCA1.3 regulates plant stomatal immunity. *Nature*. 2020;585(7826):569-573. doi:10.1038/s41586-020-2702-1

Tironi IG, Sperb R, Smith PE, Van Gunsteren WF. A generalized reaction field method for molecular dynamics simulations. *J Chem Phys*. 1995;102(13):5451-5459. doi:10.1063/1.469273

Torres MA, Dangl JL, Jones JDG. Arabidopsis gp91phox homologues Atrbohd and Atrbohf are required for accumulation of reactive oxygen intermediates in the plant defense response. *Proc Natl Acad Sci U S A*. 2002;99(1):517-522. doi:10.1073/pnas.012452499

Tran D, Petitjean H, Chebli Y, Geitmann A, Sharif-Naeini R. Mechanosensitive ion channels contribute to mechanically evoked rapid leaflet movement in Mimosa pudica. *Plant Physiol*. 2021;187(3):1704-1712. doi:10.1093/plphys/kiab333

Van der Burgh AM, Postma J, Robatzek S, Joosten MHAJ. Kinase activity of SOBIR1 and BAK1 is required for immune signalling. *Mol Plant Pathol*. 2019 Mar;20(3):410-422. doi: 10.1111/mpp.12767.

Wan WL, Zhang L, Pruitt R, et al. Comparing Arabidopsis receptor kinase and receptor protein-mediated immune signaling reveals BIK1-dependent differences. *New Phytol*. 2019;221(4):2080-2095. doi:10.1111/nph.15497

Wassenaar TA, Ingólfsson HI, Böckmann RA, Tieleman DP, Marrink SJ. Computational lipidomics with insane: A versatile tool for generating custom membranes for molecular simulations. *J Chem Theory Comput*. 2015;11(5):2144-2155. doi:10.1021/acs.jctc.5b00209

Wassenaar TA, Pluhackova K, Böckmann RA, Marrink SJ, Tieleman DP. Going backward: A flexible geometric approach to reverse transformation from coarse grained to atomistic models. *J Chem Theory Comput*. 2014;10(2):676-690. doi:10.1021/ct400617g

Waszczak C, Carmody M, Kangasjärvi J. Reactive Oxygen Species in Plant Signaling. *Annu Rev Plant Biol*. 2018;69(1):1-28. doi:10.1146/annurev-arplant-042817-040322

Wilson ME, Maksaev G, Haswell ES. MscS-like Mechanosensitive Channels in Plants and Microbes. *Biochemistry*. 2013;52(34):5708-5722. doi:10.1021/bi400804z

Wyrsch I, Domínguez-Ferreras A, Geldner N, Boller T. Tissue-specific FLAGELLIN-SENSING 2 (FLS2) expression in roots restores immune responses in Arabidopsis fls2 mutants. *New Phytol*. 2015;206(2):774-784. doi:10.1111/nph.13280

Yamanaka T, Nakagawa Y, Mori K, et al. MCA1 and MCA2 That Mediate Ca2+ Uptake Have Distinct and Overlapping Roles in Arabidopsis. *Plant Physiol*. 2010;152(3):1284-1296. doi:10.1104/pp.109.147371

Yoo SD, Cho YH, Sheen J. Arabidopsis mesophyll protoplasts: A versatile cell system for transient gene expression analysis. *Nat Protoc*. 2007;2(7):1565-1572. doi:10.1038/nprot.2007.199

Yoshimura K, Iida K, Iida H. MCAs in Arabidopsis are Ca2+-permeable mechanosensitive channels inherently sensitive to membrane tension. *Nat Commun*. 2021;12(1):6074. doi:10.1038/s41467-021-26363-z

Yu Y, Klauda JB. Symmetric and Asymmetric Models for the Arabidopsis thaliana Plasma Membrane: A Simulation Study. *J Phys Chem B*. 2021;125(41):11418-11431. doi:10.1021/acs.jpcb.1c04704

Zakharova AA, Efimova SS, Malev V V., Ostroumova OS. Fengycin induces ion channels in lipid bilayers mimicking target fungal cell membranes. Sci Rep. 2019;9(1):16034. doi:10.1038/s41598-019-52551-5

Zamioudis C, Korteland J, Van Pelt JA, et al. Rhizobacterial volatiles and photosynthesis-related signals coordinate MYB 72 expression in Arabidopsis roots during onset of induced systemic resistance and iron-deficiency responses. Delseny M, ed. Plant J. 2015;84(2):309-322. doi:10.1111/tpj.12995

Zhang J, Li W, Xiang T, et al. Receptor-like cytoplasmic kinases integrate signaling from multiple plant immune receptors and are targeted by a Pseudomonas syringae effector. *Cell Host Microbe*. 2010;7(4):290-301. doi:10.1016/j.chom.2010.03.007

Chapter 3

Signaling and defense related events activated by surfactin

1.Abstract

Induced systemic resistance (ISR) triggered by plant beneficial organisms renders plants more resistant to future unfavorable cues and thus represents an important strategy for reducing the use of chemical pesticides. However, to successfully integrate ISR as a strategy, a better understanding of this phenomenon is needed. Among the reported ISR elicitors, the cyclic lipopeptide produced by beneficial bacilli - surfactin, is considered as a promising candidate showing bioactivity in various phytopathosystems. Previous chapter described how Srf is perceived by plant cells and how subsequent early immune events are activated, thus this chapter focuses on downstream responses hormonal and defense signaling and activation of defense related genes. Collectively this data revealed qualitative and quantitative specificity of transcriptional changes induced by Srf compared to the responses to known MAMPs and showed the importance of camalexin for Srf-triggered ISR against *Botrytis cinerea*. Finally, it also provided a foundation for further investigation of hormonal and defense signaling occurring during the silent phase of Srf-triggered priming.

2. Introduction

Even though ISR has great potential as an alternative to chemical pesticides, a number of processes underpinning this phenomenon, such as signaling and activation of defense mechanisms, remain poorly understood.

During the activation of plant immunity hormonal signaling represents an important step being the link between early immune events and the activation of plant defense response. This signaling is achieved in plants by integrating information about the phytohormonal blend in the plant, the relative concentration of each hormone, the timing and sequence of the initiation of each of these molecules, and their crosstalk (Pieterse *et al*., 2012; Gimenez-Ibanez and Solano, 2013). The most thoroughly described phytohormones for their role in plant immunity are salicylic acid (SA), jasmonic acid (JA) with its derivatives, and ethylene (ET) (Berens *et al*., 2017; Vlot *et al*., 2020).

Besides phytohormones, plants can additionally use several chemical compounds to achieve defense signaling, such as azelaic acid, glycerol-3-phosphate (G3P), pipecolic acid and its derivative N-hydroxy-pipecolic acid, and volatiles like pinene or NO (Oelmüller, 2021). Although, PTI and ISR show similarities regarding the phytohormones used for signaling, studies have shown that azelaic acid (Aza) is required as defense signaling molecule for the onset of systemic resistance (Jung *et al*., 2009; Cecchini *et al*., 2015).

In most instances, ISR does not induce specific plant defense mechanisms but reinforces plant immune responses triggered upon pathogen infection, such as pathogenesis-related (PR) proteins, lipoxygenase and phenylpropanoid pathways, camalexin production, and cell wall reinforcement (De Kesel *et al*., 2021; Nguyen *et al*., 2022a,b). To date, although relatively little is known about ISR-specific defense response pathways, the production of coumarins, plant-derived secondary metabolites produced via the phenylpropanoid pathway, has emerged as a specific pathway induced in *Arabidopsis* by certain beneficials (Stringlis *et al*., 2019). Namely, the PBB *Pseudomonas simiae* WCS417, and beneficial fungi *Trichoderma harzianum* T-78 and *T. asperellum* T-34, have been shown to trigger coumarin synthesis-dependent ISR, where the MYB72 was found to be key marker transcriptional factor of this pathway (Zamioudis *et al*., 2015; Pescador *et al*., 2022). Moreover, overexpression of the enzyme b-glucosidase BGLU42, which is involved in

the production of coumarins, results in constitutive resistance against *B. cinerea*, *Pseudomonas syringae* pv. *tomato* DC3000 and *Hyaloperonospora arabidopsidis* in *Arabidopsis* indicating that elicitors activating this pathway could potentially induce ISR against these pathogens (Zamioudis *et al*., 2014).

In order to better evaluate how Srf primes plants for a reinforced immune response, the results obtained with the time series RNAseq analysis presented in the previous chapter were further investigated. In addition, *Arabidopsis* mutants lacking genes involved in the activation/synthesis pathways of different phytoalexins were used. Since coumarins have gained importance as ISR-specific phytoalexins in recent years, we used the MYB72 knockout mutant lacking this important transcription factor involved in the synthesis of these phytoalexins. We also used a mutant unable to synthesize camalexin, a phytoalexin important for *Arabidopsis* defense against *B. cinerea* (Ferrari *et al*., 2006).

3. Materials and methods

3.1. *RNAseq related experiments*

RNAseq experiment described in Chapter 2.

BLAST analysis : Protein sequences of proteins encoded by genes identified as unknown were obtained from https://www.ncbi.nlm.nih.gov/ and compared to the proteins in Pfam database (http://pfam.xfam.org/). Possible matches with the signalling peptides were investigated using SignalP (https://services.healthtech.dtu.dk/services/SignalP-5.0/).

3.2. *ISR estimation*

ISR was estimated according to the material and methods described in Chapter 2. The *pad3*, *pMYB72:GFP-GUS*, and *myb72-2* mutants used were described in Glazebrook et al., 1994, Zamioudis *et al*., 2015, Bakker et al., 2007, respectively.

3.3. *Activation of MYB72*

Seeds of *pMYB72:GFP-GUS* were sown, and plants were grown for 7 days in conditions described in Chapter 2 Materials and methods. After 7 days, uniformly grown seedlings were transferred to 96 optical bottom black microplates (Greiner 96 µClear) containing 150 µL of hydroponic solution (GENERAL HYDROPONICS FLORAMICRO 5-0-1, FLORABLOOM 0-5-4, and FLORAGRO 3-1-6, in ratio 1:1:1, each 1 mL/ 5 L of water) per well. Microplates were closed with lids and placed in a growth chamber (22°C, 12 h light/12 h dark). The 5th day plates were used for measurements. Treatment was done by adding 150µL of the treatment in each well. Measurement was done using Spark plate reader, with settings of excitation wavelength 485 nm, emission wavelength 530 nm, reading from the bottom, 9 points of measurement per well.

3.4. *Gene expression of BGLU42*

Plants were grown as described for RNAseq experiment (Chapter 2). After the growing period, roots were treated with Srf, cut off and frozen in liquid nitrogen. Plant total RNA was then extracted with Invitrogen™ TRIzol™ reagent and isolated following the method edited by Nucleospin® RNA. Expression of *BGLU*42 was quantified by qPCR (QuantStudio™ 3 System) using housekeeping gene Actin as reference and following the protocol described by Luna® Universal One-Step RT-qPCR Kit.

3.5. *Camalexin and Aza detection*

Camalexin was quantified in plants obtained from ISR experiments 96 hours after *B. cinerea* infection. Each sample (three samples per treatment) contained five plants (only rosette leaves) pooled together. Aza was detected in *Arabidopsis* roots that were elicited with Srf for 24 hours (the time point at which plants are infected with *B. cinerea* in the ISR experiment). Plant material was flash-frozen with liquid nitrogen and approximately 100 mg was taken for the extraction. Next, samples were diluted in 1 mL 80% methanol, agitated (using a bench rotating agitator) at room temperature in the dark for 2 hours and centrifuged (14000 RPM). The supernatant was dried in a rotational vacuum concentrator (2-25 CDplus, Christ) at 50°C, and the pellet was resuspended in 1 mL 100% methanol and shaken again for 1 hour. After centrifugation at 14000 RPM, the supernatant was combined with the first one for evaporation. The dry powder was resuspended in 1 mL 100% methanol. Samples were then filtered through 0.2 µm PTFE filters before LC-MS based quantification. The analysis was performed using Agilent 1290 Infinity II HPLC system (Agilent) coupled to an accurate mass detector (Jet Stream ESI-qTOF 6530, Agilent) in positive mode with MS parameters set up as follows : capillary voltage: 3.5 kV; nebulizer pressure: 35 psi; drying gas:8 l min-1; drying gas temperature: 300°C; flow rate of sheath gas: 11 l min-1; sheath gas temperature: 350°C; Nozzle voltage : 1000V; fragmentor voltage: 175 V; skimmer voltage: 65 V; octopole RF: 750 V. Accurate mass spectra was recorded in the range of m/z =100–500. Separation was performed using a C18 Acquity UPLC BEH column (2.1 × 50 mm × 1.7 µm; Waters) and 0.1% formic acid (solvent A)/acetonitrile acidified with 0.1% formic acid (solvent B) as

mobile phase with constant flow rate at 0.2 ml min-1 and column temperature set at 40°C. First, solvent B was kept at 25% during 1min followed by an increase from 25% B to 60% B in 4 min. Then, 100% solvent B was applied for 3 min before going back to initial conditions and kept as such for 5 min before next analysis. Masshunter Qualitative Analysis software (Agilent) was used for data analysis. Quantification of camalexin was performed by comparing camalexin peak area in samples with calibration curve constructed after injection of different concentration (ranging from 0.08 to 20µM) of pure camalexin standard (Sigma-Aldrich). Detection of Aza was done based on mass of the molecule and expressed through peak area/sample weight.

4. Results

4.1. *Hormonal and defense related signaling activated upon treatment with Srf*

Among the phytohormones described as immunity related, RNAseq analysis performed on *Arabidopsis* roots revealed that Srf upregulates genes involved in JA and ET. Regarding JA, both JA synthesis pathway and JA responsive genes were differentially regulated by Srf, with upregulation occurring at the same time point for both, at 1h after treatment (**Figure 37**).

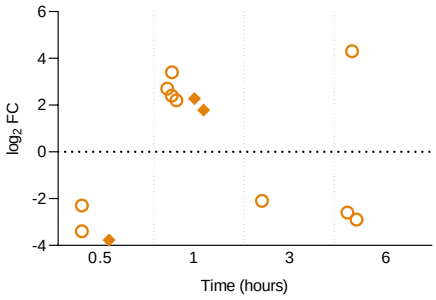

Figure 37 - Induction of genes involved in JA synthesis (circles), and JA-responsive genes (rhombuses) by Srf (**Supplementary table 6 and 7** for the list of genes represented in the graph).

This analysis also revealed a number of ERF transcription factors that are upregulated at 1 and 3h and downregulated at the last time point. Among the Srf-induced genes encoding ERFs, ERF1, ERF2, ERF4, ERF5, and ERF6 are not only related to immunity signaling but could also be JA responsive (**Figure 38;** Lorenzo *et al.*, 2002; McGrath *et al.*, 2005; Moffat *et al.*, 2012). On the other hand, up-regulation of ET synthesis genes was not observed within Srf induced DEGs, leaving it to further plant metabolome analysis to investigate whether these ERFs are induced by JA or ET.

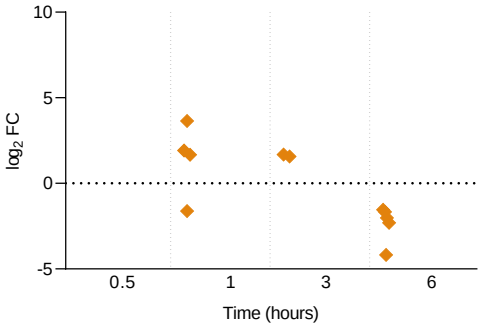

Figure 38 - Ethylene responsive genes induced by Srf (**Supplementary table 8** for the list of genes represented in the graph).

To further analyze the data, a pairwise comparison was performed between the sets of hormone signaling responsive DEGs of Srf, flg22, and chitin (flg22 and chi data were obtained from the literature Stringlis *et al*. 2018). It was observed that ET- and JA-responsive genes were induced by all treatments with different timing and amplitude (**Figure 39a,b**).

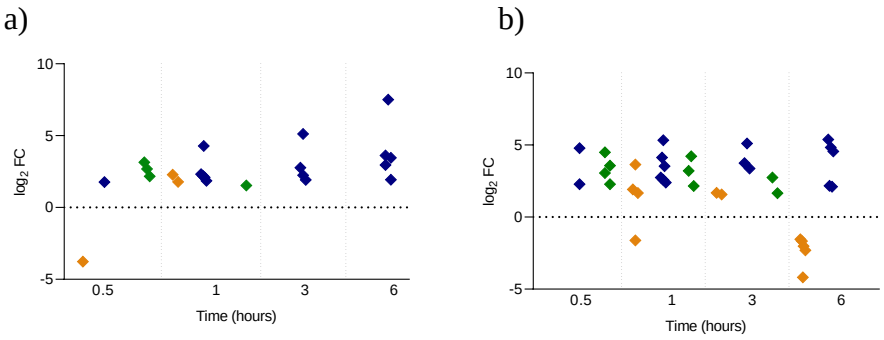

Figure 39 - A comparative analysis of hormonal responsive genes induced by Srf, chitin and flg22**. a)** JA responsive genes and **b)** ET responsive genes induced by Srf (orange), flg22 (blue), and chitin (green). Data for flg22 and chitin originates from Stringlis *et al.*, 2018 (**Supplementary table 8** for the list of genes represented in the graph).

Besides JA and ET, which could be involved in hormonal signaling, our analysis revealed three signaling molecule Aza-responsive genes. In contrast to most of the induced genes related to JA and ET, the Aza responsive genes are downregulated at 1h, whereas they are upregulated at 6 h (**Figure 40a**). In

addition, the preliminary data show a significant increase of Aza in roots upon Srf elicitation, a trend that is not observed in the MS channel mutants *msl4/5/6/9/10* and *mca1/2* impaired in mounting ISR presented in the Chapter 2 (**Figure 40b**).

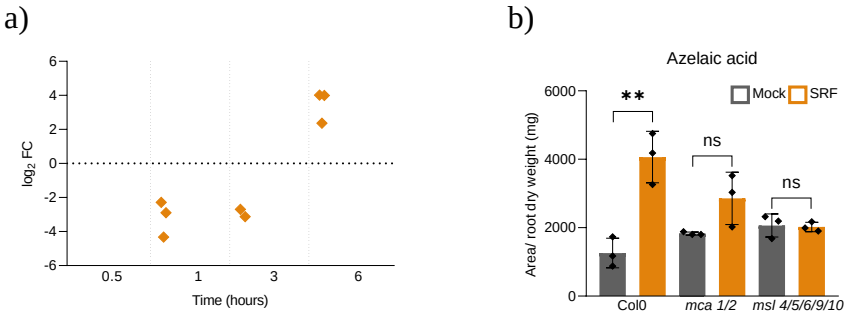

Figure 40 - Influence of Srf treatment on Aza. **a)** Aza responsive genes induced by Srf (**Supplementary table 9** for the list of genes represented in the graph). **b)** Accumulation of azelaic acid in roots of wild type *Arabidopsis* (Col-0) and mutants lacking MS channels MCA 1/2 and MSL 4/5/6/9/10. Asterisks indicate significant difference with ns, not significant; **P<0.01; two-tailed *t*-test.

Interestingly, it can be observed that Aza-responsive genes are not differentially regulated when treated with chitin, whereas flg22 induces slight upregulation of one responsive gene (accession n° At4g12480, encoding the protein pEARLI 1, upregulated at 1h with 1,7 $\log_2$ FC), below the threshold of 2 FC set up in this study. Thus both elicitors have a lower potential to induce Aza signaling than Srf.

In addition to Aza, the entry gene of pipecolic acid synthesis (Bernsdorff *et al*., 2016) can be observed in our RNAseq analysis at 3h (accession n° At2g13810, encoding the ALD1 (AGD2-like defense response protein 1), upregulated at 3,78 $\log_2$ FC). This indicates that Srf may use other defense signaling molecules in addition to Aza. On the other hand, the expression of this gene was not modulated by chitin, and flg22 induced only a slight upregulation (1,68 $\log_2$ FC) at 1h (Stringlis *et al*., 2018). Although a broader time frame of investigation is required, these results could indicate that Aza and pipecolic acid signaling is Srf-specific and not induced by MAMPs.

4.2. *Defense related plant immune responses triggered by Srf*

In contrast to PTI, which is associated with substantial transcriptional reprogramming (Bjornson *et al*., 2021), Srf stimulation of immunity does not lead to major changes in the expression of defense-related markers, such as PAL pathway related genes, pathogenesis-related (PR) proteins or receptor-like kinases, and callose deposition and lignification genes (**Figure 22**). Additionally, within the timeframe tested, Srf does not activate the 9-LOX family genes, which lead to the synthesis of the most of the oxylipins acting as phytoalexins **(Figure 4)**. However, activation of LOX3 and LOX4 enzymes belonging to the 13-LOX family (Wasternack and Song, 2017) could lead to synthesis not only of jasmonates but also of some oxylipins with antimicrobial activity such as 13-HPOT (Deboever *et al*., 2020). Such induction of the LOX pathway by Srf has also been demonstrated in tobacco cells and tomato plants (Jourdan *et al*., 2009; Cawoy *et al*., 2014). Moreover, in tomato, activation of LOX genes was corelated with the accumulation of oxylipins 13-HPOT and 13-HPOD in plant tissues, which may indicate that this also occurs in *Arabidopsis*.

To further explore pathways that could be involved in Srf induced resistance, we investigated the coumarin synthesis pathway, which has been reported as ISR specific for certain beneficials (Zamioudis *et al*., 2014), and camalexin production pathway being reported as one of the most important phytoalexins in *Arabidopsis* and having direct antimicrobial effect against *B. cinerea* (Ferrari *et al*., 2003).

4.2.1. *Activation of coumarin synthesis pathway by Srf*

Since coumarin production strongly relies on the activation of the transcription factor MYB72, we first wanted to verify whether Srf is able to activate this marker gene. To do so, a GFP-tagged line of *Arabidopsis* - *pMYB72:GFP-GUS* was used and it was observed that Srf is very efficient in activating this transcription factor (**Figure 41a**). In addition, our preliminary data show that Srf also upregulates expression of MYB72 downstream gene in the synthesis pathway *BGLU42* (**Figure 41b**).

To verify that the Srf triggered ISR is indeed dependent on this transcription factor, a *myb72-2* knockout mutant was used. When tested on *myb72-2* Srf conserved the ISR elicitor potential (**Figure 41c**), demonstrating that in this elicitor/phytopathosystem ISR is MYB72 independent and does not depend on accumulation of coumarins.

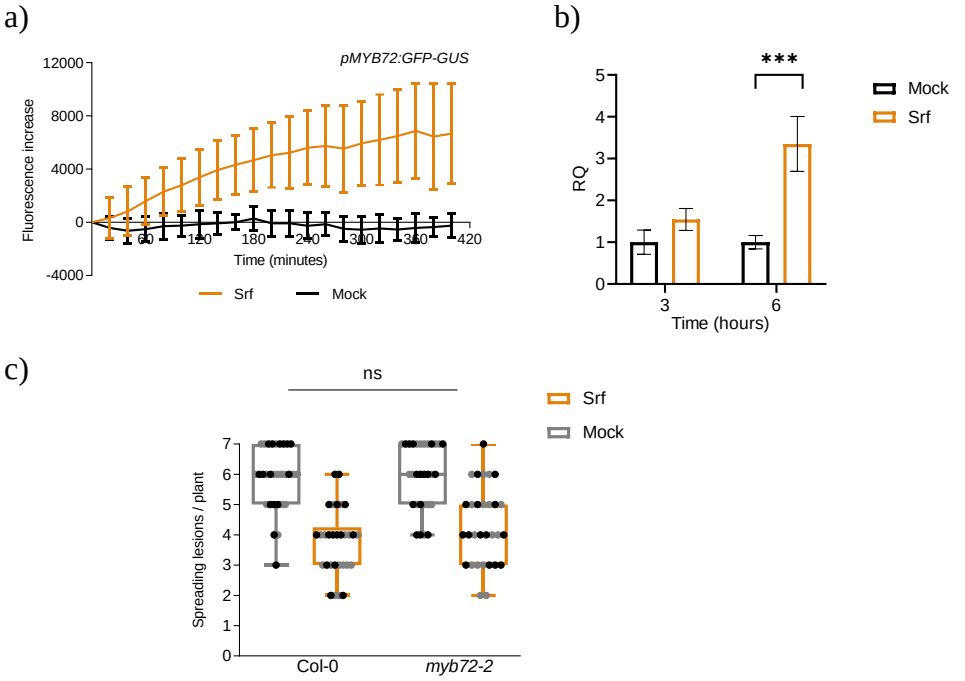

Figure 41 - Activation of coumarin synthesis pathway by Srf. **a)** Fluorescence increase measured in GFP-tagged line of *Arabidopsis* - *pMYB72:GFP-GUS* treated with Srf. Graph represents data from two experiments (each n=4). **b)** Relative quantification of *BGLU42* expression in *Arabidopsis* Col-0 roots after elicitation with Srf (10 µM). Bars represent means of 3 biological repetitions with their standard deviation. n = 8, Student t-test ($P < 0,05$). * = significant difference. **c)** Conserved ISR eliciting effect of Srf in *Arabidopsis* MYB72 transcription factor knockout mutant. n=15, Data are represented as in Figure 10. ns = not significant, two-way ANOVA and Sidak's multiple-comparison post-test.

4.2.2. *Involvement of camalexin in elevated resistance triggered by Srf against B. cinerea*

To verify the involvement of camalexin in Srf-triggered ISR, we first quantified the presence of this molecule, which showed a significantly higher amounts of this phytoalexin in infected leaves of Srf-treated plants compared

to controls (**Figure 42a**). To confirm the key role of camalexin in disease control, we also performed an ISR experiment with a mutant line *PHYTOALEXIN DEFICIENT3* (*pad3*), unable to synthesized camalexin (Denoux *et al*., 2008). The results showed that Srf loses the ISR effect in these mutant plants, confirming the importance of camalexin for Srf triggered enhanced resistance against *B. cinerea* (**Figure 42b**).

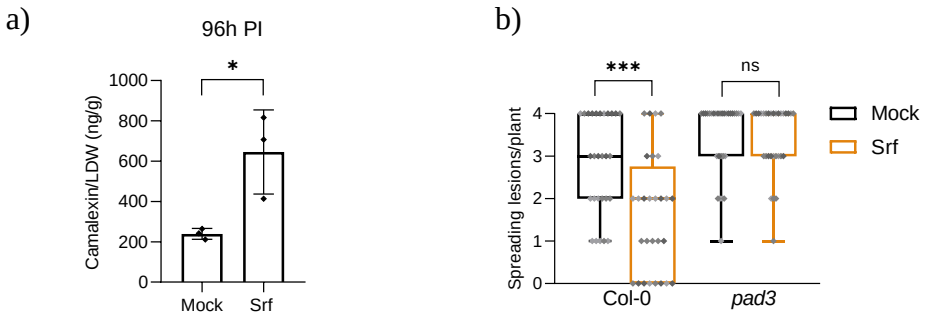

Figure 42 - a) Camalexin accumulation 96 hours post *B. cinerea* inoculation (hpi) in *Arabidopsis* Col-0 leaves of mock- or 10 µM Srf-treated plants. Graph shows values obtained in one experiment with each value representing a sample of five plants pooled together. Asterisks indicate significant difference with ns, not significant; *P<0.05; ***P<0.001; two-tailed *t*-test.
b) Disease incidence of *B. cinerea* in *pad3* mutant pretreated with 10 µM Srf or mock-treated at the root level (n=30, values obtained from three independent experiments, presented as differently shaded grey values). Data are represented as in Figure 10. Asterisks indicate significant difference with ns, not significant; *P<0.05; ***P<0.001; two-way ANOVA and Sidak's multiple-comparison post-test.

Interestingly, *CYP71A12*, encoding a key enzyme of the camalexin biosynthesis pathway (Müller *et al*., 2015), is one of the few genes strongly stimulated by Srf during the silent phase of priming, before pathogen infection. Compared to flg22 and chitin, inducing this gene already 30 minutes after the treatment, the Srf-induced upregulation of this gene at 6h is quite late. However, the *PAD3* gene, encoding the final enzyme of the synthesis pathway upregulated alongside *CYP71A12* by flg22 and chitin, is not upregulated by Srf, and even a slight downregulation can be observed at the first time point (**Figure 43**). This might indicate that Srf primes plants by accumulating precursors of this phytoalexin, such as indole-3-acetaldoxime, enabling plant to synthesize higher amounts more rapidly after the pathogen attack.

Considering that in our ISR experiments plants are elicited by Srf for 24h and then infected, a broader time frame of investigation is needed in order to confirm the aforementioned theory.

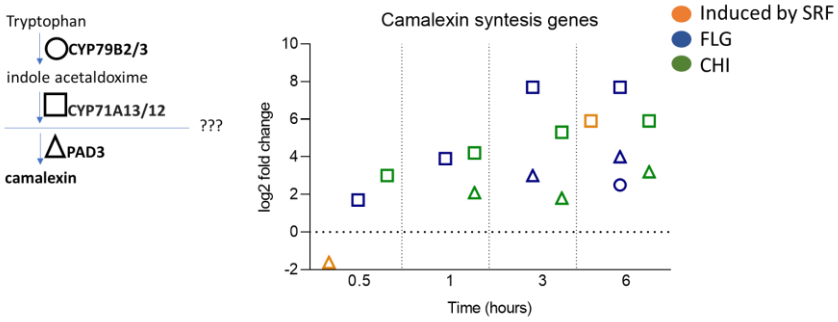

Figure 43 - Genes involved in camalexin synthesis pathway differentially regulated by Srf, flg22 (FLG) and chitin (CHI). Data for flg22 and chitin originates from Stringlis *et al.*, 2018.

4.3. *Genes encoding hypothetical/unknown proteins and proteins of unknown function modulated by Srf*

Considering that ISR is a phenomenon still to be deciphered, it is not surprising that RNSseq analysis revealed that approximately 21% of the total DEGs (85 out of 398) elicited by Srf encode hypothetical/unknown proteins and proteins of unknown function (hereafter referred to as unknowns) (**Figure 44a**). This proportion is slightly more pronounced at the first time point analyzed, 30 minutes after Srf treatment, where 28% (27 out of 98) of the DEGs are unknowns.

To better understand how these proteins might be involved in plant immunity, instead of gene sequences we further analyzed sequences of predicted proteins with a widely used database of protein families-Pfam. Out of 85 protein sequences tested, this analysis provided more information for 3 proteins (e-value < e-25, percentage of identical match > 30; alignment length > 100), giving only a vague idea about their function (**Supplementary Table 10**). To obtain more information, a web-based bioinformatics tool (SignalP-version 5.0) was used, which predicted that 20 of the unknown proteins could be secretory signal peptides transported by the Sec translocon and cleaved by

signal peptidase I (**Figure 44b**). Although, not conclusive, these data can also be used to further investigate defense signaling pathways induced by Srf.

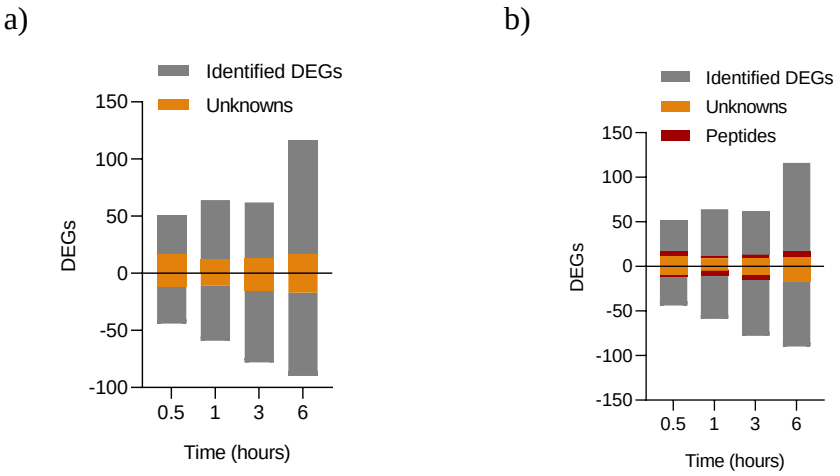

Figure 44 - Genes encoding hypothetical/unknown proteins and proteins of unknown function modulated by Srf. **a)** DEGs induced by Srf encoding hypothetical/unknown proteins and proteins of unknown function. **b)** Protein sequences of unknowns showing similarities with signaling peptides.

5. Discussion

Among the three most important hormones involved in immunity signaling, SA, JA, and ET (Chapter 1, section 3.3.), our RNAseq revealed differential regulation of genes related to JA and ET. However, neither synthesis nor responsive genes related to SA were detected. Regarding JA synthesis pathway, Srf upregulated genes were the ones acting upstream of OPDA synthesis (**Figure 28, 29**). This could indicate that the signaling is achieved by this molecule (Wasternack and Song *et al*., 2017), however, jasmonates plant metabolome upon Srf elicitation would have to be analyzed in order to confirm this hypothesis.

On the other hand, results showing Aza responsive genes being upregulated by Srf and not significantly modulated by the two MAMPs reinforce the importance of Aza in defense signaling. The possible lack of induction of Aza production by Srf in MSC mutants may be related to its synthesis pathway. Aza is produced by oxidation of linolenic acid by ROS (Shine *et al*., 2019), and since ROS is not triggered by Srf in MS mutants this could be the explanation. This indicates that Aza could be involved in onset of ISR triggered by Srf, although study on mutants lacking Aza responsive genes is needed to confirm this. Also, considering that G3P is activated by Aza, that Srf triggers NO^- production, and upregulates the entry enzyme of pipecolic acid synthesis, it can be postulated that besides Aza, Srf uses numerous defenses related signaling molecules to achieve signaling. Even though further investigation is needed, it can also be postulated that the part of unknowns that may act as signaling peptides is also important for the establishment of ISR triggered by Srf.

Even though it was shown that overexpression of BGLU42 leads to constitutive resistance against *Botrytis cinerea*, *Pseudomonas syringae* pv. *tomato* DC3000 and *Hyaloperonospora arabidopsidis* in *Arabidopsis*, this study shows that in the case of Srf triggered immunity, ISR to *B. cinerea* is independent of MYB72 (Zamioudis *et al*., 2015; Pescador *et al*., 2022). Interestingly, this trend was also observed for ISR triggered by *N*-acyl-homoserine lactones, amphiphilic molecules which are also suspected to interact with membrane lipids (Schenk *et al* 2014; Song *et al*., 2018). Although ISR is MYB72-independent in our phytopathosystem, it has already been shown that activation of MYB72 also may lead to inhibition of soil-borne

fungal pathogens *Fusarium oxysporum* and *Verticillium dahliae* (Stringlis *et al*., 2018), thus it cannot be excluded that elicitation of plant by Srf also has this beneficial effect.

As already mentioned, it remains unclear how plants are able to selectively trigger camalexin production depending on the lifestyle (beneficial or pathogenic) of the microorganism colonizing the plant (Nguyen *et al*., 2022a,b). Although this question remains unresolved, based on these results, it could be postulated that beneficials lead to the accumulation of camalexin precursors and that is how the final boost of pathogen triggered camalexin production is achieved.

Generally, since a very low transcriptional reprogramming (both in terms of number and amplitude of up- or down-regulated DEGs) is induced by surfactin compared to some MAMPs triggering PTI, it could be assumed that certain responses are induced in cell layer- or root zone-specific manner. Considering that Srf is expected to interact with PPM and not penetrate in cells nor further than root epidermis, it can be also hypothesized that outer root cells would have different response compared to the central zone of root with which cells Srf is not expected to interact. This could be overcome by using single cell RNA-seq technology which could give insight in more plant responses induced locally by Srf (especially in epidermis cells) and form a general picture of how plant roots respond to this elicitor.

All together these data give a good bases for further investigation of the silent phase of ISR triggered by Srf, and give an insight into what are possible mechanisms used for achieving ISR.

6. Data authorship

This work is a result of cooperation with different colleagues, which helped in realizing work presented in following figures:

Fig 40b, 42a, in cooperation with Anthony Arguelles Arias

44a,b in cooperation with Heba Ibrahim.

Additionally, as aforementioned raw RNAseq data was processed by Heba Ibrahim.

7. Supplementary data

Supplementary table 6 - JA synthesis and JA-responsive genes induced by Srf represented in **Figure 33**

gene		hours			
		0,5	**1**	**3**	**6**
At1g05800	Lipase (DONGEL (DGL))	-2.3	3.4		
At1g17420	LIPOXYGENASE 3, LOX3	-3,4	2,7		-2,6
At1g72520	LIPOXYGENASE 4, LOX4		2,480358		-2,9519
At3g25760	AOC 1			-2.1	4.3
At3g25770	AOC 2		2.2		
At2g34600	JAZ7, TIFY5B, jasmonate-zim-domain protein 7				-2,16484
At1g30135	JAZ8, TIFY5A, jasmonate-zim-domain protein 8	-3,7722	2,275016		-2,68958

Supplementary table 7 - JA-responsive genes induced by Srf, chi (chitin) and flg (flagellin22) represented in **Figure 35 a**.

gene		elicitor	hours			
			0,5	**1**	**3**	**6**
At1g19180	JAZ1, TIFY10A, jasmonate-zim-domain protein 1	Srf				
		chi	3,13794			
		flg				2,95655
At1g17380	JAZ5, TIFY11A, jasmonate-zim-domain protein 5	Srf				
		chi	2,16953			
		flg		2,09874		
At1g72450	JAZ6, TIFY11B, jasmonate-zim-domain protein 6	Srf				
		chi	2,68564			
		flg		2,20909	2,24085	3,45773
At2g34600	JAZ7, TIFY5B, jasmonate-zim-domain protein 7	Srf				-2,16484
		chi				
		flg				
At1g30135	JAZ8, TIFY5A, jasmonate-zim-domain protein 8	Srf	-3,7722	2,27501		-2,68958
		chi				
		flg		4,27898	5,11440	7,50034
At5g13220	JAZ10, TIFY9, jasmonate-zim-domain protein 10	Srf				
		chi				
		flg		2,32146	2,76998	3,62148

Supplementary table 8 - ET-responsive genes induced by Srf, chi (chitin) and flg (flagellin22) represented in **Figure 35 b**.

gene		elicitor	hours			
			0,5	**1**	**3**	**6**
At3g23240	ATERF1, ERF1, ethylene response factor 1	Srf				
		chi		4,220	2,738	
		flg		5,331	5,108	5,378
At4g17500	ATERF-1, ERF-1, ethylene responsive element binding factor 1	Srf				
		chi	2,625	2,036		
		flg		3,266	2,985	3,977
At5g47220	ATERF-2, ATERF2, ERF2, ethylene responsive element binding factor 2	Srf				
		chi	3,053	3,211		
		flg		4,128	3,738	4,833
At5g47230	ATERF-5, ATERF5, ERF5, ethylene responsive element binding factor 5	Srf				
		chi	2,282			
		flg		2,576		2,104
At4g17490	ATERF6, ERF-6-6, ERF6, ethylene responsive element binding factor 6	Srf				-2,303
		chi	3,572	2,157		
		flg	2,286	3,535	3,3701	4,561
At5g61600	ERF104, ethylene response factor 104	Srf				-2,014
		chi				
		flg		2,389		

Supplementary table 9 – Aza responsive genes differentially regulated by Srf represented in **Figure 36a.**

gene		hours			
		0,5	**1**	**3**	**6**
At4g12470	AZI1, azelaic acid induced 1		-2,890	-2,690	4,012
At4g12480	pEARLI 1, Bifunctional inhibitor/lipid-transfer protein/seed storage 2S albumin superfamily protein		-4,321	-3,129	3,993
At4g12500	Bifunctional inhibitor/lipid-transfer protein/seed storage 2S albumin superfamily protein		-2,289		2,366

Supplementary table 10 - Proteins with similar sequences found in the Pfam database

gene coding unknown	hours PT	log2 change	Protein with similar AA sequence
At2g44220	3h	2,3143	Domain of unknown function (DUF239). This is a family of plant and bacterial proteins, a small number of which are putative carboxy-terminal peptidases.
At4g03540	6h	2,6471	DUF588, Domain of unknown function (DUF588). This family of plant proteins contains a domain that may have a catalytic activity. It has a conserved arginine and aspartate that could form an active site. These proteins are predicted to contain 3 or 4 transmembrane helices.
At4g29780	6h	-4,0794	DDE_Tnp_4, DDE superfamily endonuclease. This family of proteins are related to pfam00665 and are probably endonucleases of the DDE superfamily. Transposase proteins are necessary for efficient DNA transposition. This domain is a member of the DDE superfamily, which contain three carboxylate residues that are believed to be responsible for coordinating metal ions needed for catalysis. The catalytic activity of this enzyme involves DNA cleavage at a specific site followed by a strand transfer reaction.

8. References

Bakker PAHM, Pieterse CMJ, Van Loon LC. Induced systemic resistance by fluorescent Pseudomonas spp. *Phytopathology*. 2007;97(2):239-243. doi:10.1094/PHYTO-97-2-0239

Berens ML, Berry HM, Mine A, Argueso CT, Tsuda K. Evolution of Hormone Signaling Networks in Plant Defense. *Annu Rev Phytopathol*. 2017;55:401-425. doi:10.1146/annurev-phyto-080516-035544

Bernsdorff F, Döring A-C, Gruner K, Schuck S, Bräutigam A, Zeier J. Pipecolic Acid Orchestrates Plant Systemic Acquired Resistance and Defense Priming via Salicylic Acid-Dependent and -Independent Pathways. *Plant Cell*. 2016;28(1):102-129. doi:10.1105/tpc.15.00496

Bjornson, M., Pimprikar, P., Nürnberger, T., Zipfel, C. The transcriptional landscape of Arabidopsis thaliana pattern-triggered immunity. *Nat. Plants* 7, 579–586 (2021).

Cawoy H, Mariutto M, Henry G, et al. Plant defense stimulation by natural isolates of Bacillus depends on efficient surfactin production. Mol *Plant-Microbe Interact*. 2014;27(2):87-100. doi:10.1094/MPMI-09-13-0262-R

Cecchini NM, Steffes K, Schläppi MR, Gifford AN, Greenberg JT. Arabidopsis AZI1 family proteins mediate signal mobilization for systemic defence priming. *Nat Commun*. 2015;6(1):7658. doi:10.1038/ncomms8658

De Kesel J, Conrath U, Flors V, et al. The Induced Resistance Lexicon: Do's and Don'ts. *Trends Plant Sci*. 2021;(January). doi:10.1016/j.tplants.2021.01.001

Denoux C, Galletti R, Mammarella N, et al. Activation of defense response pathways by OGs and Flg22 elicitors in Arabidopsis seedlings. *Mol Plant*. 2008;1(3):423-445. doi:10.1093/mp/ssn019

Estelle D, Laurence L, Marc O, Caroline DC, Magali D, Marie-Laure F. Linolenic fatty acid hydroperoxide acts as biocide on plant pathogenic

bacteria: Biophysical investigation of the mode of action. *Bioorg Chem*. 2020;100(May):103877. doi:10.1016/j.bioorg.2020.103877

Ferrari S, Galletti R, Denoux C, De Lorenzo G, Ausubel FM, Dewdney J. Resistance to Botrytis cinerea induced in arabidopsis by elicitors is independent of salicylic acid, ethylene, or jasmonate signaling but requires PHYTOALEXIN DEFICIENT3. *Plant Physiol*. 2007;144(1):367-379. doi:10.1104/pp.107.095596

Gimenez-Ibanez S, Solano R. Nuclear jasmonate and salicylate signaling and crosstalk in defense against pathogens. *Front Plant Sci*. 2013;4(APR):1-11. doi:10.3389/fpls.2013.00072

Glazebrook J, Ausubel FM. Isolation of phytoalexin-deficient mutants of Arabidopsis thaliana and characterization of their interactions with bacterial pathogens. *Proc Natl Acad Sci U S* A. 1994;91(19):8955-8959. doi:10.1073/pnas.91.19.8955

Jourdan E, Henry G, Duby F, et al. Insights into the defense-related events occurring in plant cells following perception of surfactin-type lipopeptide from Bacillus subtilis. *Mol Plant-Microbe Interact*. 2009;22(4):456-468. doi:10.1094/MPMI-22-4-0456

Jung HW, Tschaplinski TJ, Wang L, Glazebrook J, Greenberg JT. Priming in Systemic Plant Immunity. *Science* (80-). 2009;324(5923):89-91. doi:10.1126/science.1170025

Lorenzo O, Piqueras R, Sánchez-Serrano JJ, Solano R. ETHYLENE RESPONSE FACTOR1 integrates signals from ethylene and jasmonate pathways in plant defense. *Plant Cell*. 2003;15(1):165-178. doi:10.1105/tpc.007468

McGrath KC, Dombrecht B, Manners JM, et al. Repressor- and activator-type ethylene response factors functioning in jasmonate signaling and disease resistance identified via a genome-wide screen of Arabidopsis transcription factor gene expression. *Plant Physiol*. 2005;139(2):949-959. doi:10.1104/pp.105.068544

Moffat CS, Ingle RA, Wathugala DL, Saunders NJ, Knight H, Knight MR. ERF5 and ERF6 play redundant roles as positive regulators of JA/Et-

mediated defense against botrytis cinerea in arabidopsis. *PLoS One.* 2012;7(4):1-11. doi:10.1371/journal.pone.0035995

Mueller S, Hilbert B, Dueckershoff K, et al. General Detoxification and Stress Responses Are Mediated by Oxidized Lipids through TGA Transcription Factors in Arabidopsis. *Plant Cell*. 2008;20(3):768-785. doi:10.1105/tpc.107.054809

Müller TM, Böttcher C, Morbitzer R, et al. Transcription activator-like effector nuclease-mediated generation and metabolic analysis of camalexin-deficient cyp71a12 cyp71a13 double knockout lines. *Plant Physiol.* 2015;168(3):849-858. doi:10.1104/pp.15.00481

Nguyen NH, Trotel-Aziz P, Clément C, Jeandet P, Baillieul F, Aziz A. Camalexin accumulation as a component of plant immunity during interactions with pathogens and beneficial microbes. *Planta*. 2022;255(6):116. doi:10.1007/s00425-022-03907-1

Nguyen NH, Trotel-Aziz P, Villaume S, et al. Priming of camalexin accumulation in induced systemic resistance by beneficial bacteria against Botrytis cinerea and Pseudomonas syringae pv. tomato DC3000. Höfte M, ed. *J Exp Bot*. 2022;73(11):3743-3757. doi:10.1093/jxb/erac070

Oelmüller R. Threat at One End of the Plant: What Travels to Inform the Other Parts? *Int J Mol Sci*. 2021;22(6):3152. doi:10.3390/ijms22063152

Pescador L, Fernandez I, Pozo MJ, Romero-Puertas MC, Pieterse CMJ, Martínez-Medina A. Nitric oxide signalling in roots is required for MYB72-dependent systemic resistance induced by Trichoderma volatile compounds in Arabidopsis. *J Exp Bot*. 2022;73(2):584-595. doi:10.1093/jxb/erab294

Pieterse CMJ. Prime Time for Transgenerational Defense. *Plant Physiol*. 2012;158(2):545-545. doi:10.1104/pp.112.900430

Schenk ST, Hernández-Reyes C, Samans B, et al. N -Acyl-Homoserine Lactone Primes Plants for Cell Wall Reinforcement and Induces Resistance to Bacterial Pathogens via the Salicylic Acid/Oxylipin Pathway. *Plant Cell*. 2014;26(6):2708-2723. doi:10.1105/tpc.114.126763

Shine MB, Xiao X, Kachroo P, Kachroo A. Signaling mechanisms underlying systemic acquired resistance to microbial pathogens. *Plant Sci*. 2019;279(January 2018):81-86. doi:10.1016/j.plantsci.2018.01.001

Song D, Meng J, Cheng J, et al. Pseudomonas aeruginosa quorum-sensing metabolite induces host immune cell death through cell surface lipid domain dissolution. *Nat Microbiol*. 2019;4(1):97-111. doi:10.1038/s41564-018-0290-8

Stringlis IA, Yu K, Feussner K, et al. MYB72-dependent coumarin exudation shapes root microbiome assembly to promote plant health. *Proc Natl Acad Sci U S A.* 2018;115(22):E5213-E5222. doi:10.1073/pnas.1722335115

Taki N, Sasaki-Sekimoto Y, Obayashi T, et al. 12-Oxo-phytodienoic acid triggers expression of a distinct set of genes and plays a role in wound-induced gene expression in Arabidopsis. *Plant Physiol*. 2005;139(3):1268-1283. doi:10.1104/pp.105.067058

Van Der Ent S, Verhagen BWM, Van Doorn R, et al. MYB72 is required in early signaling steps of rhizobacteria-induced systemic resistance in arabidopsis. *Plant Physiol*. 2008;146(3):1293-1304. doi:10.1104/pp.107.113829

Vlot AC, Sales JH, Lenk M, et al. Systemic propagation of immunity in plants. *New Phytol*. 2021;229(3):1234-1250. doi:10.1111/nph.16953

Wasternack C, Song S. Jasmonates: Biosynthesis, metabolism, and signaling by proteins activating and repressing transcription. *J Exp Bot*. 2017;68(6):1303-1321. doi:10.1093/jxb/erw443

Zamioudis C, Hanson J, Pieterse CMJ. β-Glucosidase BGLU42 is a MYB72-dependent key regulator of rhizobacteria-induced systemic resistance and modulates iron deficiency responses in Arabidopsis roots. *New Phytol*. 2014;204(2):368-379. doi:10.1111/nph.12980

Zamioudis C, Korteland J, Van Pelt JA, et al. Rhizobacterial volatiles and photosynthesis-related signals coordinate MYB 72 expression in Arabidopsis roots during onset of induced systemic resistance and iron-

deficiency responses. *Delseny M, ed. Plant J.* 2015;84(2):309-322. doi:10.1111/tpj.12995

Zamioudis C, Korteland J, Van Pelt JA, et al. Rhizobacterial volatiles and photosynthesis-related signals coordinate MYB 72 expression in Arabidopsis roots during onset of induced systemic resistance and iron-deficiency responses. *Plant J.* 2015;84(2):309-322. doi:10.1111/tpj.12995

Chapter 4

Structural features driving the plant immunity elicitor activity of bacterial lipopeptides

1. Abstract

Cyclic lipopeptides are particularly important for triggering ISR in plants, where surfactin produced by biocontrol bacilli has a leading role having a strong elicitor potential on various plant species. Previously presented findings of this thesis demonstrated that this ISR elicitor is most likely not recognized by plant pattern recognition receptors, but that it rather interacts with the lipid part of the plasma membrane. Considering the peculiarity of the interaction as a next task an influence of the CLP structure on its potential to activate early plant immune events was estimated. As markers for early plant immune events, the CLPs potential to stimulate production of reactive oxygen and nitrogen species, being important indicators of immunity activation was measured. Additionally, for selected candidates ISR stimulation potential was also estimated. Altogether our data points out that structural changes in peptide cycle, such as one amino acid differences, have previously unsuspected importance in triggering both immune response markers and ISR itself.

2. Introduction

The bioactivity of CLPs depends on the compatibility of CLP with the plant species / organ (Chapter 1, section 4.1.7.) and it is strongly influenced by their interaction with specific PPM lipids (Chapter 2). Based on this, we suspected that variation in activity could be due to CLP/PPM interaction being bidirectionally influenced by PPM lipids and CLP structure. To investigate the extent to which structural changes of CLPs influence the interaction, we used *Arabidopsis* roots as a PPM model and CLP variants with similar structures. Among the CLPs, naturally occurring Srf-like CLPs, lichenysin and pumilacidin (**Figure 8**) were used to obtain more precise information on which are the crucial structural features for Srf's activity. As for Srf in previous chapters, these CLPs were used as a mix of homologues slightly differing in the length of the fatty acid tail (**Supplementary table 11**) as they are produced by bacilli in nature. In addition, beneficial pseudomonads produced WLIP and massetolide A (**Figure 7**) were selected as CLPs that have already been reported as ISR elicitors (Oni *et al*., 2022). Even though their structure is quite different from that of Srf, between the two of them there is only one amino acid difference, so they were used to confirm whether structure-dependent activity is generally present in CLPs.

So far, biophysical experiments investigating CLP/membrane interactions have shown that amphiphilic CLPs, such as Srf, interact with lipids of membrane mimicking bilayers in two main ways. Electrostatically with the charged headgroups, and also with the hydrophobic region of the lipid bilayer. Subsequently, the effect that Srf will have on these models, and potentially on PPM, largely depends on its properties such as geometry, charge, and hydrophobicity (Francius *et al*., 2008; Balleza *et al* 2019). Thus, at the outset of this work, considering this important role of hydrophobicity, we first estimated differences in hydrophobicity of the CLPs to be tested.

Even though, the structural differences between Srf, lichenysin, and pumilacidin are minor, they can affect their biophysical properties. CLPs are known for their high potential to reduce surface tension and for their ability to self-assemble in sphere-like micelles when the critical micellar concentration is reached in aqueous media. For instance, the change of Val4 to Leu4 that is present in pumilacidin compared to Srf, results in lower potential to reduce the

surface tension and acts unfavorably on the self-assembly (Théatre et al., 2022).

To assess the influence of the CLP structure on its bioactivity, we measured CLPs potential to stimulate early plant immune events and defense-related responses. As markers for early plant immune events, we measured the CLPs potential to stimulate the production of reactive oxygen and nitrogen species, ROS and RNS, respectively, being important indicators of immunity activation (see Chapter 1, section 3). As a defense response marker, MYB72 activation, described as specific for ISR triggered by certain beneficials (Stringlis *et al*., 2019), was measured. Finally, the ISR stimulation potential of selected CLPs was estimated as an indicator of their bioactivity.

3. Materials and methods

3.1. *Pumilacidin and lichenysin production and purification*

Srf mix was purified as previously described (Chapter 2). In order to obtain the Srf-like CLP in form of mixes of homologues as they occur in nature, two different strains of *Bacillus* sp. were used: *B. pumilus* 41 for pumilacidin and *B. licheniformis* BBG-143 for lichenysin (homologues of the mix listed in the **Supplementary Table 11**). Bacterial cultures were incubated for 24 h in LB media at 30°C with continuous shaking (180 rpm). For pumilacidin, cultures were inoculated into LB media at 10% of the flask volume and incubated on orbital shaker (180 rpm) at 30°C for 72 h. To produce lichenysin, the culture was inoculated into LB media supplemented with 1% of xylose and incubated in orbital shaker (180 rpm) at 30°C for 72 h. After 72 h, cultures were centrifuged at 10 000 rpm for 1 h to collect the supernatant. CLPs were then extracted from cell-free supernatants by acid precipitation. To do so, supernatants were acidified to pH = 2 with 4N HCl and incubated at 4°C overnight. Precipitates containing CLPs were collected by centrifugation (14 000 rpm, 1 h) and resuspended in water. Furthermore liquid-liquid extraction was conducted with solvent (50:50) composed of butanol (30%) and ethyl acetate (70%). Final CLPs purification was conducted by HPLC system (Agilent Serie 1100) with C18 reversed phase (Luna® Omega 5 µm, 250 x 10 mm) and a solution of acetonitrile and water in a ratio 90:10 was used as a mobile phase at 4 mL/min. The final concentration and purity of CLPs were determined by LC-MS analysis (QTOF, Agilent 6530) with ESI ion source in positive mode (Dual AJS ESI). The liquid chromatography (Agilent 1250 infinity 2) separation was performed on a C18 column (Acquity UPLC® BEH 1.7 µm, 2.1 x 50 mm) with H2O/ACN 53:47 at 0 min, H2O/CAN 0:100 from 0 to 14 min and H_2O/ACN 53:47 at 14,5 min. To purify the CLPs homologs, the same protocol was applied but homologs were separated during HPLC purification with the same method as the one used for the mix.

3.2. *Hydrophobicity*

Hydrophobicity index (ϕ) of the peptide of the CLPs was calculated as an average of Amino acid side chain hydrophobicities (Bigelow 1967). The method used for UPLC-MS is described in Chapter 2, section 3.1.

4. Results

4.1. *Hydrophobicity of structurally similar CLPs*

As an important feature influencing the interaction with biological membranes, we first wanted to estimate and compare the relative hydrophobicity of the selected CLPs. We used the Bigelow method, which calculates a global hydrophobicity index (ϕ) based on the type of side chains of the amino acids constituting the peptide moiety of the CLP (Bigelow 1967). We observed that changes in the amino acids in the peptide result in different hydrophobicity of lichenysin and pumilacidin, with pumilacidin being the most affected compared to Srf (**Figure 45a**). Pumilacidin's changes Val4 to Leu4 and Leu7 to Ile7 result in an increase in hydrophobicity at these two positions from 1,7 to 2,4 kcal/res, and 2,4 to 2,95 kcal/res, respectively, thus rendering pumilacidin the most hydrophobic peptide cycle among the three CLPs. The same trend was also indicated by observing the retention times in reversed-phase UPLC-MS which is related to the strength of the interaction with the C18 matrix of the column based on the relative polarity of the molecules. As shown in **Figure 45b** for homologues with a C14 fatty acid, surfactin eluted first, followed by lichenysin and lastly pumilacidin reflecting increase in apolarity of the cyclized peptide in the same order. Moreover, since hydrophobicity increases with the length of the FA chain, it is expected that pumilacidin's mix of homologues used in this study has higher hydrophobicity than Srf's and lichenysin's, having on average slightly longer length FA chains variants (**Supplementary Figure 5, Supplementary Table 11**).

Correlation between Bigelow calculation and retention times in UPLC was also observed for two pseudomonads CLPs. Namely, switch of Val that is present in position 2 of the WLIP's cycle to isoleucine that is present in massetolide A makes WLIP less hydrophobic (**Figure 45a,b**).

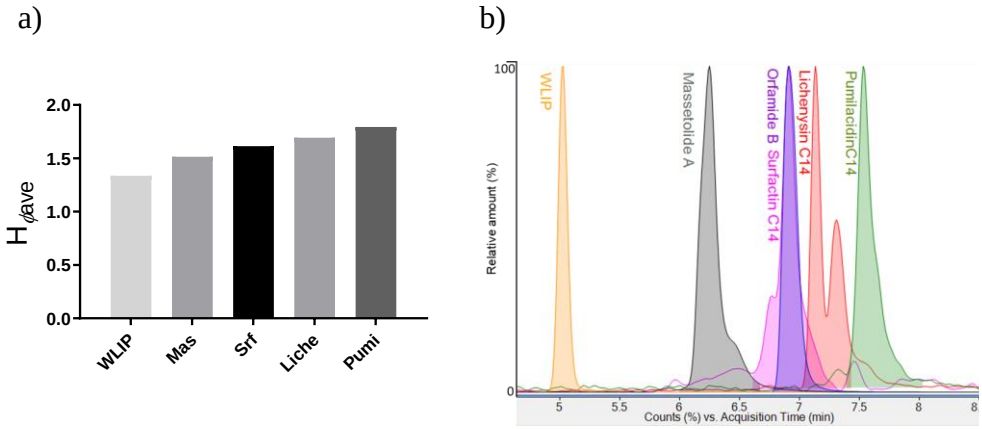

Figure 45 - Hydrophobicity of Srf, and structurally similar pumilacidin (Pumi) and lichenysin (Liche); **a)** The peptide ring hydrophobicity predicted based on amino acids side chain hydrophobicity (Bigalo calculation); **b)** Polarity of the solvent needed for C14 (Srf, lichenysin, pumilacidin and orfamide B) and C10 homologues (WLIP and Massetolide A) indicated by observing the retention times in reversed-phase UPLC-MS

4.2. *Influence of CLP structure on potential to trigger oxidative species burst*

ROS and NO^- burst are the earliest measurable immune events conferring plants with effective immune responses (Chapter 1, sections 3.2.1. and 3.2.2.), which are effectively induced by Srf (Chapter 2). Compared to other CLPs tested in this study, Srf induces production of ROS and NO^- to a similar extent as lichenysin, whereas pumilacidin does not induce either of these markers of immunity (**Figure 46b** and **Figure 46c**, respectively; **Supplementary Figure 6** for the kinetic view). Thus, although both pumilacidin and lichenysin have altered structures compared to Srf, these changes do not affect their activity in the same manner.

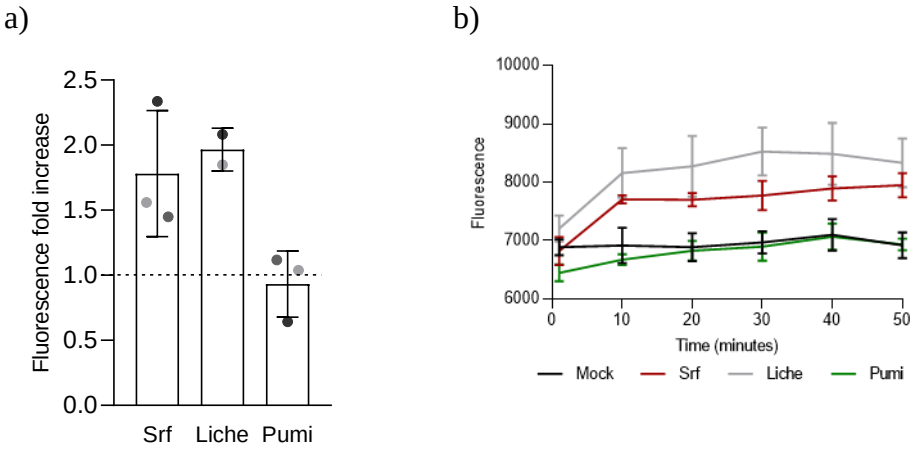

Figure 46 - Induction of oxidative species burst by surfactin (Srf), lichenysin (Liche), and pumilacidin (Pumi): **a)** $[ROS]_{intra}$ production; **b)** NO^- production. The fold change calculated by using values obtained from the mock treated roots. Dots represent values obtained from three independent experiments, each n=4 per treatment.

As shown in Chapter 2 (**Figure 27**), both pseudomonad CLPs trigger ROS production. However, a structure-dependent activity was observed in the potential for NO^- activation, where massetolide A failed and WLIP induced the production, which was slightly less pronounced compared to Srf (**Figure 47**).

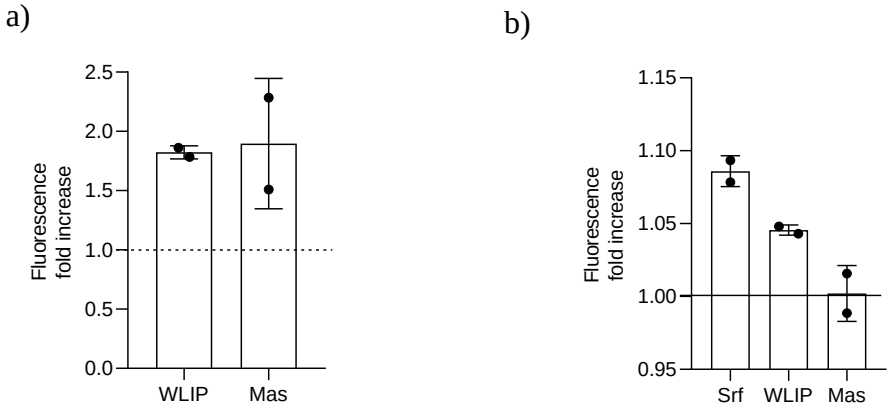

Figure 47 - Influence of structure on bioactivity of structurally similar pseudomonads produced CLPs inducing ISR; **a)** ROS production triggered by WLIP and massetolide A (Mass); **b)** Production of RNS measured in WLIP and MASS treated roots; The fold change calculated by using values obtained from the mock treated roots. Dots represent values obtained from two independent experiments, each n=4 per treatment.

4.3. *Coumarins synthesis marker gene activation by different CLPs*

As shown previously, Srf strongly activates the transcription factor MYB72 (Chapter 3, **Figure 41a**), which is often used as a marker for the coumarins synthesis pathway (Stringlis *et al*., 2019). MYB72 might not be involved in the ISR triggered by Srf against *B. cinerea* (Chapter 4**, Figure 41c**), yet this transcription factor has an important role in the production of phytoalexins coumarins and might therefore be involved in resistance to other pathogens. To test whether MYB72 activation is structure dependent, a GFP tagged *Arabidopsis* line was used as described in Chapter 3. Among all the CLPs used, only WLIP showed the potential to activate this transcription factor, although to a lower extent compared to Srf. On the other hand, pumilacidin, lichenysin, and massetolide A failed to induce this transcription factor (**Figure 48a,b**).

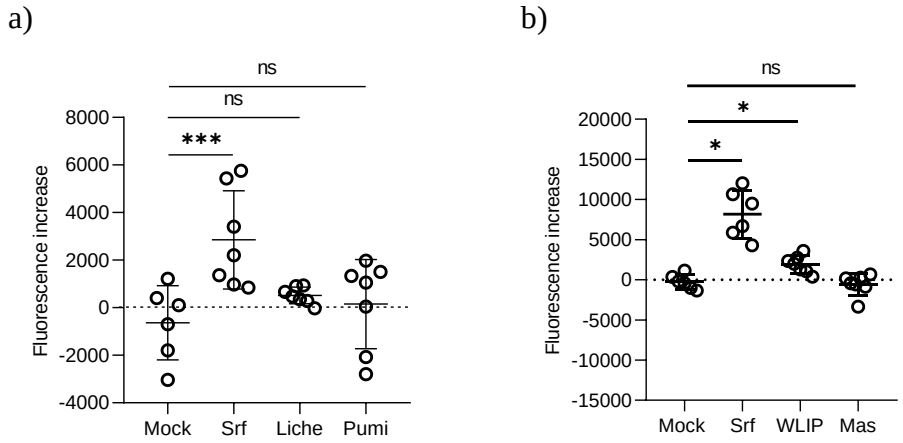

Figure 48 - Activation of MYB72 by CLPs observed as an increase of GFP fluorescence of *pMYB72:GFP-GUS*. Fluorescence values obtained at 320 minutes post elicitation by CLPs normalized to the time 0 values (T320-T0). Asterisks signify significantly different compared to the mock treated plants (*p ≤0,05; *** p ≤0.001), ns not significantly different (n=15; multiple t-test). Surfactin (Srf), lichenysin (Liche), and pumilacidin (Pumi), were applied as a mix of homologues, massetolide A (Mass) and WLIP have chain length C10.

4.4. *ISR potential of Srf-like CLPs*

As the most important functional outcome, the potential to stimulate systemic resistance in *Arabidopsis* was evaluated for lichenysin and pumilacidin in comparison to Srf. CLPs were applied as a root treatment, prior to infection of leaves with *B. cinerea*, which spores were applied 24h after elicitation with CLPs. CLPs were applied as 10 µM solution, the concentration determined as efficient for Srf (Chapter 2; Cawoy et al., 2014; Hoff *et al*., 2021). It was observed that pumilacidin has no ISR elicitor potential, whereas lichenysin and Srf show similar efficiencies (**Figure 49a,b**).

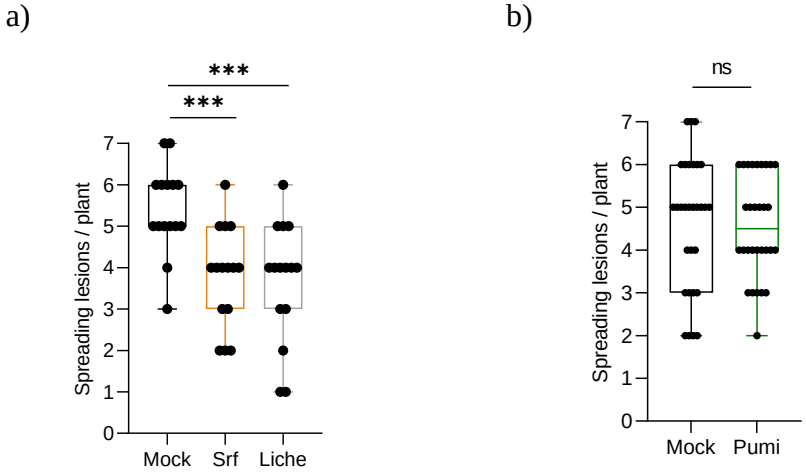

Figure 49 - ISR potential of **a)** lichenysin (Liche) and **b)** pumilacidin (Pumi). Box plots represented as in Figure 9. Data obtained from two independent experiments each n=15.

4.5. *Influence of the fatty acid chain length on the activity of Srf*

Not only for CLPs, but also for other amphiphilic molecules such as AHL and RLs (Chapter 1, section 4.1.), an influence of the alkyl chain length on their potential to induce immune responses has been observed. In the case of AHL, the most active variant is C14 whereas RLs with C12 acyl chains were the most active. For Srf, it was previously shown on tobacco roots and culture cells that variants with longer chain lengths, C14 and C15 are the most active ones in inducing immune responses and ISR (Henry *et al*., 2011; Hoff *et al*., 2021). To assess if that is also the case in *Arabidopsis*, we tested different chain length variants for ROS induction. Interestingly, our results show that C13 chain variant of Srf is the most active in triggering $[ROS]_{intra}$ production in *Arabidopsis* roots which is not in accordance with the previous results on tobacco (**Figure 50**).

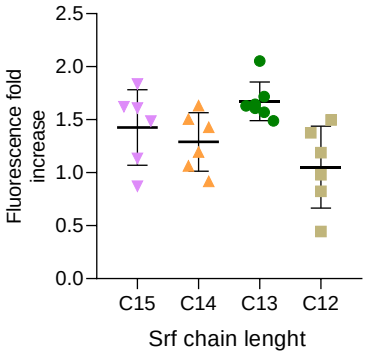

Figure 50 - Induction of $[ROS]_{intra}$ by Srf variants. Values obtained in two independent experiments, each n=3. Fold increase obtained by dividing with control values average (n=3) in each experiment separately.

5. Discussion

Taken together, these data emphasize the importance of CLP structure for its activity and demonstrate that the potential of CLPs to trigger immune-related responses and ISR is influenced by structural changes of the peptide cycle and/or acyl chain. Since structural changes did not affect the activity of lichenysin and pumilacidin in the same manner (**Figure 51**), these data also show that structural changes have to be specific regarding the position and/or amino acid alternation. To further determine which structural changes are influencing the interaction the most, additional experiments comparing homologues of different CLPs with the same chain length are needed.

Figure 51 - Schematic representation of bioactivity of CLPs. Dark blue represents events for which activity was observed, light shade blue when no activity was observed.

Moreover, massetolide A and WLIP produced by beneficial pseudomonads also exhibited such a structure-dependent immune response, suggesting that structure activity is a general CLP trend rather than specific to Srf and Srf-like CLPs.

Even though *B. licheniformis* strains are only sporadically reported as ISR inducers, our work discovers a new effective ISR elicitor – lichenysin produced by these species (Nigris *et al*., 2018; Abdelkhalek *et al*., 2020). This finding holds the potential to better implement these species as ISR inducers by selecting strains that efficiently produce lichenysin.

On the other hand, from an ecological aspect, the inactivity of pumilacidin can be interpreted based on the lifestyle of the bacteria producing this CLP. Namely, some of the *B. pumilus* species producing pumilacidin are considered to be endophytic bacilli (Dobrzyński et al., 2022), which could explain why it would not be of interest for them to trigger immune-related responses.

Interestingly, our results show that C13 chain variant of Srf is the most active in triggering $[ROS]_{intra}$ production in *Arabidopsis* roots which is not in accordance with the previous results on tobacco where variants with longest chain lengths, C14 and C15 are the most active (Henry *et al*., 2011; Hoff *et al*., 2021). This may be explained in two ways. First, previous studies showed that the effect of CLP on the lipid bilayer is bidirectionally influenced by membrane thickness (lipid chain length) and CLP chain length. In this study, it was shown that when the bilayer is composed of longer lipid chains, the CLP acyl chain must also be longer to induce pore formation (Steigenberger *et al*., 2022). In this case, this might suggest that *Arabidopsis* has a different membrane thickness than tobacco root cells and therefore different chain length variants of CLP are the most active. Knowing that the lipid composition of the membrane varies between the species, also in terms of sphingolipids (Chapter 2, section 8), another possible explanation could be that different chain length CLPs have affinity for different lipids within the membrane and thus the difference in bioactivity.

These data highlight the need for a better understanding of the exact mechanism of CLP/PPM interaction. Filling this knowledge gap could contribute to the successful integration of CLPs as biostimulants in sustainable agriculture in two main ways. It would allow optimization of the application by tactically selecting the plant species/plant organ and CLP combination depending on the plasma membrane characteristics and CLP structure, but it would also allow targeted optimization of the structure of the synthetic CLPs needed for specific plants, that are not available in nature.

6. Data authorship

This work is a result of collaboration with different colleagues, which helped in realizing work presented in following figures:

Fig 46, 48a, 49a,b experiments were conducted in collaboration with Ning Ding.

7. Supplementary data

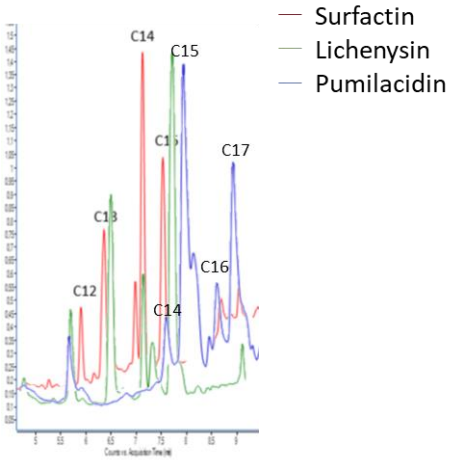

Supplementary Figure 5 – Overlapped chromatograms of CLP mixes used in this study

Supplementary Table 11: Proportional composition of different homologues of CLP mixes used in this study.

	Homologs Percentage (%)					
CLP	C12	C13	C14	C15	C16	C17
Srf	7	2	41	32	<1	
Lichenysin		29	12	59	<1	
Pumilacidin			8	43	13	37

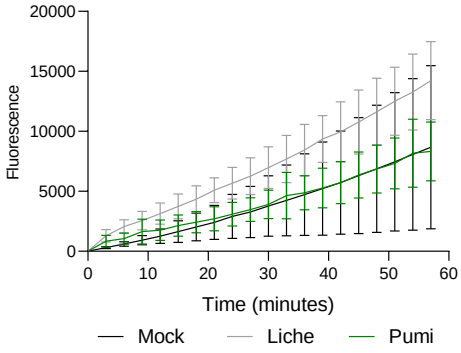

Supplementary Figure 6 – Kinetic view of ROS production triggered by lichenysin (Liche) and pumilacidin (Pumi).

8. References

Abdelkhalek A, Al-Askar AA, Behiry SI. Bacillus licheniformis strain POT1 mediated polyphenol biosynthetic pathways genes activation and systemic resistance in potato plants against Alfalfa mosaic virus. *Sci Rep*. 2020;10(1):1-16. doi:10.1038/s41598-020-72676-2

Balleza D, Alessandrini A, Beltrán García MJ. Role of Lipid Composition, Physicochemical Interactions, and Membrane Mechanics in the Molecular Actions of Microbial Cyclic Lipopeptides. *J Membr Biol*. 2019;252(2-3):131-157. doi:10.1007/s00232-019-00067-4

Bigelow CC. On the average hydrophobicity of proteins and the relation between it and protein structure. *J Theor Biol*. 1967;16(2):187-211. doi:10.1016/0022-5193(67)90004-5

Cawoy H, Mariutto M, Henry G, et al. Plant defense stimulation by natural isolates of Bacillus depends on efficient surfactin production. Mol *Plant-Microbe Interact*. 2014;27(2):87-100. doi:10.1094/MPMI-09-13-0262-R

Dobrzyński J, Jakubowska Z, Dybek B. Potential of Bacillus pumilus to directly promote plant growth. *Front Microbiol*. 2022;13(December):1-6. doi:10.3389/fmicb.2022.1069053

Francius G, Dufour S, Deleu M, Paquot M, Mingeot-Leclercq MP, Dufrêne YF. Nanoscale membrane activity of surfactins: Influence of geometry, charge and hydrophobicity. Biochim Biophys Acta - Biomembr. 2008;1778(10):2058-2068.

Henry G, Deleu M, Jourdan E, Thonart P, Ongena M. The bacterial lipopeptide surfactin targets the lipid fraction of the plant plasma membrane to trigger immune-related defence responses. *Cell Microbiol*. 2011;13(11):1824-1837. doi:10.1111/j.1462-5822.2011.01664.x

Hoff G, Arguelles Arias A, Boubsi F, et al. Surfactin Stimulated by Pectin Molecular Patterns and Root Exudates Acts as a Key Driver of the Bacillus -Plant Mutualistic Interaction. *Vidaver AK, ed. MBio*. November 2021:2021.02.22.432335. doi:10.1128/mBio.01774-21

Nigris S, Baldan E, Tondello A, et al. Biocontrol traits of Bacillus licheniformis GL174, a culturable endophyte of Vitis vinifera cv. Glera 06 Biological Sciences 0604 Genetics 06 Biological Sciences 0607 Plant Biology 06 Biological Sciences 0605 Microbiology. BMC Microbiol. 2018;18(1):1-16. doi:10.1186/s12866-018-1306-5

Oni FE, Esmaeel Q, Onyeka JT, et al. Pseudomonas Lipopeptide-Mediated Biocontrol: Chemotaxonomy and Biological Activity. 2022.

Steigenberger J, Mergen C, De Roo V, Geudens N, Martins JC, Heerklotz H. The effect of membrane thickness on the membrane permeabilizing activity of the cyclic lipopeptide tolaasin II. *Front Mol Biosci*. 2022;9(December):1-12. doi:10.3389/fmolb.2022.1064742

Stringlis IA, De Jonge R, Pieterse CMJ. The Age of Coumarins in Plant-Microbe Interactions. *Plant Cell Physiol*. 2019;60(7):1405-1419. doi:10.1093/pcp/pcz076

Théatre A, Hoste ACR, Rigolet A, et al. Bacillus sp.: A Remarkable Source of Bioactive Lipopeptides. *Adv Biochem Eng Biotechnol*. 2022;181:123-179. doi: 10.1007/10_2021_182.

Chapter 5

General discussion

Synthetic pesticides have advantages such as curative effect and being highly effective biocides, nevertheless the presence of these chemicals on the market is decreasing due to rising number of sustainable agriculture related legislations that strictly control their use (Reglinski *et al.*, 2023). PBBs are a promising alternative for phytopathogen control due to their ability to inhibit pathogens by secreting antimicrobial metabolites and by inducing ISR. However, the success of PBBs and their elicitors as plant defenses stimulators has been rather limited due to a number of factors, including our global lack of knowledge about the chemical nature of the compounds and the mechanistics underlying their resistance triggering activity.

First, although a large number of PBB species have been described to have an ISR effect on plants, the exact elicitors for most of these species remain unknown. Furthermore, even though this work partially elucidates mechanisms and pathways activated during the onset of Srf-triggered ISR, to the best of the author's knowledge, such comprehensive data is not available for other ISR elicitors.

The variety of phytopathosystems tested is also so far still limited and additional research on agriculturally important crops and pathogens is needed to better assess their potential on a larger market scale. In the case of CLPs, a more targeted approach could be achieved by using biophysical methods. While further elucidation of the physiochemical basis of the interaction of CLPs with the specific PPM lipids is needed, the results of this thesis suggest that these methods could be used as one of the approaches in order to roughly predict on which plant species/organs certain CLPs would be active. More specifically, by manipulating the composition of biomimetic liposomes, experimental biophysics and *in silico* dynamic modelling could provide a valuable information about plant species/organ candidates if appropriate models (mimicking the PPM lipidome of a specific plant species/organ) are used.

Once the plant species/pathosystem/efficient CLP combination is determined, the application of CLPs as biocontrol agents in sustainable agriculture could be developed in two directions. One would be the application of living bacterial cells producing targeted CLPs, and the other direction would be the application of pure compounds, where both of the approaches are encountering certain challenges.

Even though beneficials are good competitors in the rhizosphere, it is quite unknown how the complex interactions in this niche influence the colonization and production of different metabolites. In most instances, CLPs are active at micromolar doses, but only a few studies suggest that quantities produced by bacteria in planta are sufficient to locally reach such a threshold around the roots (Debois *et al*., 2015; Hoff *et al*., 2021; Poppeliers *et al*., 2023). Determining the amounts of CLPs produced by PBBs under natural conditions is important, but not an easy task. It would require optimal extraction from rhizosphere samples and the most-advanced MS- based metabolomics allowing high sensitivity for their detection and quantification.

Furthermore, low temperature, acidic pH or poor oxygen availability are among the rhizosphere-specific abiotic parameters that influence bacterial physiology, and which may also modulate the production of secondary metabolites, including elicitors, as reported for *Bacillus* lipopeptides (Fahim *et al*., 2012; Pertot *et al*., 2013; Zhao and Kuipers, 2016).

Biotic factors, such as interactions with other microbial species of the soil microbiome or a chemical crosstalk with the host plant, may also influence elicitor production under natural conditions (Debois *et al*., 2015; Wu *et al*., 2015; Venturi and Keel, 2016; Andrić *et al*., 2020; Hoff *et al*., 2021). A better assessment of the impact of all these factors deserves further investigation and is necessary to better anticipate inconsistencies in PBB efficacy observed upon application under field conditions.

Integrating all this missing information should also lead to a more rational determination of the range of phytopathosystems and environmental conditions in which PBB-based bioproducts would be the most effective.

An alternative for using PBB that might not produce sufficient amounts of elicitors, is making microbial-derived immunogenic compounds-based products for the phytosanitary market, guaranteeing a bioactive concentration of CLPs. However, the production and formulation in cost-effective industrial processes represent challenging but not impossible aim, as it is feasible for some *Bacillus* lipopeptides with a high production rate in bioreactors (Zanotto *et al*., 2019; Brück *et al*., 2020).

So far, solvent extraction, membrane filtration, adsorption, and size exclusion techniques are the best ranked for the purification of CLPs. Keeping

in mind that CLPs demonstrate variating structure-dependent activity, the downside of these methods is that the different families of CLPs produced are pulled together. This could be resolved by selecting species that naturally produce only one type of CLP, which is often observed in *Pseudomonas* sp., or by mutating bacteria in order to produce only targeted family of CLP. In addition, minor alternation of the CLPs could be achieved naturally by supplementing media with different amino acids. In cases where a variant that is predicted to have highest activity in certain systems is not found in nature it can also be made artificially by synthetic production (Hoste *et al*., 2023). Considering that even the CLP variants with different chain length can show differences in activity, at times when their further purification is needed, a possible solution would be an additional purification step using preparative chromatographic techniques, which provide maximum resolution with minimum contaminants (Rangarajan and Clarke, 2016).

Taken together, the dose- and structure-dependent activity should guide a rational strain selection, optimization of culture conditions for maximal CLP production and possible CLP structure alternation.

Towards the product formulation, the properties rendering CLPs advantages as biopesticides are not only their bioactivity over a wide range of temperatures, pH, and salinity, but also their biodegradability and minimal toxicity to humans (Gutiérrez-Chávez *et al*., 2021). Even though CLPs are generally stable, certain delivery methods such as liposome encapsulation and chitosan coating are under development (Kang *et al*., 2022).

Considering the important role that CLPs could play not only as biopesticides (antimicrobials and ISR elicitors), but also as anticancer and antimicrobial agents against human pathogens (Geudens and Martins, 2018), optimization of these methods could have broader benefits than solely in sustainable agriculture application.

In addition to the applied value, the results of this work also provide a good basis for future fundamental research.

Collectively, this work provides new insights into the molecular basis of the well-known long-standing process of CLP-triggered plant immunity activation by unveiling a novel lipid-mediated mechanism for sensing these molecules at the cell surface. Rather than relying on PRRs for perception, Srf inserts into

sphingolipid-enriched domains acting as docking platforms in the PPM, causing membrane deformation. Such membrane changes have been described in the literature to be perceived via MSC, and this work shows that members of these mechanosensitive ion channels are required for early immune responses and induction of ISR by Srf. To the best of the author's knowledge, this mechanism has not been previously described for triggering plant immunity, and it brings an unexpected role for mechanosensitive channels.

Such a lipid-dependent perception at the cell surface may also apply to other bacterial amphiphilic ISR elicitors, such as acyl-homoserine lactones and rhamnolipids, which also readily interact with membrane lipids and thus may be perceived via similar mechanisms (Davis *et al*., 2010; Schikora *et al*., 2016; Schellenberger *et al*., 2019; Pršić and Ongena, 2020; Schellenberger *et al*., 2021).

The nature of PPM lipids varies widely among plant species (Haslam and Feussner, 2022). This could explain, at least in the case of Srf, why this molecule triggers immunity in dicots but is not very active in monocots (Pršić and Ongena, 2020). The effect of a CLP on a particular target membrane being fine-tuned by precise structural characteristics of the molecule may explain why some CLPs produced by *Pseudomonas* leaf pathogens act as virulence factors in a wide range of plants by causing necrosis via pore formation in cell membranes (Girard *et al*., 2020). Our data supports this theory by showing that structurally different CLPs have variating activity depending on the presence of different sphingolipid classes (**Figure 26**). Also, even slight changes in the structure of the molecule can influence the outcome of the CLP/PPM interaction, such as immune-related responses and ISR activation (Chapter 4). As aforementioned, in studies using membrane mimicking models, the activity of Srf depends mainly on physico-chemical properties, such as spatial conformation, charge, and hydrophobicity (Francius *et al*., 2008; Balleza *et al* 2019). In this regard, the differences between lichenysin and Srf are particularly interesting, since Glu1 of the Srf's peptide ring is replaced by Gln in lichenysin, thus resulting in one less negative charged amino acid. In theory, during the interaction with PPM negatively charged lipids, such as sphingolipid GIPC located in the microdomains (Cassim *et al*., 2021), a more negatively charged head of Srf could induce a higher electrostatic repulsion than that of lichenysin, thus changing the interaction with the PPM (Nerurkar

et al., 2010; Coronel *et al*., 2017). However, considering that lichenysin has conserved ISR activity, and that pumilacidin has two negatively charged amino acids but no activity, it can be concluded that in our setup charge does not play a key role in the interaction with *Arabidopsis* root cells plasma membrane.

On the other hand, literature shows that methylated Srf loses activity in tobacco cells thus demonstrating contrasting data. Interestingly, tobacco culture cells also show differences in the chain variant with the highest activity, with C14 and C15 being the most active instead of C13, which is the most active in *Arabidopsis* root cells (Henry *et al*., 2011; Hoff *et al*., 2021). Thus, studying lipidome of these two models could bring additional information on specificities of Srf/PPM lipids interaction.

This work also showed that even though pumilacidin is a Srf-like CLP it loses the potential to trigger ISR. This could possibly be explained by its altered biophysical properties such as lower activity in reducing the surface tension, lower efficiency in self-assembly, increase in hydrophobicity and perhaps due to a possible change in 3D conformation. Interestingly, in pairwise comparisons of Srf-pumilacidin and WLIP-massetolide A the less hydrophobic CLPs were more active regarding immune response activation in *Arabidopsis*. However, further understanding of PPM/CLP interaction specificities is needed to narrow down which properties are crucial or complementary involved as the key players.

This work also shows that structure-dependent activity of Srf is influenced by the length of the acyl chain. This phenomenon is consistent with similar trends observed in the case of other amphiphilic molecules known to induce immune system responses, such as AHL (with C14 exhibiting the highest activity) and rhamnolipids, among which C12 is the most active. Notably, in the case of Srf, considering the proportion of its homologues present in the mixture, where C13 constitutes only up to 10%, it is conceivable that a synergistic effect on immune response elicitation may arise from the presence of various homologues. It is worth noting that MD simulations suggest that Srf is more likely to aggregate rather than insert as individual molecules, implying that the aggregation of different homologues could potentially influence the three-dimensional conformation of the agglomerate and subsequently affect Srf's interaction with the PPM.

Furthermore, this study reveals that the bioactivity of Srf is modulated by the specific PPM lipids present. When examining structurally distinct CLPs, variations in their potential to trigger immune responses in mutants lacking different classes of sphingolipids was observed (**Figure 22**). This finding suggests that, in different plant species, the interaction between CLPs and PPM lipids will result in varying immune responses, dependent upon the particular lipid composition of the plant's plasma membrane.

Another question that this study raises is whether there is a higher importance of insertion in microdomains, or CLPs that would have affinity for phospholipids would have similar effect on plants. Also, considering that proteins (thus ion channels as well) could have specific location within the PPM, would they perceive mechanical stress the same depending on the location of the membrane where the stress is caused (phospholipid fluid part or microdomains rigid area)?

However, it is important to note that this research does not directly establish that the membrane deformation induced by Srf activates MSCs. To further answer this question, a patch-clamp method could be used, a method commonly described in the literature for corelating changes in tension in the PMM and MSC activation (Haswell *et al*., 2008).

Taken together, this knowledge would only be a starting point in trying to understand how plants would differentiate a true mechanical stress response from the response to Srf.

Furthermore, although Srf does not trigger pronounced calcium elevations, this immune event is traditionally a signal of PTI. Since Srf-triggered early immune events do not result in high transcriptional changes, a possible explanation could be that Srf can modulate plant responses by downregulating genes encoding calcium binding proteins (**Figure 19**).

Downstream calcium influx, as presented, Srf specifically triggers only the production of intracellular ROS. Additionally, it is noted that the Srf can boost extracellular ROS levels, despite the fact that it alone does not induce extracellular ROS production. Literature suggests that RBOHD can be encysted within microdomains in order to differentially regulate its activity (Hao *et al*., 2014), thus it can be postulated that Srf's interaction with these microdomains may influence the overall RBOHD dynamics.

This specific behavior of Srf is raising the question whether there are differences in signaling between extracellular and intracellular ROS generally. One explanation for the divergent signaling possibly induced by these two types of ROS lies in the variance of antioxidant levels, resulting in a prolonged presence of "signaling active ROS" in apoplast (Chapter 1, 3.2.2.). In the past, it was widely assumed that transfer of extracellular ROS into the cell via aquaporins was necessary to activate responses in plants. However, recent research has uncovered a key receptor in *Arabidopsis* which serves as the receptor for apoplastic H_2O_2, a leucine rich repeat-receptor kinase - HPCA1 (HYDROGEN-PEROXIDE-INDUCED Ca^{2+} INCREASES 1). This receptor plays a crucial role in activating calcium influx and the subsequent downstream response directly by perceiving extracellular ROS (Wu *et al*., 2020).

Even though existing literature has shown that ROS can be exclusively produced intracellularly in response to various abiotic and biotic stimuli, the reasons behind this phenomenon remain unexplained (Lee et al., 2023). Besides, while the activation of extracellular ROS by calcium has been comprehensively documented in the literature (Marcec *et al*., 2019), the mechanisms underlying calcium-induced intracellular ROS production remain unexplored.

Although, the results of this work demonstrate for the first time involvement of MSCs, interaction with lipid phase of PPM was already postulated for RLs (Herzog *et al*., 2020; Schellenberger *et al*., 2021), NLP toxins (Lenarčič *et al*., 2017), and pathogenic immunity elicitor cryptogein (CRY; Gerbeau-Pissot *et al*., 2014). CRY is secreted by the pathogenic oomycete *Phytophthora cryptogea* and it induces a hypersensitive response in plants, resulting in plant cell death. Although it has been reported to be perceived by a PRR at nM concentrations, its ability to bind sterols in the PPM has also been demonstrated. Interestingly, a structure-activity relationship for the activation of NO^- and ROS production was also observed for this elicitor. Janků *et al.* compared the elicitation of oxidative burst by two elicitins, CRY and infestin 1 (INF1), secreted by the oomycete *P. infestans* which has significantly weaker capacity for inducing hypersensitive response in plants. The data presented showed that INF1 is not able to trigger ROS nor NO^- production, however with only one amino acid change (valine substituted for lysine at position 13, or valine at position 84 substituted for phenylalanine), the activity increased to a

level similar to active CRY. This study also suggested that the increase in activity of the phenylalanine containing variant is due to its increased ability to trap sterols, which would enhance ROS production. The same study suggested that the NO^- is produced intracellularly and then transferred to the apoplast at later time points, possibly suggesting that NO can serve as a signal for neighboring cells (Janků et al., 2022). On the other hand, Kulik *et al*. showed that CRY induced NO^- production is partially triggered by ROS, but also that NO^- downregulates the level of H_2O_2. Furthermore, a transcriptomic analysis revealed that NO^- and ROS upregulated genes are downregulated by another RNS species $ONOO^-$ (Kulik *et al*., 2015). Srf does not induce hypersensitive response in plants, it is active at µM concentrations, and Srf triggered NO^- is independent of ROS (based on the results on MSC mutants), however studies performed on CRY could be a good starting point to further investigate the role of NO^- in Srf-induced resistance. It would be interesting to test whether Srf triggered NO^- would lower the H_2O_2 levels, whether there is a switch in intra to extracellular NO^-, but also whether $ONOO^-$ production is triggered by Srf. If Srf indeed triggers $ONOO^-$ production, it could be interesting to further investigate whether $ONOO^-$ is responsible for the high downregulation of genes by Srf. Furthermore, resolving what are the downstream events of calcium and ROS and on the other hand NO^- signaling, would give more information on how the signal specificity is achieved by the interplay of these early immune events and how it creates the final plant response - ISR.

Step further along immunity elicitation, this work provides the basis for further investigation of defense signaling molecule azelaic acid (Aza) involvement in SAR and ISR. Besides Aza, RNAseq analysis provides other candidates (Chapter 3, Discussion), that could also serve as signaling molecules.

Considering that Srf can also trigger ISR in *Arabidopsis* against *Pseudomonas syringae pv. maculicola* (Altrão *et al*., 2022), the data obtained in this work provide a basis for estimating how Srf achieves priming of plants against pathogens with different lifestyles. At the outset of this work, ISR against *Pseudomonas syringae pv. maculicola* could be evaluated on *pad3* and *myb72* mutants in order to evaluate if elevated resistance is camalexin or coumarins dependent. The activation of MYB72 occurs downstream of NO^-

production as previously shown in the literature (Zamioudis *et al*., 2015). Although it remains a speculative hypothesis, it is conceivable that activation of MYB72 may represent an MSC-independent event, as NO^- production was demonstrated to be MSC-independent in this study. In summary, this suggests that Srf has the capability to independently activate two distinct phytoalexin pathways (coumarin and camalexin).

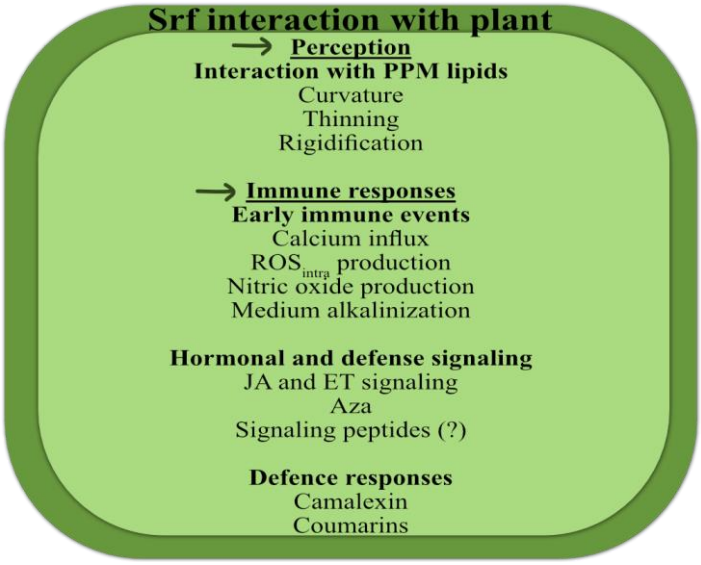

Figure 52 – Schematic representation of Srf perception and activation of immune responses in plants.

Taken together, this work partially explains how an ISR elicitor is sensed by plant cells, what are the following early immune events, and gives indications how ISR might be achieved. This not only provides a framework for further investigation of ISR underlying mechanisms, but also it provides a starting point for the successful establishment of CLPs as a strategy in sustainable agriculture.

References

Andrić S, Meyer T, Ongena M. Bacillus Responses to Plant-Associated Fungal and Bacterial Communities. *Front Microbiol*. 2020;11(June):1-9. doi:10.3389/fmicb.2020.01350

Anuradha S. N. Structural and Molecular Characteristics of Lichenysin and Its Relationship with Surface Activity. In: Sen R, ed. New York, NY: Springer New York; 2010:304-315. doi:10.1007/978-1-4419-5979-9_23

Balleza D, Alessandrini A, Beltrán García MJ. Role of Lipid Composition, Physicochemical Interactions, and Membrane Mechanics in the Molecular Actions of Microbial Cyclic Lipopeptides. *J Membr Biol*. 2019;252(2-3):131-157. doi:10.1007/s00232-019-00067-4

Brück HL, Coutte F, Dhulster P, Gofflot S, Jacques P, Delvigne F. Growth dynamics of bacterial populations in a two-compartment biofilm bioreactor designed for continuous surfactin biosynthesis. *Microorganisms*. 2020;8(5). doi:10.3390/microorganisms8050679

Cassim AM, Navon Y, Gao Y, et al. Biophysical analysis of the plant-specific GIPC sphingolipids reveals multiple modes of membrane regulation. *J Biol Chem*. 2021;296(7):100602.

doi:10.1016/j.jbc.2021.100602

Cawoy H, Debois D, Franzil L, De Pauw E, Thonart P, Ongena M. Lipopeptides as main ingredients for inhibition of fungal phytopathogens by Bacillus subtilis/amyloliquefaciens. *Microb Biotechnol*. 2015;8(2):281-295. doi:10.1111/1751-7915.12238

Coronel JR, Marqués A, Manresa Á, Aranda FJ, Teruel JA, Ortiz A. Interaction of the Lipopeptide Biosurfactant Lichenysin with Phosphatidylcholine Model Membranes. *Langmuir*. 2017;33(38):9997-10005. doi:10.1021/acs.langmuir.7b01827

Davis BM, Jensen R, Williams P, O'Shea P. The Interaction of N-Acylhomoserine Lactone Quorum Sensing Signaling Molecules with Biological Membranes: Implications for Inter-Kingdom Signaling. II

RMR, ed. *PLoS One*. 2010;5(10):e13522. doi:10.1371/journal.pone.0013522

Fahim S, Dimitrov K, Gancel F, Vauchel P, Jacques P, Nikov I. Impact of energy supply and oxygen transfer on selective lipopeptide production by Bacillus subtilis BBG21. *Bioresour Technol*. 2012;126:1-6. doi:https://doi.org/10.1016/j.biortech.2012.09.019

Francius G, Dufour S, Deleu M, Paquot M, Mingeot-Leclercq MP, Dufrêne YF. Nanoscale membrane activity of surfactins: Influence of geometry, charge and hydrophobicity. *Biochim Biophys Acta - Biomembr*. 2008;1778(10):2058-2068. doi:10.1016/j.bbamem.2008.03.023

García-Gutiérrez L, Zeriouh H, Romero D, Cubero J, de Vicente A, Pérez-García A. The antagonistic strain Bacillus subtilis UMAF6639 also confers protection to melon plants against cucurbit powdery mildew by activation of jasmonate- and salicylic acid-dependent defence responses. *Microb Biotechnol*. 2013;6(3):264-274. doi:10.1111/1751-7915.12028

Gerbeau-Pissot P, Der C, Thomas D, et al. Modification of plasma membrane organization in tobacco cells elicited by cryptogein. *Plant Physiol*. 2014;164(1):273-286. doi:10.1104/pp.113.225755

Geudens N, Martins JC. Cyclic lipodepsipeptides from Pseudomonas spp. - Biological Swiss-Army knives. *Front Microbiol*. 2018;9(AUG):1-18. doi:10.3389/fmicb.2018.01867

Girard L, Höfte M, Mot R De. Lipopeptide families at the interface between pathogenic and beneficial Pseudomonas -plant interactions. *Crit Rev Microbiol*. 2020;46(4):397-419.

Hao H, Fan L, Chen T, et al. Clathrin and Membrane Microdomains Cooperatively Regulate RbohD Dynamics and Activity in Arabidopsis. *Plant Cell*. 2014;26(4):1729-1745. doi:10.1105/tpc.113.122358

Haslam TM, Feussner I. Diversity in sphingolipid metabolism across land plants. *J Exp Bot*. 2022;73(9):2785-2798. doi:10.1093/jxb/erab558

Haswell ES, Peyronnet R, Barbier-Brygoo H, Meyerowitz EM, Frachisse JM. Two MscS Homologs Provide Mechanosensitive Channel Activities

in the Arabidopsis Root. *Curr Biol*. 2008;18(10):730-734. doi:10.1016/j.cub.2008.04.039

Herzog M, Tiso T, Blank LM, Winter R. Interaction of rhamnolipids with model biomembranes of varying complexity. *Biochim Biophys Acta - Biomembr*. 2020;1862(11):183431. doi:10.1016/j.bbamem.2020.183431

Hoff G, Arguelles Arias A, Boubsi F, et al. Surfactin Stimulated by Pectin Molecular Patterns and Root Exudates Acts as a Key Driver of the Bacillus -Plant Mutualistic Interaction. Vidaver AK, ed. *MBio*. November 2021:2021.02.22.432335. doi:10.1128/mBio.01774-21

Kang BR, Park JS, Ryu GR, Jung W, Choi J, Shin H. Effect of Chitosan Coating for Efficient Encapsulation and Improved Stability under Loading Preparation and Storage Conditions of Bacillus Lipopeptides. *Nanomaterials* (Basel). 2022 Nov 25;12(23):4 189. doi:10.3390/nano12234189.

Lee J, Han M, Shin Y, Lee JM, Heo G, Lee Y. How Extracellular Reactive Oxygen Species Reach Their Intracellular Targets in Plants. *Mol Cells*. 2023;46(6):329-336. doi:10.14348/molcells.2023.2158

Marcec MJ, Gilroy S, Poovaiah BW, Tanaka K. Mutual interplay of Ca2+ and ROS signaling in plant immune response. *Plant Sci*. 2019;283(March):343-354. doi:10.1016/j.plantsci.2019.03.004

Nerurkar AS. Structural and molecular characteristics of lichenysin and its relationship with surface activity. *Adv Exp Med Biol*. 2010;672:304-315. doi:10.1007/978-1-4419-5979-9_23

Pertot I, Puopolo G, Hosni T, Pedrotti L, Jourdan E, Ongena M. Limited impact of abiotic stress on surfactin production in planta and on disease resistance induced by Bacillus amyloliquefaciens S499 in tomato and bean. *FEMS Microbiol Ecol*. 2013;86(3):505-519. doi:10.1111/1574-6941.12177

Pršić J, Ongena M. Elicitors of Plant Immunity Triggered by Beneficial Bacteria. *Front Plant Sci*. 2020;11(November):1-12. doi:10.3389/fpls.2020.594530

Rangarajan V, Clarke KG. Towards bacterial lipopeptide products for specific applications — a review of appropriate downstream processing schemes. *Process Biochem*. 201 6;51(12):2176-2185. doi:10.1016/j.procbio.2016.08.026

Schellenberger R, Crouzet J, Nickzad A, et al. Bacterial rhamnolipids and their 3-hydroxyalkanoate precursors activate Arabidopsis innate immunity through two independent mechanisms. *Proc Natl Acad Sci U S A*. 2021;118(39):1-10. doi:10.1073/PNAS.2101366118

Schellenberger R, Touchard M, Clément C, et al. Apoplastic invasion patterns triggering plant immunity: plasma membrane sensing at the frontline. *Mol Plant Pathol*. 2019;20(11):1602-1616. doi:10.1111/mpp.12857

Schikora A, Schenk ST, Hartmann A. Beneficial effects of bacteria-plant communication based on quorum sensing molecules of the N -acyl homoserine lactone group. *Plant Mol Biol*. 2016;90(6):605-612. doi:10.1007/s11103-016-0457-8

Venturi V, Keel C. Signaling in the Rhizosphere. *Trends Plant Sci*. 2016;21(3):187-198. doi:10.1016/j.tplants.2016.01.005

Wu K, Fang Z, Guo R, et al. Pectin enhances bio-control efficacy by inducing colonization and secretion of secondary metabolites by Bacillus amyloliquefaciens SQY 162 in the rhizosphere of tobacco. *PLoS One*. 2015;10(5):1-17. doi:10.1371/journal.pone.0127418

Wu F, Chi Y, Jiang Z, et al. Hydrogen peroxide sensor HPCA1 is an LRR receptor kinase in Arabidopsis. *Nature.* 2020;578(February):1-5. doi:10.1038/s41586-020-2032-3

Zamioudis C, Korteland J, Van Pelt JA, et al. Rhizobacterial volatiles and photosynthesis-related signals coordinate MYB 72 expression in Arabidopsis roots during onset of induced systemic resistance and iron-deficiency responses. *Plant J.* 2015;84(2):309-322. doi:10.1111/tpj.12995

Zanotto AW, Valério A, de Andrade CJ, Pastore GM. New sustainable alternatives to reduce the production costs for surfactin 50 years after the

discovery. *Appl Microbiol Biotechnol*. 2019;103(21-22):8647-8656. doi:10.1007/s00253-019-10123-7

Zhao X, Kuipers OP. Identification and classification of known and putative antimicrobial compounds produced by a wide variety of Bacillales species. *BMC Genomics*. 2016;17(1):1-18. doi:10.1186/s12864-016-3224-y